Evaluation of a Ball Bearings

Dynamical Response Under Different

Conditions Using the Recurrence Analysis

Faculty of Management and Technology
Leuphana University Lüneburg

Submitted as a requirement for the award of the title of
Doctor of Engineering

Thesis submitted by MSc Eng. Bartłomiej Ambrożkiewicz
born 15.08.1993 in Kraśnik

Submitted on:

Main supervisor and reviewer: Prof. Dr Anthimos Georgiadis
                                  (Leuphana University of Lüneburg)

Second supervisor and reviewer: Prof. Dr Grzegorz Litak
                                  (Lublin University of Technology - Lublin)

Third reviewer: Prof. Dr Jörn Mehnen
                                  (University of Strathclyde - Scotland)

Contents

Abstract

The doctoral dissertation deals with the problems of the diagnosis of rolling bearings using recurrence analysis. The main topic is the influence of radial internal clearance on the change of dynamics in a self-aligning double-row ball bearing with a tapered bore, in which the axial preload can control this parameter in a wide range. The dissertation began with an analysis of the state of knowledge, where the works related to the analyzes of the impact of radial clearance on the dynamics of rolling bearings have been cited so far. In the next part of the dissertation, the thesis was formulated and activities related to its proving were defined. The theoretical part was supplemented with the basics related to vibroacoustic diagnostics of rolling bearings and presented methods that can be used for their diagnostics.

The research on proving the thesis was started with the preparation of a mathematical model in which a change in the damping coefficient in the field of radial clearance was adopted, a difference in the clearance value for a given row of balls was proposed, and the influence of shape errors and radial shaft endplay on the dynamics of the tested bearing was taken into account. During the dynamics tests, the radial clearance was adopted as a bifurcation parameter, and on the basis of the bifurcation diagram, it was possible to indicate the characteristic areas of bearing operation due to the radial internal clearance. In order to verify the model, experimental tests

were carried out with a series of bearings in which the radial clearance was changed in a wide range possible to be physically realized. Recurrence analysis was used for both the dynamic response obtained from model and experimental studies.

Owing to the comparative analysis of the dynamic response, recurrence quantificators were selected that are most susceptible to changes in radial clearance to bearing dynamics. Moreover, as a result of the research, it was possible to select a narrow range of radial clearance, ensuring the smoothest operation of the tested bearing.

INTRODUCTION AND OBJECTIVES

1.1 Introduction

The continuous development of mechanical systems is increasingly focused on high quality and high-reliability products applied in modern industry. In order to meet still growing requirements of customers, a variety of novel methods are applied in structural health monitoring and predictive maintenance, such as artificial intelligence, fuzzy logic, machine, and deep learning, acoustic emission, or advanced signal processing methods. Recently, mentioned methods gained popularity, as non-destructive testing is popularized for its sustainability and environmentally friendly approach.

Among rotational elements, rolling-element bearings play an important role as they are used in a wide range of mechanical systems for automotive, machinery, robotics, or space solutions. Growing demands of ball bearings impose its high reliability, maintenance-free operation, better performance, and longer durability. To meet the demands, especially for a rapidly grow-

ing market of e-drives, bearing manufacturers focus mainly on the quality of used materials, manufacturing precision, and customized profiles of rolling surfaces. Additionally, the diagnostics systems for diagnosis are still under the development often implementing the Industrial Internet of Things and the cloud computing. One of the solutions is the term "Smart Bearing", which corresponds to the online-condition monitoring of rolling-element bearings analyzed in its application, called in-situ. In modern engineering, the term "prevention is better than cure" is in force, that early diagnosed alarming behavior prevent undesirable serious damage or expensive downtime in the production.

The history of bearings dates back to ancient times, however, studies on their reliability and diagnostics were initiated in the XXth century applying accessible tools of engineering. In 1939, Swedish engineer Waloddi Weibull proposed the chain model explaining the structural strength [10]. The main assumption was that the mechanical structure consists of several n-pieces components composing the n-rings chain, for which the lifetime depends on the weakest one [24]. To find the lifetime distribution of the structure states the problem of finding the distribution of the weakest element. During the industrial development in XXth century, among various diagnostics methods, the vibrational analysis has been mostly utilized in industrial practice [91] allowing to detect mechanical failure issues like defects, imbalance, or misalignments and describing it in a quantitative way with amplitudes and characteristic frequencies.

Except for vibrational analysis in the rolling-element bearings diagnostics, it is worth mention the methods based on acoustic emission, electrostatic, ultrasonic, Shock Pulse Method, wear analysis, and modal analysis, however, methods often require special vibration sensors that can be applied easily. equipment and sublime knowledge. An unquestionable advantage

of frequency-based signal processing methods [142] is the extraction of a specific frequency, which can be assigned to the characteristic frequency of damaged element [106]. The challenge in modern diagnostics is the evaluation and quantitative or qualitative description of time-varying relevant operational parameters during the operation of a rotational system. The quantitative and qualitative evaluation of the influence of radial internal clearance on the dynamical response in self-aligning ball-bearings was the motivation to continue an ongoing trend in mechanical engineering.

The aim of this work is the application of time-based method called recurrences in the diagnostics of the dynamical response of self-aligning ball bearing with different radial internal clearance.

In order to achieve the set goal, the mathematical model is derived for the studied self-aligning ball bearing with conical bore in which it is possible to control the value of radial clearance in wide range. Development of the mathematical model and the experimental verification allow to conduct the comparative analysis with the recurrence-based methods in qualitative way (recurrence plots) and quantitative way (recurrence quantification analysis). The main advantage of proposed method over the linear analysis is the possibility to based it on the short-time intervals and conduct fine study to find the minor changes introduced by clearance into the dynamics of ball bearing. The radial internal clearance is one of the most important operating parameters in ball bearings influencing the bearing life and the level of generated vibrations during operation. The novelty of the work is not only the application of sublime signal analysis method, but the approach of quantitative description of the ball bearing's dynamics due to different operating radial clearance. To this time, the application of linear methods was proposed for the description of bearing's dynamics in reference to the value of clearance, but it was not referenced to the mathematical model and ver-

ified with the experiment. The proposed methodology can be undoubtedly applied in the dedicated diagnostic system.

STATE OF THE ART OF RESEARCH ON RADIAL INTERNAL CLEARANCE INFLUENCE IN ROLLING-ELEMENT BEARINGS

2.1 State of the Art

Radial internal clearance in ball bearings is the total distance that one ring can be moved in relation to the second ring being one of the most important parameters affecting the bearing's performance. The importance of the radial clearance relies on its direct influence on bearing life, too little leads to increased friction, while too big leads to decreased contact and undesirable sliding of rolling elements.

The research on the influence of radial internal clearance on the dynamics of rolling-element bearings was initiated with the analysis of State of the Art. Special attention was paid to research works considering radial

clearance as the variable parameter both in experimental and mathematical modeling way.

It is worth notice, that the first studies on the influence of radial clearance on the dynamics of ball bearings have been started in the 60s of the XXth century. In the work [62], authors studied undesirable slip and spin phenomena affecting the bearing's dynamics and they classified clearance as one of the parameters having a negative impact on it.

Starting with the end of the previous century, Lynagh et al. [93] employ the mathematical model of rolling-element bearing based on the Hertzian contact. In his work, he emphasizes the influence of clearance on the dynamics of the rotor system and on the emerged contact during its operation.

Tiwari et al. [128–130] studied the effect of radial internal clearance on the dynamics of a balanced horizontal rotor. He conducted the stability analysis of the rotor-bearing system, taking the radial clearance as the bifurcation parameter. Based on his mathematical modeling and experimental results, a general conclusion was provided that increased clearance leads to chaotic solutions with the increased strength of superharmonics and leads to wider regions of the system's instability.

Harsha et al. [59–61, 109, 133] demonstrated the nonlinear response of a balanced rotor for some specific combination of rotational velocity combined with varying radial internal clearance to provide sufficient nonlinearity. He pointed, that the radial clearance value changes effectively stiffness and damping of the system. It is another source of nonlinearity.

Yakout [151] confirmed experimentally the dependence of damping characteristics with clearance, additionally he studied the impact of radial clearance on the bearing life. With the highest clearance value, the damping factor had the smallest value and the bearing life was the shortest. The relation between bearing life and radial clearance is studied as well by Oswald

et al. [108] observing the negative influence of big clearance. Moreover, he analyzed the load distribution in reference to the clearance value. The deeper analysis on the calculation of load distribution due to positive, negative, and zero-clearance is studied by Xiaoli et al. [147]. Another factor related to the internal clearance is the thermal effect caused by frictional forces on rolling surfaces. The higher the temperature, the operational clearance is more reduced due to the thermal expansion of bearing rings [102].

The mathematical model of rolling-element bearing based on Hertzian elastic contact deformation theory and deformation compatibility theory provides satisfying results of dynamical response and is mostly utilized in scientific research. Balls and raceways are considered as nonlinear springs and the main nonlinearities introduced to the system are the description of the contact, internal clearance, and shape errors. The following papers provide deep insight into the mathematical description of multi-body ball bearing system considering radial internal clearance in the equation describing the Hertzian contact [25, 28, 35, 159].

The trend of online monitoring is observed in the diagnostics of radial clearance, which should provide an early-stage and interpretable indication of bearing health condition. Wang et al. [139] compared the vibrational data for different deep-groove bearings with induced local defects and various radial clearances observing differences in frequency spectra with modulations excitations with very low amplitudes submerged in noises. Moreover, he proposed the combination of quantificators consisting of Modulation Signal Bispectrum (MSB) for identification of noisy signal and Gini index for representation the peakedness of MSB. The applied signal-processing method allowed for identification between 20μm of radial clearance. In other reference, [149], it was claimed that the MSB indicator has the ad-

vantage over RMS, kurtosis, and BPFO (Ball Pass Frequency Outer) in the clearance online monitoring.

Xu et al. [148] proposed RMS and Spectral Centroid as the quantificator for online monitoring of radial clearance and compared it with the results of a mathematical model. He presumed mentioned quantificators allow the approximate clearance indication, but they exhibit fluctuating behavior due to nonlinear vibration. Comparison of model and experimental results didn't provide the same result and he emphasized the need to look for optimal indicators to control radial clearance.

One possible approach for real-time diagnostics can be the application of artificial intelligence in form of neural networks. The analysis proposed by Knezevic et al. [78] shows the acceptable accuracy based on RMS values, however, he emphasized that application of Deep Learning Neural Network could improve obtained classification's accuracy.

To sum up the review of the state-of-the-art regarding the real-time diagnostics of the radial internal clearance in ball bearings, it can be stated that the problem solving is considered both in an experimental and mathematical way. Primarily, the scientists face the problem to analyze chaotic solutions due to the specific radial clearance and finding accurate indicators based on the vibrational response signalizing the value of operational clearance. Most certainly, the aspect of providing the mathematical indicators being sensitive to the change of clearance is the present topic, which should be explained and discussed.

2.2   Objectives, Research Thesis and Scope

Observing the problem of identification of operational radial clearance based on the dynamical response and seeing the global trend directed to the real-

time condition monitoring, the main aim of the dissertation is to find the quantitative indicators providing the identification of operational radial clearance. Considering the above statement, the research thesis is formulated:

The dynamical response of rolling-element bearing is changing with different radial internal clearance and it can be distinguished in quantitative way with help of recurrence analysis.

The scope of the thesis includes the following tasks:

- derivation of the classical nonlinear 2-DOF mathematical model of rolling-element bearing based on the Hertzian contact theory,

- development of extended mathematical model based on the literature review considering the impact of radial internal clearance on bearing's performance,

- conduction of extended experiment for a set of bearings by different radial internal clearance and various operational velocities,

- study of experimental data with frequency-based methods,

- application of recurrence-based methods for qualitative and quantitative description of bearing's operation by specific clearance and velocity, the method is particularly applied for analysis of short-time intervals,

- comparative analysis of dynamical responses obtained with the mathematical model and in the experiment,

- selection of the most accurate recurrence quantificators prone to the change of radial clearance value based on the test of a set of bearings.

In the following text, the quantitative and qualitative description of radial internal clearance influence on the rolling-element bearing's dynam-

ics. In most cases, the application of new signal processing in real-time ball bearing diagnostics was referred to as its damage. Dealing with online clearance monitoring is definitely an important step-change in the development of the diagnostics of bearings. Moreover, the novelty of the approach is based on application in the experiment of the self-aligning ball bearings with a conical bore in which it is possible to control the radial clearance in a wide range. Referring to the already published papers, the analysis was conducted on different bearings with pre-determined clearance. Then, shape errors were not considered what might disturb the real frequency spectra. Additionally, the preparation of quantitative analysis based on more number bearings is the first step to the potential application of artificial intelligence for the diagnostics of operational radial clearance.

The dissertation consists of 8 chapters and the remainder is the following. In Chapter 3, the basics and theoretical aspects regarding rolling-element bearings are presented, emphasizing their role in the development of mechanical systems. Next, the commonly used methods applied in the online condition monitoring of ball bearings and other rotational systems are discussed. In Chapter 5, the mathematical model for ball bearings based on Hertzian contact theory is presented focusing on the additional parameters regarding the self-aligning ball bearings applied in the experiment. Chapter 6 contains the information on test rigs applied in the experimental part and its possibilities. Additionally, the experimental procedure with signal processing is described. In Chapter 7, the comparison of results obtained from the experimental part and simulations is presented. In the last chapter, the conclusions coming from the analysis are summarized and further steps of the research are established.

THEORETICAL ASPECTS AND BASICS

This chapter aims to provide essential information on the basics of bearing theory, i.e. types of rolling element bearings and their design. The main elements of ball bearings are described excluding special types of bearings. The most important issue considered in this chapter is the definition of clearance and its influence on rolling-element bearings performance. Types of radial clearances in reference to the stage of bearings operation are presented.

3.1 Bearing Theory

Bearings are the key elements in modern industry, which are used for supporting heavy loads and enabling rotational motion with the least possible friction. Industrial development over the last century forced the need for increased application of bearings wherever the movement and forces are

transferred. By the general overview of rolling-element bearings, two types of bearings can be defined according to the type of contact, i.e. point contact in ball bearings and linear contact in roller bearings [2]. What binds the two of them is the fact that they can be dedicated to carrying radial or axial load, but they differ completely from each other in operating velocities and the value of friction [6].

The idea of the research is focused on rolling-element bearings and they are classified according to the type of rolling element or direction of subjected load (radial bearings, thrust bearings). Referring the bearing division by the type of element, its classification is presented in Figure 3.1.

3.2   Design of Rolling-Element Bearings

The vast majority of rolling-element bearings consist of four main parts, i.e. inner and outer ring, rolling elements, and cage (Figure 3.2). The role of rolling elements and rings is to carry the subjected load and provide the rotational movement with the least possible friction. Cage separates consecutive balls or rollers in a row, however, complement bearings (without retainer) are available on the market.

3.2.1   Rings

The inner ring (IR) is mounted on the shaft and in a vast number of applications, it translates the rotational movement. In rolling-element bearings, there are two shapes of the bore, cylindrical (most applications) and conical. On the other hand, the outer ring (OR) in most cases is fixed in the housing or plummer block. The role of the rings is to carry the subjected load with the highest possible reliability, to ensure it, they are heat-treated to obtain proper hardness of rolling surfaces and thermal stabilization.
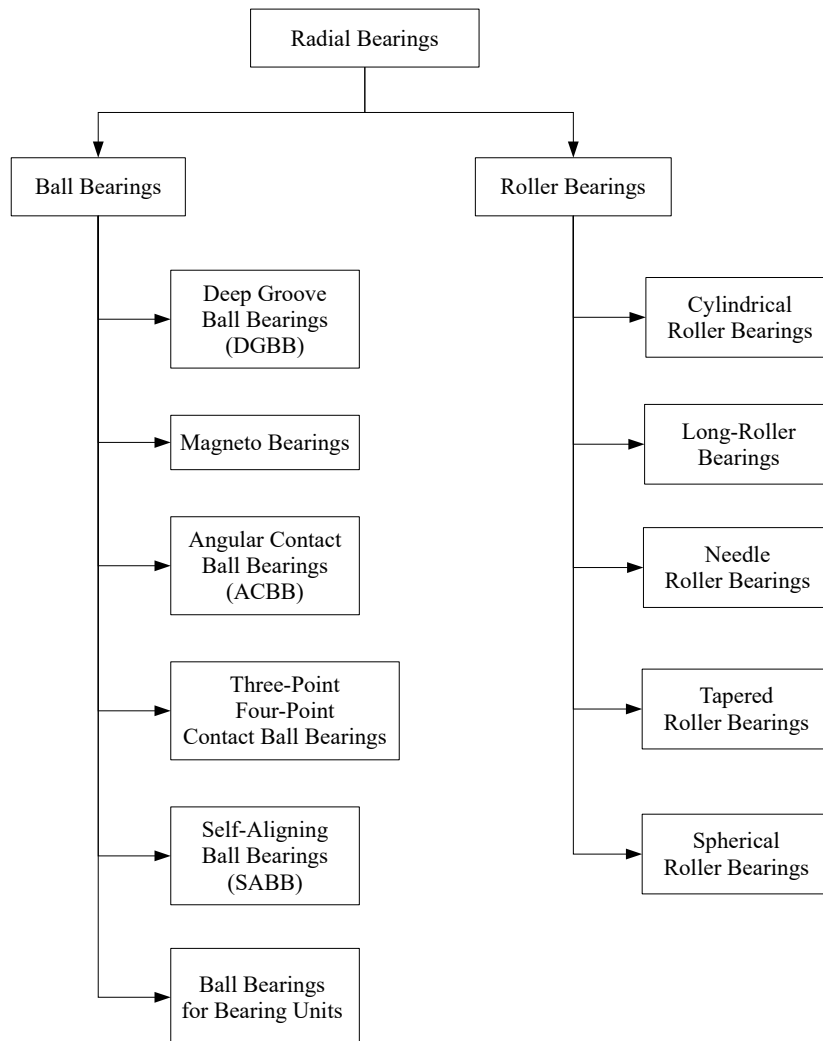
```
                        ┌──────────────────┐
                        │ Radial Bearings  │
                        └──────────────────┘
              ┌───────────────────────┴───────────────────────┐
   ┌──────────────────┐                            ┌──────────────────┐
   │  Ball Bearings   │                            │ Roller Bearings  │
   └──────────────────┘                            └──────────────────┘
        │   ┌──────────────────┐                        │   ┌──────────────────┐
        ├──▶│   Deep Groove    │                        ├──▶│   Cylindrical    │
        │   │  Ball Bearings   │                        │   │ Roller Bearings  │
        │   │     (DGBB)       │                        │   └──────────────────┘
        │   └──────────────────┘                        │
        │   ┌──────────────────┐                        │   ┌──────────────────┐
        ├──▶│ Magneto Bearings │                        ├──▶│   Long-Roller    │
        │   └──────────────────┘                        │   │    Bearings      │
        │   ┌──────────────────┐                        │   └──────────────────┘
        │   │  Angular Contact │                        │   ┌──────────────────┐
        ├──▶│  Ball Bearings   │                        ├──▶│     Needle       │
        │   │     (ACBB)       │                        │   │ Roller Bearings  │
        │   └──────────────────┘                        │   └──────────────────┘
        │   ┌──────────────────┐                        │   ┌──────────────────┐
        │   │   Three-Point    │                        ├──▶│     Tapered      │
        ├──▶│    Four-Point    │                        │   │ Roller Bearings  │
        │   │ Contact Ball     │                        │   └──────────────────┘
        │   │    Bearings      │                        │   ┌──────────────────┐
        │   └──────────────────┘                        └──▶│    Spherical     │
        │   ┌──────────────────┐                            │ Roller Bearings  │
        │   │  Self-Aligning   │                            └──────────────────┘
        ├──▶│  Ball Bearings   │
        │   │     (SABB)       │
        │   └──────────────────┘
        │   ┌──────────────────┐
        │   │  Ball Bearings   │
        └──▶│ for Bearing Units│
            └──────────────────┘
```

Figure 3.1. *Types of rolling-element bearings*

3.2.2 Rolling elements

The role of rolling elements is the transfer of subjected load (radial or axial) to the bearing and the rotational movement. Depending on the type of contact in rolling-element bearings, they can be in form of balls (ball bearings), tapered rollers, cylinders, spherical rollers, or needles (roller bearings). To ensure the high reliability of rolling elements, they are made of bearing steel 100Cr6 and the lubrication is added to reduce the frictional forces.

3.2.3 Cage

The cage (sometimes called a retainer) provides the separation of neighboring rolling elements in the bearing to avoid contact between them. The element doesn't carry the load, however in case of poor bearing's performance (push and pull phenomena), the rolling element can interact with it, which is why it is made of brass or metal sheet or plastics in most cases.

3.2.4 Seals

The aim of seals application in bearings is protection from external contamination, which could get into the grease or on rolling surfaces, causing the radical decrease of a lifetime. Its role is as well the prevention from grease leakage from the internal space of bearing, which could lead to a drastic increase of temperature and damage as a result.

3.3   Radial Internal Clearance in Ball Bearings

Depending on the type of rolling-element bearing, two types of internal clearance can be distinguished, namely radial clearance in ball bearings and axial clearance in tapered roller bearings [7]. The definition of internal
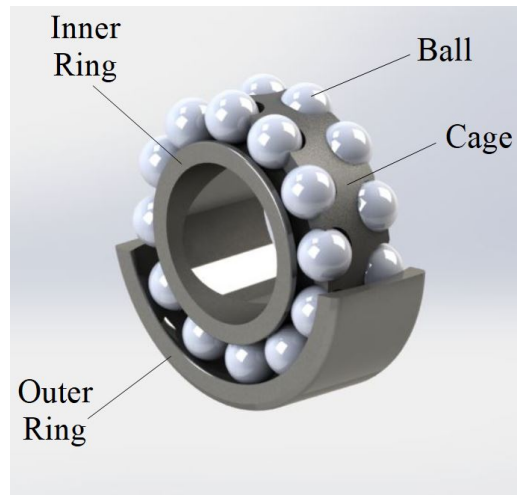
Figure 3.2. *Main component of rolling-element bearing*

clearance refers to the total distance through which one bearing ring can be moved relative to the other. The main role of the clearance is to provide the smoothest possible bearing operation with reduced friction torque and temperature. The value of initial clearance differs and is estimated by designers to the predicted operating conditions, i.e subjected load, possible temperatures, or mounting specifications. Inappropriately adjusted, i.e. too little or too small will lead to factors such as heat, vibration, noise, and fatigue life.

Referring to the stage of clearance depending on stage of bearing's application, the following types of it can be determined: [9]

- initial clearance - the value of clearance measured after assembly after bearing's manufacturing,

- mounted (reduced) clearance - after bearing mounting on shaft's journal with interference fit and subjected preload,

- operating clearance - the final clearance value after thermal stabilization of rings during operation.
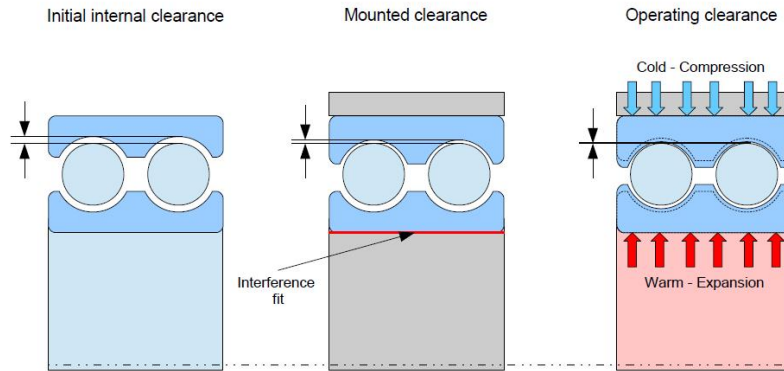
Figure 3.3. *Types of clearance in rolling-element bearing*

Mentioned three types of clearance are presented in the Figure 3.3.

To select appropriate initial radial clearance and next to achieve the correct operational clearance, bearings are usually manufactured in 5 different clearance classes according to ISO-5753-1:2009. Many bearing's manufacturers established the radial clearance designation referring to Normal as following specified in Table 3.1 [8]

Important notice, referring to rolling-element bearings with conical bore, its normalized values are bigger than in case of bearings with cylindrical bore. Their values are specified in the standard ISO-5753-1:2009.

3.4 Factors Influencing the Radial Internal Clearance

Referring to the analysis of dynamics of rolling-element bearings, only its operating clearance should be considered during bearing rotation. However, its value is decreased compared to the initial clearance and is affected by the following factors [77]:

Table 3.1. *Clearance classes designation and operating conditions*

ISO clearance class	Designation suffix	Internal clearance	Operating condition
Group 2	C2	Smaller than Normal	Clearance fitting on both rings, small load and no preload, little tolerance for endplay and operation by low temperature
Group N	CN	Normal	Low frictional torque, modearate loads and small preload, slight interference on one of rings depending on which is rotating, low and medium operational velocities, average temperature
Group 3	C3	Greater than Normal	Very low value of frictional torque, heavy loads, high interference, high temperatures and applied preload
Group 4	C4	Greater than C3	Same conditions as in C3
Group 5	C5	Greater than C4	Same conditions as in C3

- interference fit - bearing's seating on the shaft's journal causes the reduction of radial clearance beacuse of the pressure acting from the assembly on rings. The interference from shaft acts on the inner ring, while fitting in the housing has the effect on outer ring. Both of situations lead to the decrease of radial clearance based mostly on the geometry and material properies related to its elasticity.

- thermal effects - bearing's rings are usually made of bearing steel 100Cr6, which is characterizing with the linear expansion coefficient. Bearings are usually mounted at the room temperature, however during its rotation the heat is generated as a result of frictional forces on rolling surfaces. That leads to clearance reduction which can be calcuated with reference to the temperature difference of both rings or its difference in relation to the room temperature.

- pressing force - the effect of pressing force on the radial clearance reduction is usually applied in case of bigger interference. Then, the minimal values of axial forces for bearing's mounting can be estimated, taking into consideration frictional forces and geometry of assembly diameters.

Referring to conducted research, the effect of thermal expansion on the radial clearance reduction will be considered for different operating conditions. This will be conducted in the chapter referring to the experimental procedure, where it is going to be analyzed for various operating conditions.

METHODS APPLIED FOR DIAGONSIS OF ROLLING-ELEMENT BEARINGS

In this chapter, the overview of methods applied in the diagnostics of rolling-element bearings is presented. All discussed methods are based on the analysis of vibrational response of bearings. The general selection of discussed methods can be divided into signal processing, information fusion, statistical analysis and pattern recognition.

4.1   Introduction

Rolling-element bearings like all dynamical systems, characterize with a specific vibration profile showing its general performance related to its operational conditions, external conditions, and operational parameters. The methods applied for studying the vibration response are based on various approaches, which can be divided into four main root analyses, i.e. signal processing, information fusion, statistical analysis, and pattern recognition

(Figure 4.1) making them the basis of predictive maintenance and diagnostics [119]. Mentioned methods were mostly applied in the diagnostics of bearing's damages, but they can be applied as well in the diagnostics of frictional torque, misalignments, eccentricity (imbalance), or clearance.
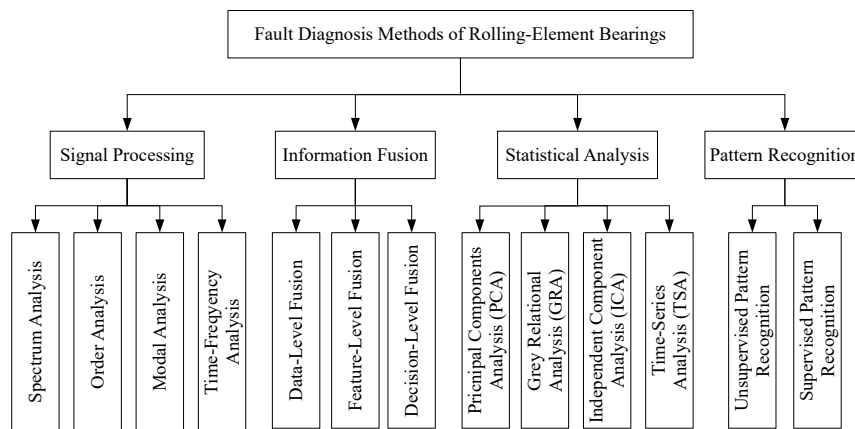
Figure 4.1. *Classification of fault diagnosis methods for rolling-element bearings*

Vibrational response of bearings is presented in form of impulses in the recorded time-series as numerous local discontinuities in contact of rolling surfaces. The accelerometer for registration of the vibrational response is mounted in most cases on the surface of the outer ring, so the vibrations induced by rotating elements are modulated by the transmission paths. Then, in its spectra, additional noise is present, which should be not considered for the analysis. This leads to the conclusion, that there is no universal method directly describing the defect or other bearing's feature without critical thinking of the applied method. In the following subsections, the calculation of characteristic frequencies in the rolling-element bearing will be presented and four mentioned diagnostics methods will be described in

relation to the condition-monitoring of rolling-element bearings describing its characteristics.

4.2   Characteristic frequencies of ball bearings

Referring to the design of rolling-element bearing (Figure 4.2) and taking into consideration a few assumptions of a constant velocity of both raceways, no special state such as slippage and constant pressure angle during operation, it is possible to determine the characteristic frequencies of bearing, which are related to the specific element (Equations 4.1-4.4) [101, 118]. The calculated frequencies provide the fundamental information on frequency analysis of ball bearings, which should next refer to obtained amplitude and detection of the potential defect.

FTF denotes Fundamental Train Frequency referring to the frequency of cage.

$$FTF = \frac{1}{2}F_s(1 - \frac{D}{d_m}\cos\alpha) \qquad (4.1)$$

BPFO denotes Ball Passing Frequency Outer referring to the frequency of outer ring.

$$BPFO = \frac{N}{2}F_s(1 - \frac{D}{d_m}\cos\alpha) \qquad (4.2)$$

BPFI denotes Ball Passing Frequency Inner referring to the frequency of outer ring.

$$BPFI = \frac{N}{2}F_s(1 + \frac{D}{d_m}\cos\alpha) \qquad (4.3)$$

BSF denotes Ball Spin Frequency referring to the frequency of rolling-element.

$$BSF = \frac{F_s d_m}{2D}(1 - \frac{D^2}{d_m^2}\cos^2\alpha) \qquad (4.4)$$

where: d_m is the pitch diameter, D is rolling-element diameter, F_s is the operational velocity, N is the number of rolling-elements, α is the contact angle.
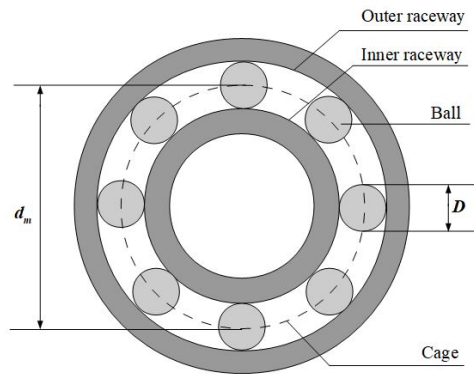
Figure 4.2. *Elements of rolling-element bearing considered in calculation of its characteristic frequencies*

The calculation of characteristical frequencies should be always the first step in the diagnostics of ball bearings, however, it doesn't provide the information of influence of other factors influencing the bearing's vibration.

4.3   Signal processing-based methods

Signal processing-based methods in the diagnostics or rolling-element bearings are the fundamental approach being extensively developed for a long time and its main advantage is fast computing on the raw time series. Some methods, like Fast Fourier Transform (FFT), have been even standardized as the accurate method in diagnostics of bearing failure. However, the experimental signal is strictly nonlinear characterizing with non-stationarity and the presence of numerous frequency components affecting the frequency spectra. The solution before coming to conclusions is it's preprocessing in

form of filtering, demodulation, or noise reduction. The specific feature extraction in signal processing-based methods can be obtained with frequency, order, modal or time-frequency analysis, what fundamentals will be presented in the following subsections.

4.3.1 Spectrum analysis

- Fast Fourier Transform - is the most popular frequency-based diagnostics method of mechanical systems giving the information about the frequencies dominating in the spectra [15]. The obtained time series is decomposed in sinusoidal signals with dominating frequency. The transition from the time domain into the frequency domain is shown in form of a spectrogram consisting of frequency peaks in the spectra with specific amplitude, which corresponds to the specific element of the analyzed mechanism.

For the discrete signals $x[N]$, the Fourier transform is described with following formula [113]:

$$X(k) = \sum_{n=0}^{N-1} x[n]e^{-j\left(\frac{2\pi nk}{N}\right)} \tag{4.5}$$

where: N is harmonic index referring to the exponential function for $k = 0, 1, ..., N-1$.

The scaling of the FFT spectra into frequency domain is calculated with the following equation:

$$f[k] = k\frac{f_p}{N} \tag{4.6}$$

where: f_p is sampling frequency.

- Envelope analysis - is one of the methods applied in the diagnostics of rolling-element bearings. In the calculation of the analytic envelope, the applied filter extracts the main harmonics from the frequency spectra for which the bandpass filter, rectifier, and smoothing circuit are applied. Then the envelope of the main harmonics is calculated, which can be analyzed. The obtained envelope signal is calculated in the following way [63]:

$$r(x) = \sum_p A_p e^{j2\pi(p-z)x} \tag{4.7}$$

where: p are frequency components passing through the low pass filter, A_p is the Fourier coefficient, z is resonant frequency, x is time-series.

- Hilbert-Huang Transform (HHT) - allow decomposing the experimental signal $x(t)$ into several intrinsic mode functions representing the average trend of the signal. Obtained IMFs with empirical mode decomposition, represent the input signal in specific frequency bands [64, 121]. The mathematical representation of HHT is following:

$$H(y(t)) = \frac{1}{\pi} PV(\int_{-\infty}^{+\infty} \frac{y(t)}{t-\tau} d\tau) \tag{4.8}$$

where: $PV(\int_{-\infty}^{+\infty})$ is the Cauchy principal value of the integral, τ.

4.3.2 Order analysis

- Power Spectrum (PS) - refers to the power distribution of the time series in the frequency domain. The influence of specific features in the bearing causes an increase in the amplitude of the power spectrum.

Power spectrum represents the time-varying time-domain signal into a set of the fixed-length vector representing the square magnitude of the harmonics [14, 115]. The mathematical representation of PS is following:

$$Px_i(e^{-j\omega}) = \frac{1}{KLU} \sum_{i=0}^{K-1} \sum_{n=0}^{L-1} W_n x_{n+iD} e^{-jn\omega} \tag{4.9}$$

where: W_i is applied window function of length $L-1$, K refers to the number of time-series segments x_n divided into with D points overlapping between two consecutive segments, U is the normalizing factor.

- Modulation Signal Bispectrum (MSB) - another order-based method is the modulation signal bispectrum (MSB), which advantage is the effective reveal of modulation characteristics and detection of interference components of a signal with modulation characteristics buried in strong noise [56, 57, 127]. The MSB for discrete-time series can be represented in the following way:

$$B_{MS}(f_1, f_2 = E < X(f_1 + f_2)X(f_1 - f_2)X(f_1) >) \tag{4.10}$$

where: $B_{MS}(f_1, f_2)$ is the bispectrum of discrete signal, E indicates expectation operator, f_1 is carrier frequency, f_2 is modulating frequency, $(f_1 + f_2)$ and $(f_1 - f_2)$ are the higher and lower sideband frequencies.

4.3.3 Modal analysis

Modal analysis is a process of extracting modal features, i.e. natural frequencies, damping loss factors, modal constants from vibration data. The modal analysis can be divided into frequency domain analysis from frequency response functions or time-domain analysis from impulse responses.

The dynamics of a system are physically decomposed by frequency and position providing the analytical solution in form of partial differential equations. The analyzed vibration response of the mechanical system can be expressed in form of a set of simple harmonic motions called natural modes of vibration. Referring to the modal analysis to study of ball bearings' vibrational response, it can be useful both in the identification of damages and influence of other features buried in the spectra [41, 55, 84].

4.3.4 Time-Frequency analysis

- Short-Time Fourier Transform (STFT) - the STFT is similar to the Fourier Transform, but it provides extended information, what is the influence of specific frequency in the time domain. As the method is "short-time", the experimental signal is divided into segments according to the applied window, next the standard Fourier Transform is calculated [21, 134]. The STFT can be defined with weighting function and window function $h(t)$, for which, the mathematical formula is following:

$$STFTx(t)(t, \omega) = \int_{-\infty}^{+\infty} x(t)h(t - \tau)e^{-j\omega t}dt \qquad (4.11)$$

where: $h(t - \tau)$ is applied window function, $e^{-j\omega t}$ is weighting function, τ is time shift.

- Spectral Kurtosis (SK) - the approach is similar to the STFT algorithm and provides the measure of the impulsiveness of the time series in form of frequency function. The advantage of SK is its usefulness in the detection of transient states in short-time series, by analyzing their characteristic frequencies in the specific frequency band. The signal is decomposed with the power of a signal with respect to frequency,

except that fourth-order statistics are used instead of second-order [83, 114]. The mathematical formula for this is following:

$$K(f) = \frac{< H^4(t,f) >}{< H^2(t,f) >} - 2 \qquad (4.12)$$

where: $H(t, f)$ is time/frequency envelope of the time-series.

4.4 Information fusion-based methods

Information fusion-based methods are related to the data combination obtained with the sensor-fusion approach having the information from few sources. Based on this approach, data-level fusion and feature-level fusion can be selected, the third final level is the decision-level related to the classification of processed data to the phenomena. The idea of information fusion is focused on the reduction of the dimension of experimental data into principal vectors. Then, making computations on compressed data set, the complementary and redundant information is utilized. That the data fusion approach is a very broad field of science, each level will be briefly described according to the review paper of Castanedo [26].

Classification of Information Fusion methods

- Classification based on the relations between the data sources - the classification consists of three following criteria:

  1. Complementary, when the infromation provided by the input sources represents different parts of the scene and could thus be used to obtain more complete global information.

  2. Redundant, when two or more input sources provide information about the same target and could thus be fused to increment the confi-

dence.

3. Cooperative, when the provided information is combined into new information that is typically more complex than the original information.

- Dasarathy's Classification - this classification is composed of five categories [150]

1. Data in-data out - this type of data fusion process inputs and outputs raw data. The results are typically more reliable or accurate. Data fusion at this level is conducted immediately after the data are collected from sensors.

2. Data in-feature out - at this next step, the data fusion process employs raw data from the sources to extract features or characteristics that describe an entity in the environment.

3. Feature in-feature out - both the input and output of the data fusion process are features. Thus, the data fusion process addresses a set of features with to improve, refine or obtain new features.

4. Feature in-decision out - obtains a set of features as input and provides a set of decisions as output.

5. Decision in-decision out - it fuses input decisions to obtain better or new decisions.

- Classification based on the abstraction levels - this classification consists of four abstraction levels [92]

1. Signal level: directly addresses the signals that are acquired from the sensors.

2. Pixel level: operates at the image level and could be used to improve image processing tasks.

3. Characteristic: employs features that are extracted from the images

or signals.

4. Symbol: the decision level, then the information is represented as symbols.

- JDL data fusion classification - consists of five following data processing levels:

1. Level 0 - source preprocessing and information extraction process. This level reduces the amount of data and maintains useful information for the high-level processes.

2. Level 1 - object refinement, the procedures at this level include spatio-temporal alignment, association, correlation, clustering or grouping techniques, state estimation, the removal of false positives, identity fusion. The data is formed into consistent data structures.

3. Level 2 - situation assessment, it aims to identify the likely situations given the observed events and obtained data and relationships between objects are established.

4. Level 3 - impact assessment, the impact of activities is evaluated to obtain a proper perspective. The current situation is evaluated, and a future projection is performed to identify possible risks, vulnerabilities, and operational opportunities.

5. Level 4 - process refinement, the aim of the last level is to achieve efficient resource management while accounting for task priorities, scheduling, and control of available resources.

- Classification based on the type of architecture - referring to the final application of data fusion, four architecture can be distinguished:

1. Centralized architecture - in a centralized architecture, the fusion node resides in the central processor that receives the information from all of the input sources. Therefore, all of the fusion processes

are executed in a central processor that uses the provided raw measurements from the sources.

2. Decentralized architecture - a decentralized architecture is composed of a network of nodes in which each node has its own processing capabilities and there is no single point of data fusion. Therefore, each node fuses its local information with the information that is received from its peers. Data fusion is performed autonomously, with each node accounting for its local information and the information received from its peers.

3. Distributed architecture - in a distributed architecture, measurements from each source node are processed independently before the information is sent to the fusion node; the fusion node accounts for the information that is received from the other nodes. In other words, the data association and state estimation are performed in the source node before the information is communicated to the fusion node. This type of architecture provides different options and variations that range from only one fusion node to several intermediate fusion nodes.

4. Hierarchical architecture - other architectures comprise a combination of decentralized and distributed nodes, generating hierarchical schemes in which the data fusion process is performed at different levels in the hierarchy.

Data-Level fusion

- Nearest Neighbors and K-Means - Nearest neighbor [126] is the simplest data association technique. NN is a well-known clustering algorithm that selects or groups the most similar values. How close the one measurement is to another depends on the employed distance metric and typically depends on the threshold that is established by

the designer. K-Means method is a well-known modification of the NN algorithm. K-Means divides the dataset values into K different clusters. K-Means algorithm [122] finds the best localization of the cluster centroids, where best means a centroid that is in the center of the data cluster.

- Probabilistic Data Association - the algorithm is also known as the modified filter of all neighbors. This algorithm assigns an association probability to each hypothesis from a valid measurement of a target. A valid measurement refers to the observation that falls in the validation gate of the target at that time instant.

- Joint Probabilistic Data Association - Joint probabilistic data association [43] is a suboptimal approach for tracking multiple targets in cluttered environments.

- Multiple Hypothesis Test - the method was developed to track multiple targets in cluttered environments [104]. As a result, it combines the data association problem and tracking into a unified framework, becoming an estimation technique as well. The test considers all of the possibilities, including both the track maintenance and the initialization and removal of tracks in an integrated framework. Moreover, it calculates the possibility of having an object after the generation of a set of measurements using an exhaustive approach, and the algorithm does not assume a fixed number of targets.

- Graphical Models - Graphical models [29] are a formalism for representing and reasoning with probabilities and independence. A graphical model represents a conditional decomposition of the joint probability. A graphical model can be represented as a graph in which the

nodes denote random variables; the edges denote the possible dependence between the random variables, and the plates denote the replication of a substructure, with the appropriate indexing of the relevant variables. The graph captures the joint distribution over the random variables, which can be decomposed into a product of factors that each depend on only a subset of variables.

Feature-Level fusion

- Maximum Likelihood and Maximum Posterior - the maximum likelihood technique is an estimation method [107] that is based on probabilistic theory. This function expresses the probability of the observed data. The maximum posterior (MAP) method is based on the Bayesian theory. It is employed when the parameter x to be estimated is the output of a random variable that has a known probability density function $p(x)$. Both methods (ML and MAP) aim to find the most likely value for the state x. However, ML assumes that x is a fixed but an unknown point from the parameter space, whereas MAP considers x to be the output of a random variable with a known a priori probability density function.

- Kalman Filter - the Kalman filter is mainly employed to fuse low-level data. If the system could be described as a linear model and the error could be modeled as the Gaussian noise, then the recursive Kalman filter obtains optimal statistical estimations.

- Particle Filter - particle filters [33] are recursive implementations of the sequential Monte Carlo methods. This method builds the posterior density function using several random samples called particles. Particles are propagated over time with a combination of sampling and

resampling steps. At each iteration, the sampling step is employed to discard some particles, increasing the relevance of regions with a higher posterior probability. In the filtering process, several particles of the same state variable are employed, and each particle has an associated weight that indicates the quality of the particle.

- Covariance Consistency - this method [132] is general and fault-tolerant frameworks for maintaining covariance means and estimations in a distributed network. These methods do not comprise estimation techniques, instead, they are similar to an estimation fusion technique.

Decision-Level fusion

- Bayesian Methods - information fusion based on the Bayesian inference [67] provides a formalism for combining evidence according to the probability theory rules.

- Dempster-Shafer Interference - the Dempster-Shafer theory [37, 116] provides a formalism that could be used to represent incomplete knowledge, updating beliefs, and a combination of evidence and allows us to represent the uncertainty explicitly.

- Abductive Reasoning - abductive reasoning [117], or inferring the best explanation, is a reasoning method in which a hypothesis is chosen under the assumption that in case it is true, it explains the observed event most accurately. In other words, when an event is observed, the abduction method attempts to find the best explanation.

- Semantic Methods - Semantic information fusion [144] is essentially a scheme in which raw sensor data are processed such that the nodes exchange only the resultant semantic information. Semantic informa-

tion fusion typically covers two phases: (1) building the knowledge and (2) pattern matching (inference). The first phase (typically offline) incorporates the most appropriate knowledge into semantic information. Then, the second phase (typically online or in real-time) fuses relevant attributes and provides a semantic interpretation of the sensor data.

4.5 Statistical analysis-based methods

The statistical analysis of experimental time-series is a very wide range and there are numerous indicators, which refer to the dynamical state of rolling-element bearing. There are two approaches in the statistical-based analysis, i.e. univariate - the analysis is based on the evaluation of one indicator, multivariate - the analysis is based on the correlation estimation between two or more of them [31]. The decision of choosing the particular approach is usually made by the number of random samples and the accuracy of studied features. In the following subsections, the discussion will be started with the presentation of the univariate approach with the definition of indicators and next the multivariate approach will be presented.

4.5.1 Time-Series Analysis

There are number of time-series features referring to the specific dynamical state of bearings and other rotational mechanisms. The discussion and definition of each of them will be conducted on following works [70,82,94, 112].

1. Time-domain feature extraction:

- Root Mean Square (RMS) - is the square root of the average of the sum of the squares of the signal:

$$RMS_x = \sqrt{\frac{1}{N}[\sum_{i=1}^{N}(x_i)^2]} \qquad (4.13)$$

where: N is number of samples in the signal x.

- Crest Factor (CF) - is the maximum positive peak value of the signal divided by its RMS:

$$CF = \frac{x_{0-pk}}{RMS} \qquad (4.14)$$

where: pk is is the index for the maximum positive peak of the signal and x_{0-pk} is the value of x at pk.

- Energy Ratio (ER) - refers to the condition of the system and is the ratio of RMS of of the difference signal d to the RMS of signal containing regular meshing components y_d:

$$ER = \frac{RMS_d}{RMS_{y_d}} \qquad (4.15)$$

- FM0 - is the indicator signalizing the faults. It is a ratio of the maximum peak-to-peak amplitude to the sum of amplitudes:

$$FM0 = \frac{PP_x}{\sum_{n=0}^{H} P_n} \qquad (4.16)$$

where: PP_x is the maximum peak-to-peak amplitude, P_n is the amplitude of the nth harmonic, H is the total number of harmonics in the frequency range.

- Kurtosis - is the fourth normalized moment of the studied signal and gives the information on the number of amplitudes in the spectra:

$$Kurtosis = \frac{N \sum_{i=1}^{N} (x_i - \bar{x})^4}{[\sum_{i=1}^{N} (x_i - \bar{x})^2]^2} \tag{4.17}$$

- FM4 - refers to the detection of initial faults:

$$FM4 = \frac{N \sum_{i=1}^{N} (d_i - \bar{d})^4}{[\sum_{i=1}^{N} (d_i - \bar{d})^2]^2} \tag{4.18}$$

where: $\bar{d}$ is the mean of the difference signal, N is the total number of data points.

- NA4 - refers to the diagnostics of propagation of faults or specific state:

$$NA4 = \frac{N \sum_{i=1}^{N} (r_{iM} - \bar{r}_M)^4}{\frac{1}{M} \sum_{j=1}^{M} [\sum_{j=1}^{N} (r_{ij}) - \bar{r}_j)^2]^2} \tag{4.19}$$

where: $\bar{r}$ is the mean of the residual signal, N is the total number of data points, M is the number of current time-series, j is the index of the time signal in the run ensemble.

- M6A - this indicator is applied in surface degradation:

$$M6A = \frac{N^2 \sum_{i=1}^{N} (d_i - \bar{d})^6}{[\sum_{i=1}^{N} (d_i - \bar{d})^2]^3} \tag{4.20}$$

- M8A - the more sensitive indicator than M4A and M8A usually applied in the diagnostics of buried states in the spectra:

$$M6A = \frac{N^3 \sum_{i=1}^{N}(d_i - \overline{d})^8}{[\sum_{i=1}^{N}(d_i - \overline{d})^2]^4} \qquad (4.21)$$

- NB4 - indicator refering to the diagnostics of transient states caused by damage:

$$NB4 = \frac{\frac{1}{N}\sum_{i=1}^{N}(s_i - \overline{s}_i)^4}{(\frac{1}{N}\sum_{j=1}^{N}(\frac{1}{n}\sum_{k=1}^{n}(s_{jk} - \overline{s}_j)^2))^2} \qquad (4.22)$$

where: s is the signal's envelope, s_{jk} is the kth measurement in the jth time record envelope.

2. Frequency-domain feature extraction:

- Mean Frequency (MF) - indicates the vibration energy in the frequency domain:

$$MF = \frac{1}{K}\sum_{k=1}^{K}X_k \qquad (4.23)$$

where: X_k is the kth measurement of the frequency spectrum of signal, K is the total number of spectrum lines.

- Frequency Center (FC) - shows the position changes of the main frequencies:

$$FC = \frac{\sum_{k=1}^{K}f_k X_k}{\sum_{k=1}^{K}X_k} \qquad (4.24)$$

where: f_k is the frequency value of the kth spectrum line and X_k is the kth measurement of the frequency spectrum.

- Root Mean Square Frequency (RMSF) - calculates RMS of FC indicator:

$$RMSF = \sqrt{\frac{\sum_{k=1}^{K} f_k^2 X_k}{\sum_{k=1}^{K} X_k}} \tag{4.25}$$

- Standard Deviation Frequency (STDF) - describes the convergence level of the spectrum power:

$$RMSF = \sqrt{\frac{\sum_{k=1}^{K} (f_k - FC)^2 X_k}{\sum_{k=1}^{K} X_k}} \tag{4.26}$$

3. Recurrence quantificators:

- Determinism (DET) - refers to the periodicity of the response, demonstrates by diagonal lines of different lengths. Determinism expresses the ratio of the number of recurrence points forming the diagonal line to the overall number of recurrence points creating the 0-1 matrix:

$$DET = \frac{\sum_{l=l_{min}}^{N} lP(l)}{\sum_{l=1}^{N} lP(l)} \tag{4.27}$$

where: $P(l)$ is the historgram of the diagonal line, N is vector length of a data series, l_{min} is predefined minimal length of a diagonal line.

- Average line length of the diagonal lines (L) - mentions the average time that two segments of the phase space trajectory are close to each other, and can be interpreted as the mean prediction time [13]:

$$L = \frac{\sum_{l=l_{min}}^{N} lP(l)}{\sum_{l=min}^{N} lP(l)} \tag{4.28}$$

- Length of the longest diagonal line (L_{max}) - is related to the exponential divergence of the phase space trajectory. The faster the trajectory segments diverge, the shorter are the diagonal lines and the higher is the divergence *DIV* (inversion of L_{max}):

$$L_{max} = max(l_{i=1}^{N_l})$$ (4.29)

where: $N_l = \sum_{l \geq l_{min}} P(l)$ corresponds to the total number of diagonal lines in the matrix.

- Entropy (*ENTR*) - the last of the diagonal-based quantificators calculates the complexity of the recurrence plot in reference to the diagonal lines, the lower complexity of the signal, the lower value of the entropy:

$$ENTR = -\sum_{l=l_{min}}^{N} p(l)lnp(l)$$ (4.30)

where: $p(l)$ is the probability of finding a line of with exactly l length.

- Laminarity (*LAM*) - refers to the occurrence of laminar states in the system without describing the length of the laminar phases. The value of laminarity is lower if the recurrence plot consists of more single, isolated points than vertical structures. In the mathematical notation, the laminarity is similar to the determinism denoting the ratio between the recurrence points creating the vertical structures and the entire set of recurrence points:

$$LAM = \frac{\sum_{v=v_{min}}^{N} vP(v)}{\sum_{v=1}^{N} vP(v)}$$ (4.31)

where: $P(v)$ is the historgram of the vertical line, N is vector length of a data series, v_{min} is predefined minimal length of a diagonal line.

- Trapping Time (TT) - defines the mean time that the system will be at a specific state or how long this state will be trapped. In the mathematical notation, this quantificator takes into account the minimal length of the vertical line:

$$TT = \frac{\sum_{v=v_{min}}^{N} v P(v)}{\sum_{v=v_{min}}^{N} P(v)} \tag{4.32}$$

- Maximal length of the vertical lines (V_{max}) – refers to the exponential divergence of the phase space trajectory, the same as in the case of Lmax. The only difference is that it is based on vertical lines:

$$V_{max} = max(v_{i=1}^{N_v}) \tag{4.33}$$

where: N_v is the absolute number of vertical lines.

- Recurrence Time of the 1st type (T^1) - allows to detect weak transitions of the system's dynamics, the quantificator is based on the distribution and analysis of recurrence points [22, 47, 48]:

$$T^1 \sim \varepsilon^{-D_p(i)} \tag{4.34}$$

where: D_p is point-wise dimension.

- Recurrence Time of the 2nd type (T^2) - allows to detect transient states in the signals characterized with low energy, the quantificator is based on the analysis of the average of lengths of white vertical lines [22, 47, 48]:

$$T^2 \sim \varepsilon^{-D_1(i)} \tag{4.35}$$

where: D_1 is information dimension.

- Recurrence Period Density Entropy (*RPDE*) - this quantificator refers to the extent of recurrences [89, 95, 105]. For the dynamical systems it has the following mathematical notation:

$$RPDE = -\sum_{i}^{T_{max}} P(i) ln P(i) \tag{4.36}$$

where: $P(i)$ is recurrence probability density, T_{max} is maximum recurrence time found in the embedded state space.

- Clustering (*CLS*) - represents the probability that two recurrences of any state are also neighbors. It is obtained as the average of the local clustering coefficients and refers to the characteristic of recurrence plot based on the low degree nodes [39, 105].

$$CLS = \frac{\sum_{i,j=1}^{N} R_{v,i} R_{i,j} R_{j,v}}{k_v(k_v - 1)} \tag{4.37}$$

where: k_v is degree of centrality.

- Transitivity (*TRANS*) - allows detecting the periodic and chaotic response of the system [95]. The quantificator refers to the characteristic of recurrence plot based on the high degree nodes [105].

$$TRANS = \frac{\sum_{i,j,k=1}^{N} R_{j,k} R_{i,j} R_{i,k}}{\sum_{i,j,k=1}^{N} R_{i,j} R_{i,k}(1 - \delta_{j,k})} \tag{4.38}$$

where: $\delta_{j,k}$ is main diagonal equal to zero.

That the recurrence analysis is the main method applied to the conducted analysis, its the most important steps will be described briefly. The details on full recurrence analysis for exemplary experimental acceleration time-series, i.e recurrence plots (RPs) method and recurrence quantification analysis (RQA) will be presented in Chapter 7. This chapter discusses basics of applied signal processing and analysis for experimental data.
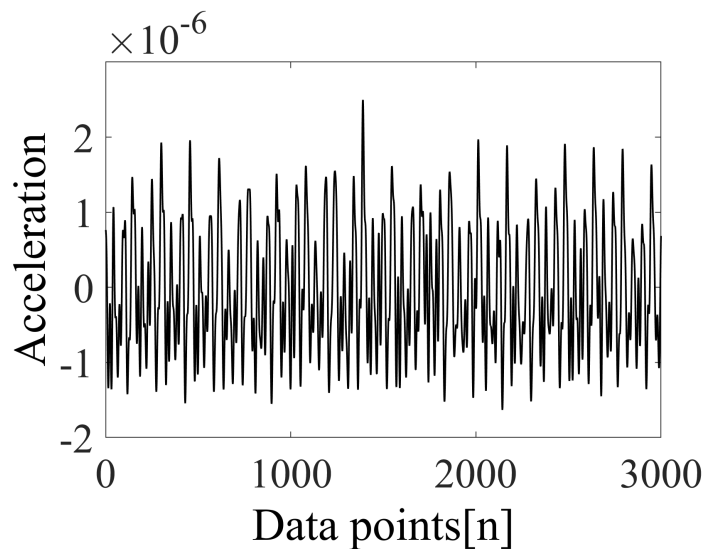
Figure 4.3. *Exemplary acceleration short-time series.*

The analysis starts with the partition of the long acceleration time-series into shorter consisting of 3000 data points (Figure 4.3). The studied signal is firstly normalized to compare it between cases and next is filtered to get rid of not necessary frequencies in the spectra. The frequency spectra of the signal is presented in Figure 4.4 after Fast Fourier Transform calculation. Next step is the determination of parameters for the phase-space reconstruction, i.e. embedding dimension, time delay and threshold. After the determination of mentioned parameters, it is possible to draw the recurrence plot (Figure 4.5) for the considered time-series. That, the interpretation of the recurrence map is sometimes hard, its quantification is needed.

In Table 4.1., the recurrence quantificators for obtained recurrence plot are presented, they correspond to the description of the dynamical properties of studied system. The continuation of the analysis will be conducted in Chapter 7, referring to the entire experiement.
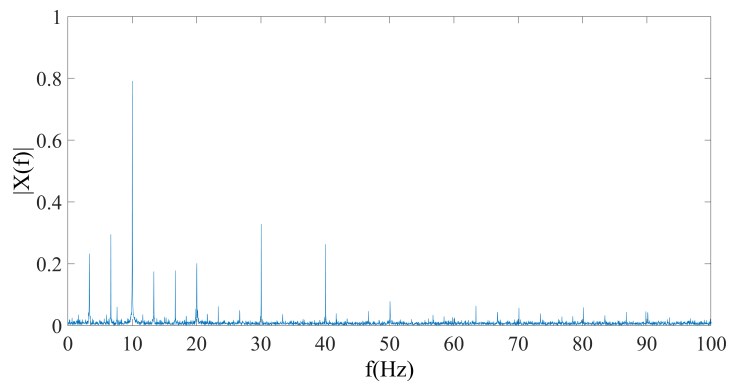
Figure 4.4. *Exemplary acceleration short-time series.*
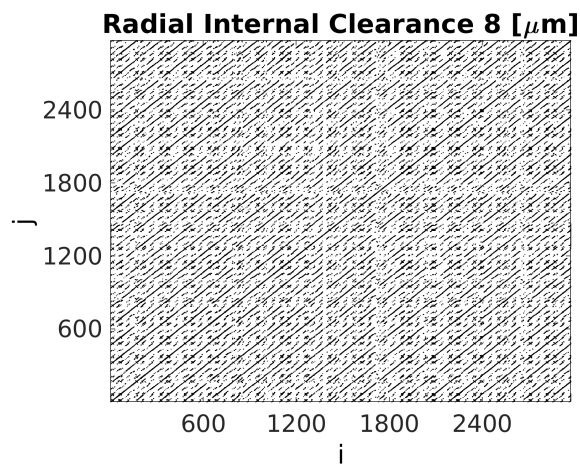
Figure 4.5. *Recurrence plot for analysed time-series.*

Table 4.1. *Values of recurrence quantificators calculated for one short-time series.*

Recurrence Quantificator	Value
DET	0.9120
L	5.725
L_{max}	2983
ENTR	0.281
LAM	0.9484
TT	4.0845
V_{max}	24
$T^{(1)}$	20.1351
$T^{(2)}$	70.9559
RPDE	0.6292
CLS	0.5726
TRANS	0.5521

4.5.2   Principal Components Analysis

Principal Component Analysis is the fundamental of multivariate data analysis based on graphical methods. The analyzed big data is compounded into a smaller set of variables called indices, by which it is possible to observe final dependencies between features in form trends, jumps, clusters or outliers [11, 143]. PCA as the method allows analyzing datasets containing multicollinearity, missing data, imprecise measures, or categorical data. As the final result, the summary indices "Principal Components" are obtained showing the information of studied datasets. By statistical meaning, the PCS finds lines, planes in the n-dimensional space that adjust the data as well as possible in a least-squares manner. Approximated main line or plane of datasets makes the variance of the coordinates on the line or plane

as large as possible [72]. The PCA method has been already applied for studying the damages of rolling-element bearings [58, 103].

4.5.3   Grey Relational Analysis

The Grey Relational Analysis is another multivariate data method referring to the systems which lack information, treated as "Grey Systems" dealing with poor, incomplete, or uncertain information [46]. The method is based on the grey system theory that is used for studying complex interrelationships between multiple performance features allowing to estimate the behavior of an uncertainty system or problem of stochastic data. Following the idea of the method, there are 3 types of systems, i.e. black (no information), white (all information), and grey (imperfect information) by which the correct properties of systems are discovered under poorly-informed situations. Then, the Grey System seeks for only the intrinsic structure of the system given such as limited data [65]. In the GRA, the following characteristic steps can be distinguished [152].

- Definition of problem, response variables or quality characteristics,

- Data collection,

- Data normalization for smaller or bigger datasets for better quality characteristics,

- Finding of grey relation coefficient for normalized data,

- Calculation of grey relation grade,

- Selection of optimum level based on grade value.

The GRA founded its application as in the diagnostics of bearing's faults [85] and analysis of friction torque [145].

4.5.4 Independent Component Analysis

Another multivariate data analysis is the Independent Component Analysis (ICA), by which the generative model is derived for a large dataset. In the obtained mode, the studied features are presumed to be linear mixtures of unknown latent variables with unknown mixing systems [23]. The hidden features are assumed nongaussian and relatively independent, that is why they are called independent components. ICA is particularly useful, when standard methods such as PCA fail, and can be used for mixed data, e.g. speech signals obtained with different microphones, acceleration signals of the rotating system obtained from different sensors, interfering radio signals received at a mobile phone [66]. The ICA has been applied to study the fault detection in the rolling-element bearings [42].

4.6 Pattern recognition-based methods

The general division of pattern recognition-based methods is unsupervised (when classification rule is unknown)and supervised (when the classification rule is known beforehand) [53]. Regarding unsupervised methods, only similarities and discrepancies between features are considered without predefined information on them. On the other hand, in supervised methods, the information on classes is predefined and the rule or characteristic used for features grouping is known. In the following subsections, the main unsupervised and supervised pattern recognition methods are presented.

4.6.1 Unsupervised pattern recognition

- Cluster Analysis - according to this method, the analyzed features are classified into the same cluster based on the level of similarity between them. It is used for the development of the new classification of

features and as well as for confirmation of already existing grouping. The Cluster Analysis was applied to the analysis of bearing's dynamics and classification obtained features referring to the damages [80],

- Artificial Neural Networks - this method is particularly useful for overcoming the difficulty encountered during the classification process. The procedure of ANN starts with a data-training set based on different samples with predefined properties (concentration level or spectra) calculating the probability of the dataset to be assigned to the specific class. The application of Neural Networks in the diagnostics of rolling-element bearings, which results can be found in following papers [27, 36, 74],

- Methods based on factor models - the aim of the factor models approach is to reduce the n-dimensional information on features into a more representative dimension. The reduced dataset can be analyzed in two following ways, multi-set - data tables are handled simultaneously in common and an irregular structure or meaning, multi-way - 2D data tables with several modes in common, and a cube or hypercube structure are considered.

4.6.2 Supervised pattern recognition

- Parametric/Non-parametric - referring to the parametric approach, it utilizes the mathematical models that have adjustable parameters to conduct the features classification, while the non-parametric approach is not using any model to carry on the classification,

- Discriminant/Class-modelling - the discriminant techniques place features in one hyperspace class and there is no other placement of it in

another one. Referring to class modelling, samples fitting are considered to be a part of the class, but those of them, which don't fit are rejected,

- Deterministic/Probabilistic - like in the name of techniques, the deterministic way relies on the class assignments to each sample without the statement of the reliability of the decision. While probabilistic methods estimate mentioned classification reliability for class assignments.

MATHEMATICAL MODEL OF A SELF-ALIGNING BALL BEARING

In order to have the mathematical description and refer it to the planned experiment, the 2-DOF mathematical model of double-row self-aligning ball bearing (SABB) was derived. The model in the majority reflects the design and operation of bearing design for SABB NTN 2309K studied in the experiment. The simulation with the derived model allows adjusting the radial internal clearance in a wide range as in the real bearing. To implement the influence of RIC on the dynamical response of bearing, the Hertzian contact theory was implemented.

5.1   Introduction

A mathematical model is the process of encoding and decoding reality, in which a real phenomenon is presented in formal numerical description by a casual structure [30, 140]. Derived mathematical model allow for the im-

plementation of various operating conditions and various design (e.g. shape errors) in rolling-element bearing providing satisfying results without the need of conducting physical tests on the dedicated test rig. Then, the obtained dynamical response in form of time-series can be processed as usual experimental signal providing comparable results. Another advantage of the mathematical model is the understanding of how specific nonlinear effects influence the bearing's dynamics. Among the nonlinear factors, the following can be distinguished, which will be applied in the mathematical model:

- Variable stiffness in time, related to Hertzian contact theory [51, 90],

- Shape errors [73, 110],

- Radial internal clearance [157],

- Subjected external forces [137],

- Eccentricity [159],

- Thermal effects [49, 50].

Above mentioned nonlinear effects are the main sources of nonlinearities in the operation of rolling-element bearing and that is why they will be applied in the studied mathematical model. In the following subsections, its meaning and mathematical formulation will be described.

5.2 Description of the 2-DOF Mathematical Model of the Rolling Element Bearing

In Figure 5.1, the rolling-element bearing model is presented in form of the nonlinear spring-damper oscillator with the rotating shaft and inner ring

handled as one mass (rotor-bearing system) driven by a constant angular velocity ω_s and fixed outer ring. The proposed 2-DOF mathematical model realizes the operation of the deep groove ball bearings (DGBB) in x-y plane. In order to provide a realistic dynamic response of ball bearing, the following assumptions and considerations have been taken into account:

- rolling-elements are aligned equidistantly around the shaft and there is no relative interactions between them,

- the study is performed under isothermal conditions, the reduced clerance due to thermal effect is studied in the experiment and can be applied to the specific case in the model,

- the inner ring and shaft are treated as one mass and they are rotational part,

- the external forces can be subjected to the model, however they are small as in the experimental part,

- the interactions between rolling-elements and raceways are described according to the Hertzian contact theory,

- damping due to lubrication is neglected, however the damping factor is variable in radial clearance domain and rotational velocity,

- effect of shape-error is studied with relatively realistic parameters of waviness of the bearing's raceways,

- gyroscopic effect and rolling-element slipping are not studied rotational velocities are much smaller than the limiting speed of the bearing,

- analysis of friction torque is neglected, that there are no fluctuations in the rotational velocity during simulation.

In the model, as it was mentioned, rotational elements are distributed equidistantly over circumference with the constant angle ψ_i, that the angular position of $i - th$ ball is calculated from the vertical axis according to the following formula:

$$\psi_i = \psi_0 + \int_0^t \omega_c(t) \, dt \tag{5.1}$$

$$\psi_o = \frac{2\pi(i - 1)}{n} \tag{5.2}$$

where: ψ_0 is the angular position of the first ball, i is the angular position of the ball (i=0,1,...,n-1), n is the number of rolling elements, ω_c is the rotational velocity of the cage.

The value of the rotational velocity of the cage ω_c is determined by the internal geometry of the ball bearing and subjected velocity to the shaft. It is worth notice, that the cage's velocity is the same as the velocity of rolling-elements held by cage assuming no slipping effect of them.

$$\omega_c = \frac{\omega_s}{2}(1 - \frac{D\cos(\alpha_0)}{d_p}) \tag{5.3}$$

where: D is the ball diameter, d_p is the pitch diameter, α_0 is the pressure angle.

5.3 Hertzian Contact Theory and Radial Internal Clearance

Hertzian contact theory refers to the interactions between rolling surfaces, i.e. rolling elements and raceways in rolling-element bearings, that changes
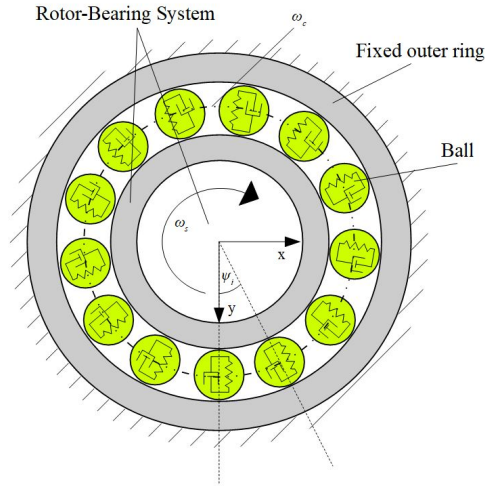
Figure 5.1. *Mathematical model of the rolling-element bearing. The inner ring with shaft are treated as one rotating mass of the bearing (Rotor-Bearing System)*

in contact have a relevant influence on the dynamics. The load distribution on the raceways depends mostly on subjected external forces, but the influence of shape errors and rotor-bearing system's eccentricity shouldn't be neglected. The acting loads form two kinds of contact, i.e. elliptical in the loaded area and the point contact in the unloaded area. It is worth notice, that defects are as well introduced in the mathematical model in form of variable contact [34, 100]. Referring to the variable contact between rolling surfaces, also the effect of radial internal clearance must be considered. The term referring to the clearance is applied in the equation calculating nonlinear load deformations according to the Hertzian theory.

The elastic contact deformation δ_i is calculated for i^{th} ball in its actual angular position ψ_i. The deformations are calculated according to the following formula including the effect of radial clearance *RIC* and shape errors:

$$\delta_i = \delta_{xs}sin(\psi_i) + \delta_{ys}cos(\psi_i) - RICcos(\alpha_0) - (U_{inner})_i - (U_{outer})_i \quad (5.4)$$

where: δ_{xs}, δ_{ys} are relative displacement between inner and outer ring in the x - horizontal and y - vertical directions, RIC - value of radial internal clearance, $(U_{inner})_i$,$(U_{outer})_i$ - shape errors on inner and outer raceway respectively. Effect of clearance and shape errors on the bearing's dynamics and its mathematical formulation will be discussed in the following sections.

After the determination of elastic deformation, the acting Hertzian contact forces [79,158] can be calculated accroding to the following mathematical notation:

$$K_x = k_b \sum_{i=1}^{n} H(\delta_i)\delta_i^{\gamma-1}sin(\psi_i) \quad (5.5)$$

$$K_y = k_b \sum_{i=1}^{n} H(\delta_i)\delta_i^{\gamma-1}cos(\psi_i) \quad (5.6)$$

where: k_b is the stiffness of ball, γ is the contact coefficient (for the point contact in ball bearing γ=3/2, for the linear contact in ball bearing γ=10/9) [81], $H()$ is the Heaviside function referring to the instantaneous contact.

The value of Heaviside function refers to the contact between rolling surfaces and its mathematical notation is following:

$$0 \text{ for } x < 0 \text{ - no contact}$$
$$1 \text{ for } x \geq 0 \text{ - in contact}$$

The novelty introduced into the mathematical model of SABB is based on the design of the bearing and separated cage. Into the calculation of

deformations, the clearance in one row is smaller about 10% than in the second row, due to the axial pre-load subjected to the bearing's face. This action slightly influences the dynamical output but reflects the real situation in the assembly.

5.4   Shape Errors on Rolling Surfaces

As the effect of the manufacturing process and normal operation of rolling-element bearings, the shape errors (waviness, roughness) appear on the rolling surfaces in form of smaller and bigger undulations over the bearing's circumference. Rolling elements over rolling over the imperfect surface lead to the appearance in the frequency spectra of additional frequency peaks usually with small amplitude. The value of the peak's amplitude related to the shape error depends on the number of undulations and the amplitude of imperfection [12]. In Figure 5.2, the graphical representation of the waviness profile studied in the mathematical model is presented considering the undulations on the inner and outer ring. The waviness of rolling elements is not studied, that they have neglectable shape errors due to the more demanding manufacturing process and low amplitudes of imperfections. The shape errors have usually a small impact on the bearing's dynamics, but they should be considered as the real source of vibrations. In the real operation of ball bearings, the amplitude of undulations is increasing due to the tribological effect leading to the bearing damage. The term referring shape errors is applied in the definition of Hertzian contact and has the following mathematical notation:

$$(U_{inner})_i = U_{inner} sin(N_{inner} \psi_0) \qquad (5.7)$$

$$(U_{outer})_i = U_{outer} sin(N_{outer} \psi_0) \tag{5.8}$$

where: $U_{inner/outer}$ is the amplitude of inner/outer raceway surface waviness, $N_{inner/outer}$ is the number of undulations on the inner/outer raceway
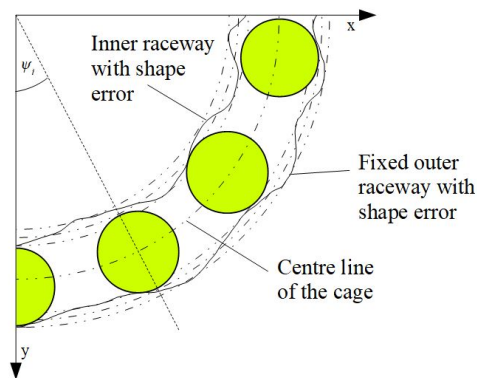
Figure 5.2. *Shape error on rolling surfaces of inner and outer ring*

5.5   Subjected External Forces

In the proposed mathematical model, the effect of subjected external forces is considered. In ball bearings, the radial forces are acting on it, and its critical value during operation is defined by the dynamic load capacity. Following the planned experiment, minor values of forces will be applied to the bearing, that the radial load can disturb the reduced clearance after the measurement. The term referring to external forces will be mentioned in the section referring to the equations of motion.

5.6 Eccentricity

Another factor referring to the nonlinearity is the eccentricity of the system consisting of inner ring and shaft treated as one mass (Rotor-Bearing System) [138, 155]. Shaft's eccentricity is caused by two main factors, i.e. improper manufacturing (irregular mass distribution) or improper coupling with the motor, however, both factors have an impact on bearing's dynamics. In Figure 5.3, the effect of eccentricity on the rotor-bearing system is visualized. The occurrence of centrifugal force F_g is caused by the shifted center of gravity due to factors as eccentricity, gravitational acceleration, and deformations.
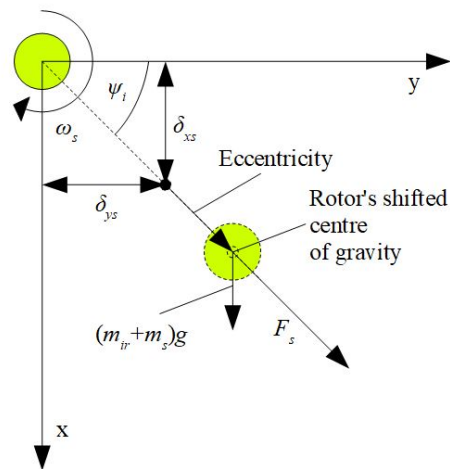
Figure 5.3. *The graphical representation of the eccentricity of the rotor-bearing system. The gravitational acceleration and acting loads affect the rotating system [157]*

5.7   Equations of Motion

Referring to described influences of nonlinear effects in the rolling-element bearings, the dynamical solution can be formulated in the set of differential equations of motion. The extension of the formulas considers terms of external forces, eccentricity of the rotor-bearing system, elastic Hertzian contact deformations and damping. The equations of motion (Equations 5.9 and 5.10) for the derived mathematical model are following:

$$m\ddot{\delta}_{xs} + c_x \dot{\delta}_{xs} + k\delta_{xs} = F_x + e\omega_s^2 cos(\omega_s t) \tag{5.9}$$

$$m\ddot{\delta}_{ys} + c_y \dot{\delta}_{ys} + k\delta_{ys} = F_y + e\omega_s^2 cos(\omega_s t) \tag{5.10}$$

where: $F_{x,y}$ is the external force shubjected to the bearing in horizontal/vertical direction, $c_{x,y}$ is the linearized bearing damping factor in the horizontal/vertical direction.

In the chapter referring the simulations and experimental verifications, the derived mathematical model will be studied following the cases realized in the experiment.

EXPERIMENTAL SETUP AND MEASUREMENTS

In the next chapter, the test rigs applied in the experiment are presented in which two main branches can be distinguished, i.e. the measurement of radial internal clearance after mounting and the dynamical test of self-aligning ball bearings with measurement of acceleration, temperature, and shaft's endplay. Moreover, the detailed data of the tested bearing type and the plan of the experiment are described. The whole experiment was conducted in the laboratory of the Institute of Process and Product Innovation at Leuphana University of Lüneburg.

6.1 Introduction

In order to check the influence of radial internal clearance on the dynamical response, the experiment was conducted for a batch of 10 bearings of the same type, i.e. self-aligning ball bearing NTN 2309SK with a conical bore

in which it is possible to control radial clearance in wide range with help of the alignment of the adapter sleeve and the nut. This is the unquestionable advantage, that comparison of two different bearings with pre-defined radial clearance is risky because of different quality of rolling surfaces and repeatability of the assembly process. That the thermal effects affect the reduction of the radial clearance, during the measurements also the temperature is recorded by stable thermal conditions and defined rotational velocity. Then, the clearance reduction can be calculated by estimation of the temperature difference on each bearing's ring. Tests for each bearing with defined radial clearance and rotational velocity are conducted in 10 minutes intervals after reaching its stable thermal conditions. For recording the acceleration of ball bearings, the professional equipment utilized in the industrial practice of bearings' diagnostics is applied characterizing with high accuracy and noise reduction. Next, the experimental time-series are preprocessed for further qualitative and quantitative analysis. In the following sections, particular test rigs and measurement procedures of the unit will be discussed finishing the chapter with the details of ball bearing studied in the experiment and the plan of the experiment itself.

6.2   Measurement of Radial Internal Clearance

In order to define the value of radial internal clearance (RIC) in the self-aligning ball bearing, the automated system for measuring the radial internal clearance after mounting of rolling bearings was applied (Figure 6.1) [97, 98]. At the beginning of the discussion, it is worth to mention, that reduced clearance after mounting on adapter sleeve was studied (Figure 6.2). The adapter sleeve is applied for bearings with a conical bore and this feature allows to reduce clearance with the locknut pressing on the inner ring.
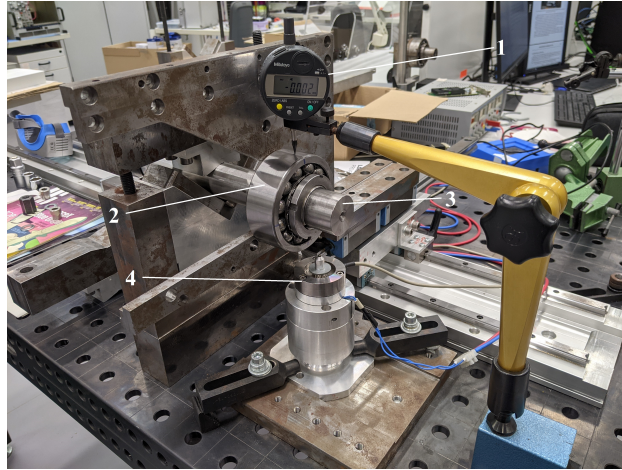
Figure 6.1. *Automated system with the automatic radial internal clearance after mounting with measured ball bearing NTN 2309SK. 1 - dial gauge, 2 - seated bearing, 3 - shaft, 4 - electromagnetic actuator and holder.*
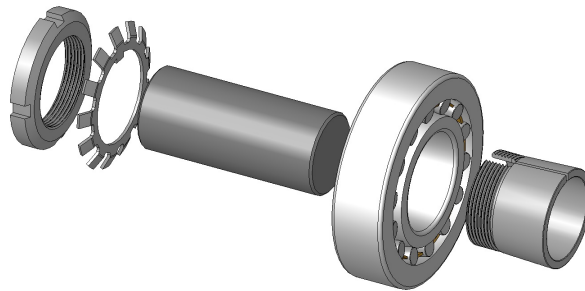
Figure 6.2. *Exploded view of all components for mounting a rolling bearing with conical inner ring on a shaft by means of an adapter sleeve. Arranged from left to right are locknut, locking plate, section of shaft, rolling bearing, adapter sleeve. [1]*

Next, the reduced radial clearance due to bearing fit on the shaft is measured. The determination of actual radial clearance is conducted according to the standard ISO 1132-2 referring to the guidelines for measurement of dimensions, running accuracy, and internal clearance of rolling bearings. In Figure 6.3, the flowchart for the radial clearance measurement is presented. During the measurement, the outer ring is lifted up with a vertical force of about 30N by activating the electromagnetic actuator at the bottom of the supporting bearing. The final result is measured with a dial gauge at the top of the bearing and can be written into the database. The measurement is repeated 3 times with a constant lifting force subjected by the actuator. Next, the bearing is rotated about $120°$ and the procedure is repeated. Later on, in two other 2 positions, there are 6 more measurements (3 by each angle). At the and, mean value and standard deviation are calculated of resultant radial internal clearance. After pressing with the locknut on the inner ring, the radial clearance is reduced, and then the new measurement can be conducted. The system can be introduced into industrial practice as it meets the requirements for Measurement System Analysis (MSA) by giving repeatable and reproducible clearance measurements. In the test rig, the software is written in the C language and is managed with Arduino Due microcontroller.

6.3 Dynamical Test

After the determination of reduced radial internal clearance, then the bearing is ready for mounting in the plummer block in the test rig. In Figure 6.4, the exploded view is presented of the bearing's mounting, additionally, in Figure 6.2, the locating rings are used on both sides of the bearing to prevent its tilting. That the bearing is working in the clean laboratory environment, in the place of seals, the rings were applied in which the cables for
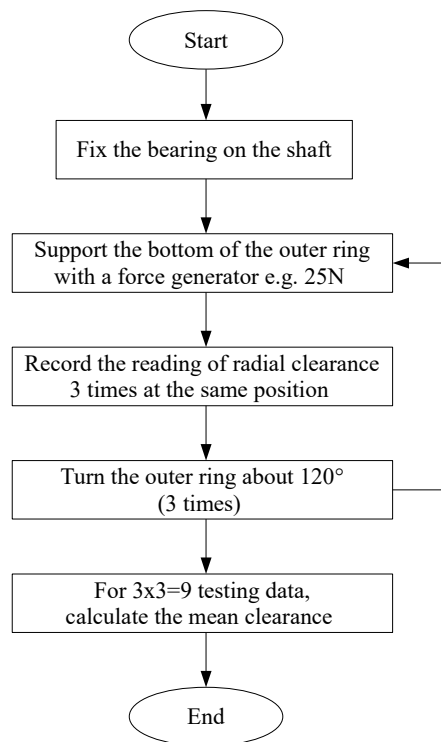
Figure 6.3. *Flowchart of radial internal clearance measurement according to ISO 1132-2*

temperature sensors and sensors itself are mounted. More about the temperature measurements will be mentioned in the next section. The plummer is modified and equipped with two accelerometers piezoelectric recording vibrations in the vertical direction and MEMS-based recording vibrations in the horizontal direction. Details referring to the measurements of acceleration will be provided in a separate section. In Figure 6.5, the whole experimental setup is presented, the mounted bearing is coupled with the DC motor controlled with the inverter. The applied motor allows for the tests up to 3000 rpm, which corresponds to half of the limiting speed for studied bearing. The test rig is reassembled by changing the radial clearance in the bearing, referring to the measurements by different rotational velocities to reach the thermal stability, the interval time is 10 minutes the same as for recording all features. The influence of variable load is neglected as the experiment is focused on the impact of clearance on dynamical response, there is only constant force subjected by a split-block housing and the shaft's eccentricity as the result of imperfect coupling. In order to avoid undesirable couplings between bearing, only one bearing is studied without classical bearing-node approach with fixed and locating bearing. For the experiment, only brand-new bearings are used and it is assumed that there is no influence of characteristic bearing defects on the measured acceleration. In Table 6.1, the equipment for the experimental setup is specified.

6.4 Measurement of Temperature

One of the factors influencing the reduction of radial clearance during its operation is the thermal effect caused by the frictional forces induced on the rolling surfaces. That the bearing steel has linear properties for low temperatures, it is possible to determine its expansion or compression with

Table 6.1. *Equipment for the experimental setup*

Component	Type
Ball Bearing	NTN 2309SK
Adapter Sleeve	NTN H2309
Locating Ring	NTN FR 100x4
Bearing Housings	NTN SNC 511-609
3-Phase Motor	Siemens 1LA5090-4AA60-Z
Frequency Converter	Siemens SIMOVERT 6SE2103
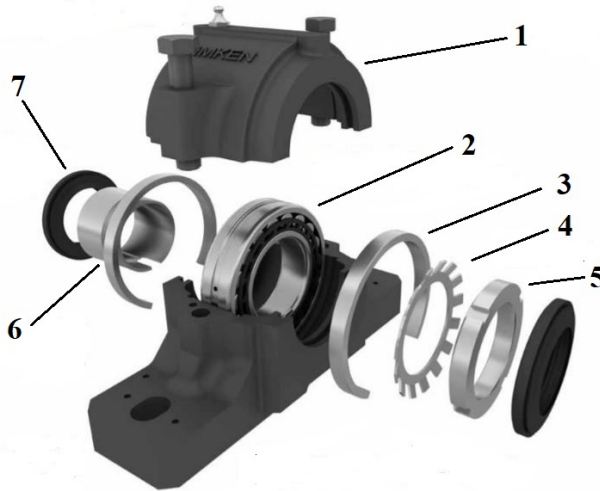
Figure 6.4. *Design of plummer block: 1 - split-block housing, 2 - bearing, 3 - locating ring, 4 - locking plate, 5 - locknut, 6 - adapter sleeve, 7 - seal [5]*
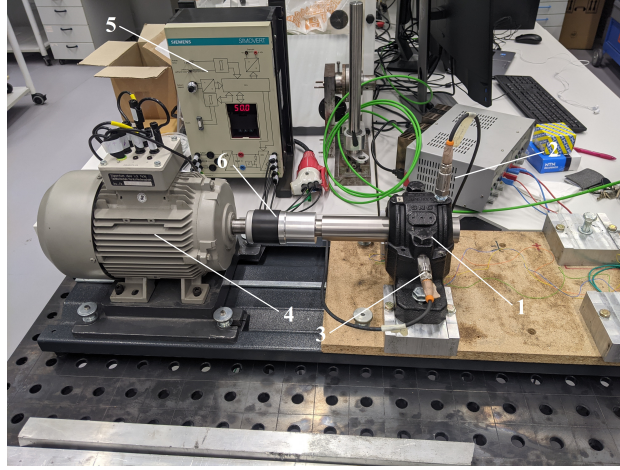
Figure 6.5. *Experimental setup: 1 - plummer block with mounted ball bearing, 2 - vertical accelerometer, 3 - horizontal accelerometer, 4 - 3-phase DC motor, 5 - inverter, 6 - coupling*

coefficient describing its expansion. The final result of the temperature gradient allows to estimate the real value of operating clearance, which in the bearing is calculated with the following formula:

$$\Delta RIC_{(Temp)} = \alpha \Delta T d_m \tag{6.1}$$

where: α is the linear thermal expansion coefficient (for steel shaft and cast iron housing, $\alpha = 12 * 10^{-6} \, [°C^{-1}]$).

In the test rig, two thermistors NTC $10k\Omega$ 3434K, Murata (NXRT15 XH103FA1B040 type) were attached to the bearing's rings. There was contact between the outer ring and thermistor, while another thermistor was placed in the closest possible distance to the rotating inner ring (Figure 6.6). For each radial clearance and velocity, the data of temperature was recorded in form of output voltage time-series, which was estimated with the Steinhart-Hart equation as the model of the resistance of a semicon-

ductor at different temperatures. First, the resistance of the thermistor was calculated with the following formula for the voltage divider:

$$R_1 = R_2(\frac{V_{in}}{V_{out}} - 1) \tag{6.2}$$

where: R_2 is the additional resistance (10 kOhm), V_{in} is the input voltage (5V) and V_{out} is the output voltage (recorded temperature time-series in voltage unit).

Next, after the estimation of thermisor's resistance, the value of temperature can be calculated with the Steinhart-Hart equation as following:

$$T = \frac{1}{(\frac{1}{T_0} + \frac{1}{B})ln(\frac{R_1}{R_0})} \tag{6.3}$$

where: B - is the B thermistor coefficient (3455K for temperature 25°), T_0 is the referrence temperature (25°).

The application of contactless sensors to the inner ring leads to certain measurement errors, but based on obtain result the clearance reduction due to thermal effects is approximate to the value specified by bearing manufacturers. The obtained clearance reduction in the experiment will be referred to the specific case derived in the mathematical model. The maps of clearance reduction by specific *RIC* and rotational velocity will be presented in the next chapter.

6.5 Measurement of Shaft's Endplay

One of the factors influencing the bearing's operation and inducing additional frequencies to the system is the endplay of the shaft. For the mea-
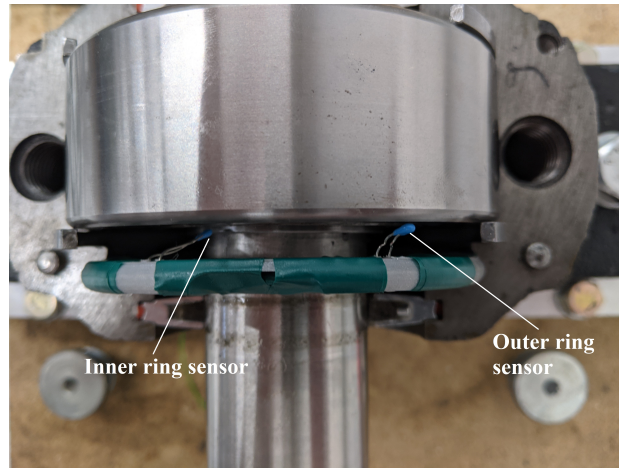
Figure 6.6. *Temperature sensors in the proximity of inner and outer ring*

surement of the eccentricity, the eddy current sensor (modular eddyNCDT Compact Eddy Current Sensor - DT 3300) (Figure 6.7) is applied to ensure high precision of measurements. The eddyNCDT 3300 controllers are equipped with high-performance processors for signal processing and further processing. Three-point linearization enables almost fully automatic linearization, which provides high accuracies for any metallic target and installation environment. The high resolution enables reliable detection of very small changes in displacement and distance in the sub-micrometre range. In Table 6.2, the most relevant features of Eddy Current sensor system are listed:

6.6 Measurement of Acceleration and Data Acquisition Software

As in the planned experiment, the diagnostics of bearing's acceleration played the most important role, the professional condition monitoring setup

Table 6.2. *Data-sheet for eddy currence sensor*

Feature	Value/Description
13 measuring ranges [mm]	0.4; 0.5; 0.8; 1; 2; 3; 4; 6; 8; 15; 22; 40; 80
Resolution max. [μm]	0.02
Linearity max. [μm]	0.8
Sensor robustness	IP67
Frequency response [kHz]	100
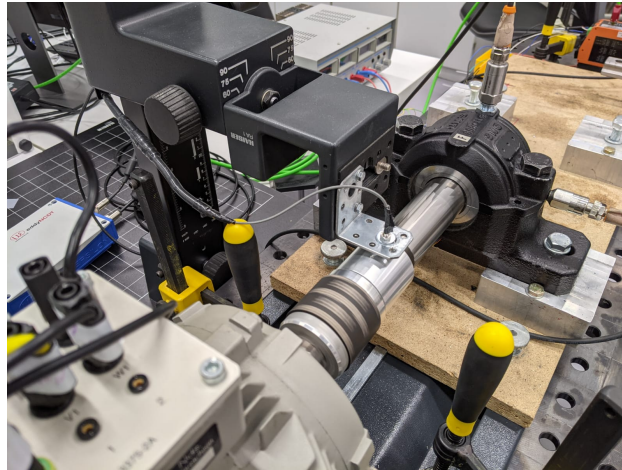
Figure 6.7. *Eddy current sensor with Kaiser RA1 holder*

Table 6.3. *Data-sheet for piezo-based accelerometer VSP001*

Feature	Value/Description
Vibration measuring range [g]	-50...50
Range of frequencies [Hz]	2...10000
Measuring principle	Piezoelectric effect
Precision [%]	5
Measuring sensitivity $\frac{mV}{g}$	100
Shock resistance [g]	5000

was applied for its recording provided by IFM. The whole setup consisted of the software and two accelerometers:

- software for vibration diagnostics VES004 - V2.16.02 - allowed to connect accelerometers and temperature sensors. The options in the program allow to conduct simple signal data processing as Fast Fourier Transform (FFT) calculation, signal filtering, averaging, statistics of recorded data or setting the alarm by exceeded critical value. The software can be connected with any computer with Ethernet connection and cloud-computing is also allowed.

- piezo-based vibration sensor VSP001 (vertical direction) - is the professional vibration sensor of rotational systems applied in the industrial applications characterizing with high resilience meeting the requirements of tough industrial environments by large operating temperatures and high protection class. Additionally, the sensor is distinguished with high repeatability and low linearity error. In Table 6.3, the most important features for accelerometer are specified.

Table 6.4. *Data-sheet for MEMS-based accelerometer VSA001*

Feature	Value/Description
Vibration measuring range [g]	-25...25
Range of frequencies [Hz]	1...6000
Measuring principle	Capacitative
Precision [%]	0.2
Measuring sensitivity $\frac{\mu m}{g}$	142
Shock resistance [g]	500

- MEMS-based vibration sensor VSA001 (horizontal direction) - similarly to piezo-based accelerometer, VSA001 is the professional vibration sensor of rotational systems applied in the industrial applications characterizing with high resilience meeting the requirements of tough industrial environments by large operating temperatures and high protection class. Additionally, the sensor is distinguished with high repeatability and low linearity error. In Table 6.4, the most important features for accelerometer are specified.

- Diagnostics electronics for vibration sensors VSE100 - in order to organize the communication between the accelerometers and diagnostics software. In Table 6.5, the most important features for the communication box are specified:

The time-series of acceleration were recorded with the sampling time equal to 0.64ms, which corresponds to 1562.5Hz sampling frequency. The data were saved in the CSV format and used in the further DSP analysis.

Table 6.5. *Data-sheet for diagnostics electronics for vibration sensors VSE100*

Feature	Value/Description
Range of frequencies [Hz]	0...12000
Design PC software VES004	Parameter setting via
Precision [%]	0.2
Total number of inputs and outputs	16 (configurable)
Communication interface	Ethernet
Protocol	TCP/IP
Data memory type	ring memory, FIFO
Memory size	881664 data records

6.7   Data of Self-Aligning Ball Bearing

In Figure 6.8, the technical drawing of self-aligning ball bearing 2309SK NTN applied for the tests is presented, while in Figure 6.9, the photo of the real bearing with pre-defined clearance in C3 class is shown. In Table 6.6, the most important geometric dimensions are listed, in Table 6.7. the characteristic frequencies for SABB NTN 2309SK, in Table 6.8., the clearance classes for studied bearing are specified.

6.8   Plan of the Experiment

After the measurement of the radial clearance, the bearing is mounted with the biggest possible RIC in the test rig. Then, the dynamical test starts with the slowest operational velocity, and after 10 minutes, when bearings reach the thermal stability by specific clearance and velocity, the accelera-
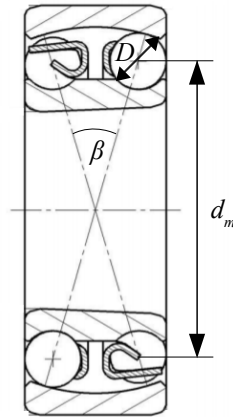
Figure 6.8. *Drawing of SABB NTN 2309SK with relevant dimensions for calculation of characteristic frequencies β - pressure angle, D - ball diameter, d_m - pitch diameter*
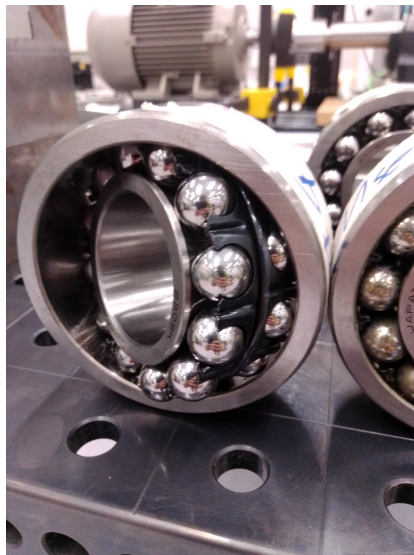
Figure 6.9. *Photo of one of tested bearings*

Table 6.6. *Dimensions of bearing*

Feature	Value
Bore diameter [mm]	45
Outer diameter [mm]	100
Pitch diameter [mm]	71.810
Ball diameter [mm]	15.870
Pressure angle [°]	15.52
Number of rolling elements	26 (13 per row)
Width [mm]	36
Dynamic load capacity [kN]	55
Static load capacity [kN]	16.7
Limiting speed [rpm] (oil)	7100
Limiting speed [rpm] (grease)	5600

Table 6.7. *Characteristic frequencies*

Characteristic frequency	Value
FTF [Hz]	0.394
BPFO [Hz]	5.116
BPFI [Hz]	7.884
BSF [Hz]	2.160

Table 6.8. *Clearance classes for tested bearing*

Clearance Class	C2	CN	C3	C4
Clearance Range [μm]	14-27	22-39	33-52	45-65
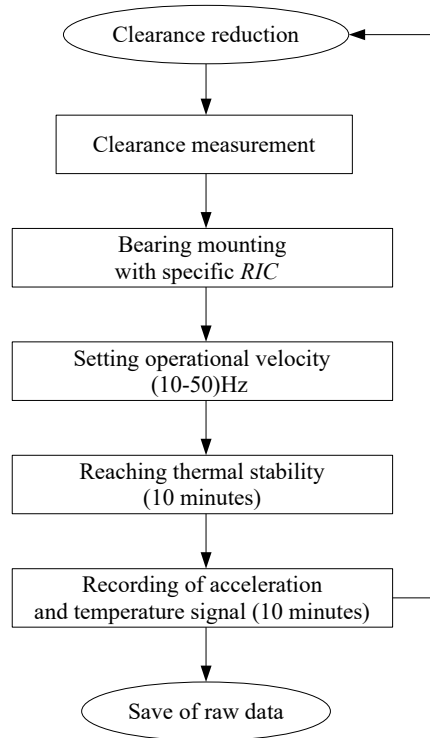
Figure 6.10. *Flowchart of data acquisition by radial clearance reduction and measurements*

tion is recorded. Later, the procedure is repeated with different clearance and for different velocities (Figure 6.10). The experiment is performed for 10 bearings (Figure 6.11) to reproduce the comparison tests between them and observe the repeatability. For each bearing, it was possible to get the 5-6 values of radial clearance that the values in specific bearing had small deviation. Between the definition of radial clearance, it was necessary to wait to cool down the bearing to the room temperature.

After the realization of the whole plan of the experiment, the data are pre-processed in MATLAB software, however, the details on it will be dis-
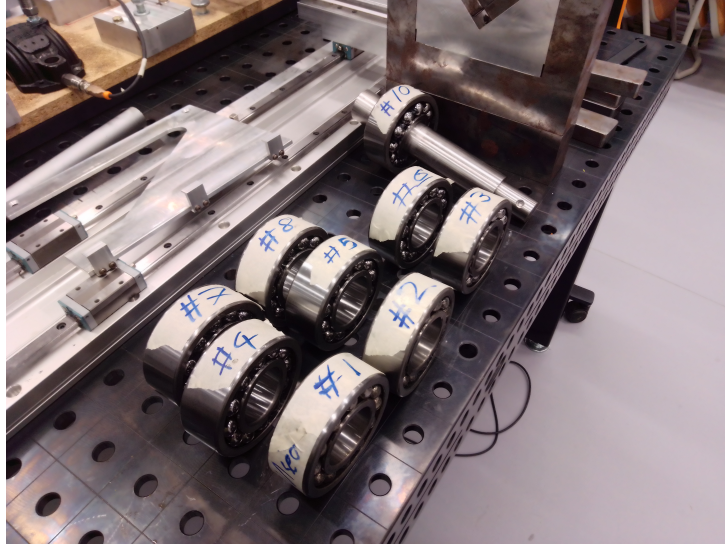
Figure 6.11. *Photo of bearing batch for the experiment, one bearing is mounted on the test rig*

cussed in the next chapter. The applied experimental setup allows providing the precise data acquisition for its further analysis.

SIMULATIONS AND EXPERIMENTAL VERIFICATION OF THE MODEL

This chapter refers to the comparison of the dynamical response of self-aligning ball bearing obtained with the 2-DOF mathematical model and in the experiment. Firstly, the mathematical model discussed in Chapter 5 is studied with terms based on the design of bearing and obtained by the conducted experiment. Its role is to examine the influence of the radial internal clearance on the dynamic response and to find the optimal operating conditions. Next, the experiment for 10 bearings is conducted according to the plan and comparative analysis is performed with the recurrence-based methods. The most sensitive recurrence quantificators to the influence of radial internal clearance are selected and proposed for the diagnostics of bearing's dynamics.

7.1   Model parameters

The mathematical model of a self-aligning ball bearing was derived to get the information on the influence of radial internal clearance on the dynamic response. One of the challenges is to obtain the realistic response of ball bearing, that terms used in the studied model must be close to the reality considering non-linear contact, shape errors or forces subjected to the bearing, and other factors mentioned in Chapter 5. The applied features can be divided into geometric parameters related to the design of tested bearing and physical related to the material properties of the ball bearing.

The value of eccentricity by specific rotational velocity of the studied system was measured with the eddy current sensor. Moreover, the value of the damping coefficient is dependent on the value of radial clearance according to the paper [151], and has more or less characteristics by obtaining it in the experimental analysis. It is reported [4, 141], that the damping factor is changing with subjected load, amount of lubrication, and rotational velocity. During the experiment, the subjected load is constant for all cases and it is assumed that lubrication is equal for all bearings because of the impossibility of its estimation for non-sealed bearings. The additional assumption is the variability of the damping factor with the rotational velocity. The distribution of damping factor in radial clearance and rotational velocity is presented in Figure 7.1.

7.2   Simulation and Bifurcation analysis

For the analysis of bearing's dynamics, the MATLAB software 2020a was applied in which the solver was ode45 (4th order Runge-Kutta) providing

Table 7.1. *Bearing properties for simulation study*

Term	Symbol	Unit	Value
Rotational velocity	ω_s	Hz	10; 20; 30; 40; 50
Ball diameter	D	mm	15.875
Pitch diameter	d_m	mm	71.810
Pressure angle	α	°	15.520
Radial Clearance	RIC	mm	0.0005:0.0005:0.050
Load deflection factor	K	N/mm	1874580
Damping factor in vertical direction	c_y	Ns/mm	RIC and rotational velocity dependent
Damping factor in horizontal direction	c_x	Ns/mm	RIC and rotational velocity dependent
Mass of inner ring and shaft	m	kg	1
Amplitude of the biggest undulation on inner ring	U_{inner}	mm	0.0004
Amplitude of the biggest undulation on outer ring	U_{outer}	mm	0.00028
Number of undulations on the perimeter of inner ring	N_{inner}	-	28
Number of undulations on the perimeter of outer ring	N_{outer}	-	19
Number of rolling elements	n	-	26
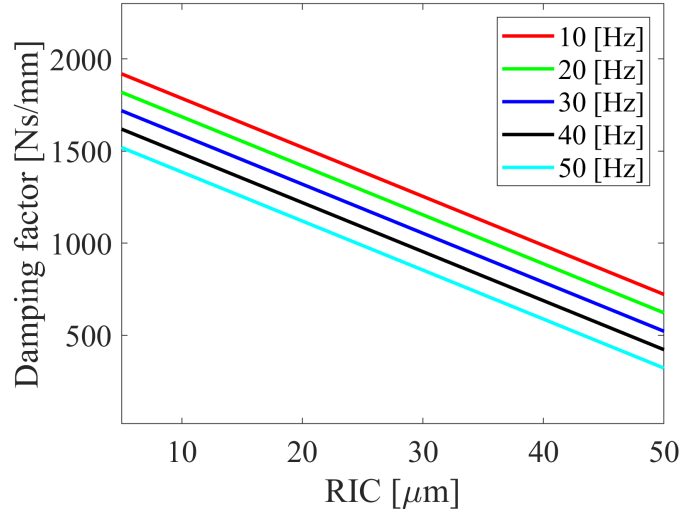
Figure 7.1. *Damping factor functions variable in radial internal clearance and rotational velocity domain.*

Table 7.2. *Bearing properties for simulation study (continuation of Table 7.1)*

Term	Symbol	Unit	Value
Eccentricity	*ecc*	mm	0.00035 - 10Hz; 0.00080 - 20Hz; 0.00071 - 30Hz; 0.00059 - 40Hz; 0.00065 - 50Hz;
External vertical force	F_y	N	50
External horizontal force	F_x	N	0

easy implementation and stability of calculations. Initial conditions and step value are extremely vital to the numerical solution, and during the initial step, the displacements and velocities in both directions are set to zeroes. An incorrect initial conditions mean a sudden change of dynamic response or rotor speed at the beginning, which will cause severe vibration and is not permitted in several case studies, that is why the stable conditions of ball bearing are taken into account. The time step in the calculations is the rotational velocity-dependent by each case, to refer to the real movement of bearing. At each time step, the equations of motion are solved according to the actual position of rolling elements.

The analysis of dynamics of a ball bearing was started with the classical qualitative tool for its investigation, i.e. bifurcation diagram. The bifurcation parameter was radial internal clearance investigated in the range from 0 to 50 μm with 0.5 μm incrementing step. The derived mathematical model has nonlinear characteristics, so the occurrence of bifurcation points or characteristic areas is expected. That in the system, the force is applied in the vertical direction, only mentioned response is taken for further analysis. The external force is considered as the upper part of split-block housing and the accelerometers attached to it. The bifurcation analysis is conducted for all rotational velocities following the planned experiment.

In Figures 7.2-7.6, the bifurcation plots by different operational velocities are presented in which the bifurcation parameter is the radial internal clearance and the acceleration response and its range is studied. At the first glance, bifurcation plots for all velocities have the same response differing slightly in amplitude. Referring to the observed qualitative changes in the response of the self-aligning ball bearing, few characteristic response can be observed. Up to 5 μm, the amplitude of acceleration response is in a really small range, which reflects strong damping in the bearing. For C2 and

CN clearance classes up to 30 μm, the bearing characterizes with relatively small amplitudes with slight discontinuity at 16 μm. The exact bifurcation point is found at 30 μm, where at normal clearance, the optimal clearance is found in the respect of the operation with a small range of amplitudes. This point shows the qualitative difference between the response with relatively small amplitudes and the response with the constantly increasing number of solutions in the clearance domain for C3 and C4 clearance classes. The found optimal clearance is worth further investigation and the experimental verification for studied bearing. The additional observation is, that the velocity has no strong impact on the variability of response, however, with its increase, the number of solutions is getting lower. For found radial clearance values of interest, the recurrence-based methods have been applied in the following subsections.

In the beginning, to identify and observe the dynamical behaviour by 4 specific radial internal clearance values, i.e. $RIC = 5\mu m, 16\mu m, 30\mu m$ $48\mu m$, the orbit plots and corresponding δ_{ys}-phase plots are presented (Figures 7.7-7.10). For the comparative analysis, the results are shown for the one rotational velocity n=30Hz. Referring to the obtained orbit plots, the value of elastic deformations in the vertical direction oscillates around the value of defined operating radial clearance. In the horizontal direction, the amplitude of elastic deformations is negligibly small, that only vertical directions will be considered for further analysis, where a small load is applied coming from the upper part of split housing and attached accelerometers. All cases characterize with closed trajectories, which reflects in the periodic response with dominating main frequency. In the phase portraits, the almost periodic response is observed too, the Poincare points are almost in the same place, which reflects a non-changing period of the bearing's dynamics.
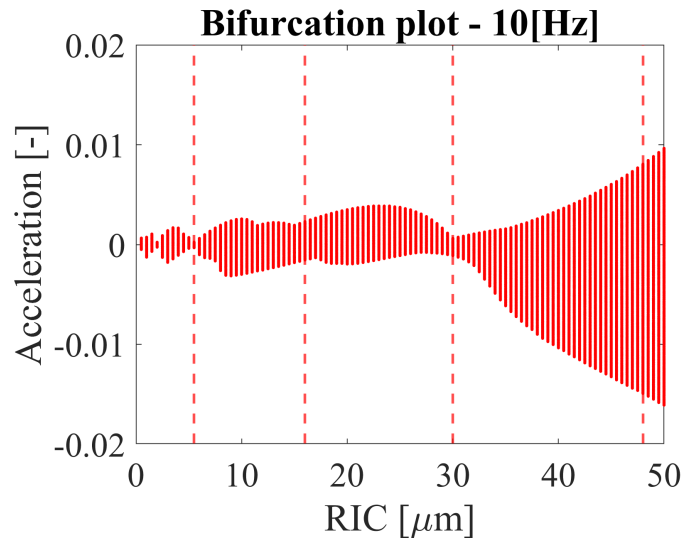
Figure 7.2. *Bifurcation diagram for the rotational velocity n=10[Hz].*

The next step in the investigation of the dynamical response of bearing is the calculation of the Fast Fourier Transform (FFT) (Figures 7.11-7.14). Its results reflect the results of bifurcation analysis, the magnitude of the elastic deformations response in the vertical direction has smaller values by small clearance $5\mu m$ and normal clearance $30\mu m$. The main harmonics in the case of $16\mu m$ and $48\mu m$ has a bigger magnitude. Despite the occurrence of other frequencies (Figures 7.11-7.14 - right panel, time-series), their magnitude don't have a strong influence on the dynamics.

The application of the fundamental tools for the diagnostics of dynamical systems shows the qualitative changes in the dynamical response of bearing in the radial clearance domain, but more sensitive tools are required to show the quantitative and qualitative changes in the system. In the next part, the recurrence analysis will be performed to capture the sophisticated changes by the variable clearance in the dynamic response both with the mathematical model and in the experiment.
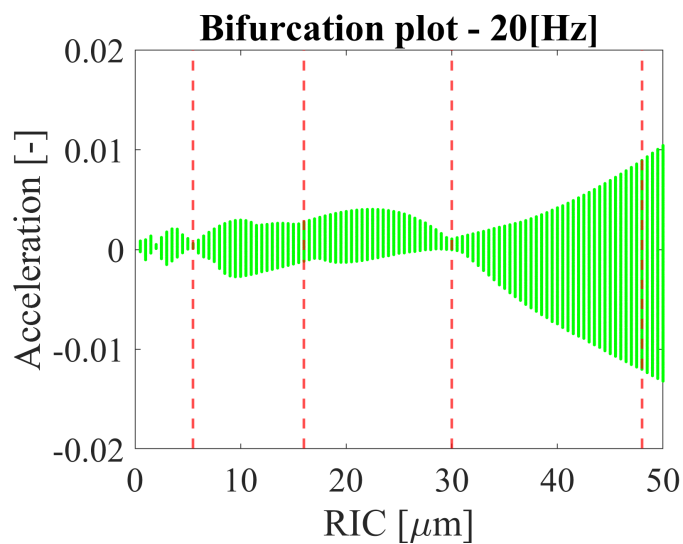
Figure 7.3. *Bifurcation diagram for the rotational velocity n=20[Hz].*
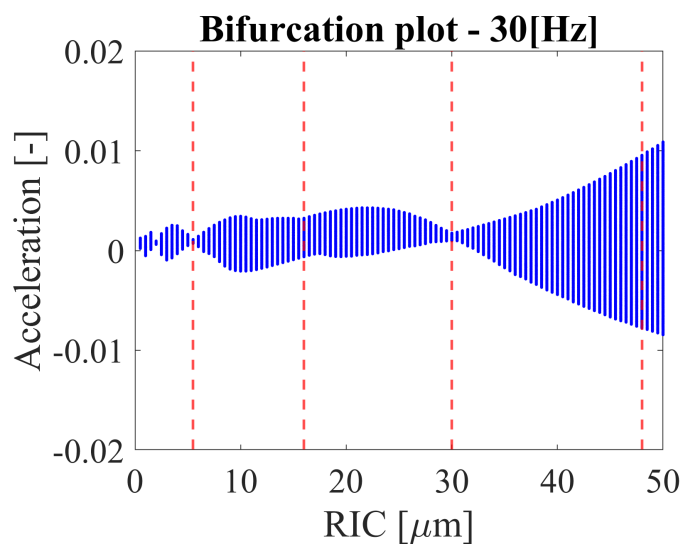
Figure 7.4. *Bifurcation diagram for the rotational velocity n=30[Hz].*
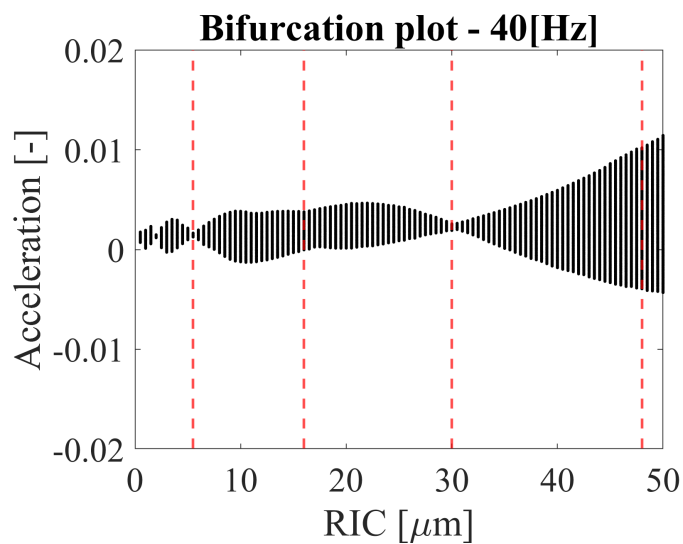
Figure 7.5. *Bifurcation diagram for the rotational velocity n=40[Hz].*
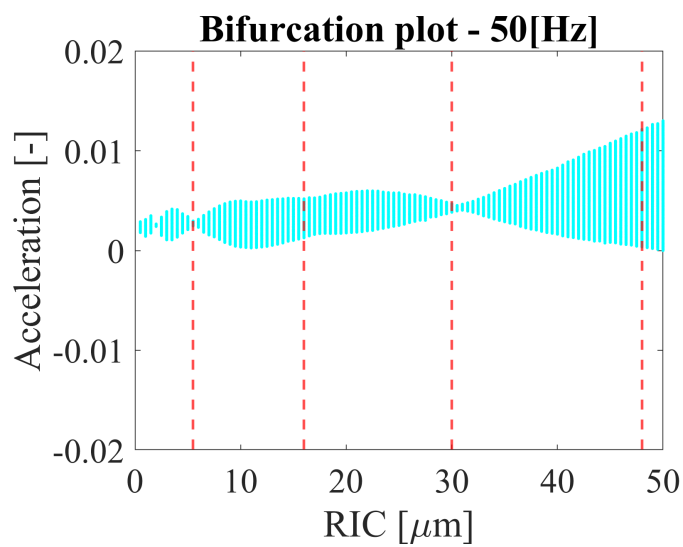
Figure 7.6. *Bifurcation diagram for the rotational velocity n=50[Hz].*
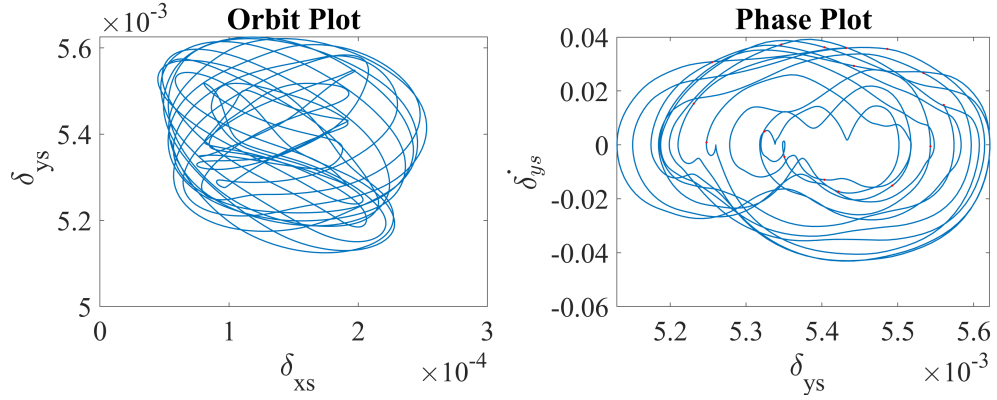
Figure 7.7. *Orbit and phase plot by RIC=5.5[µm] n=30[Hz].*
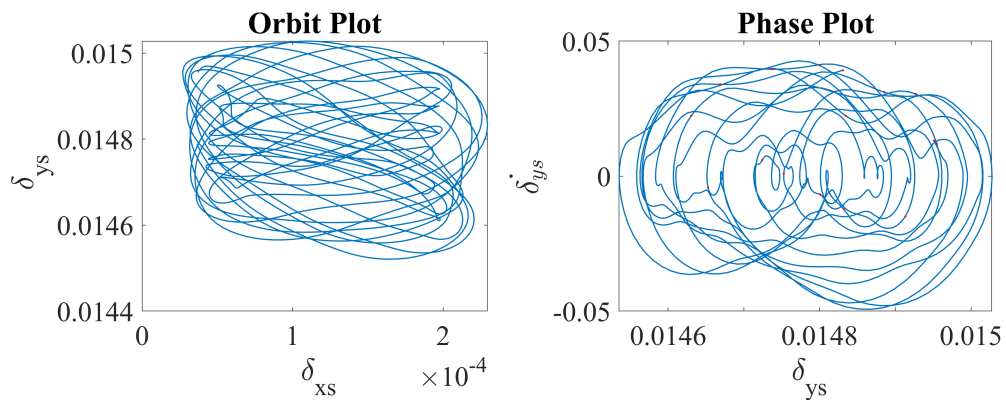
Figure 7.8. *Orbit and phase plot by RIC=16[µm] n=30[Hz].*
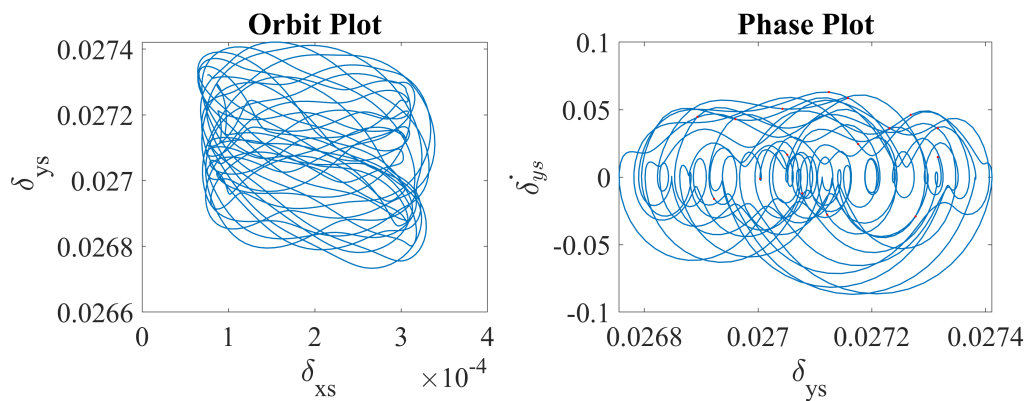
Figure 7.9. *Orbit and phase plot by RIC=30[µm] n=30[Hz].*
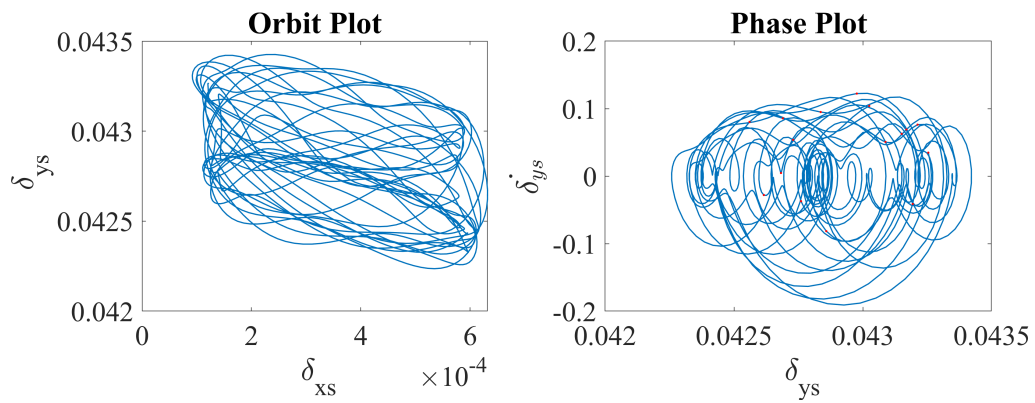
Figure 7.10. *Orbit and phase plot by RIC=48[μm] n=30[Hz].*
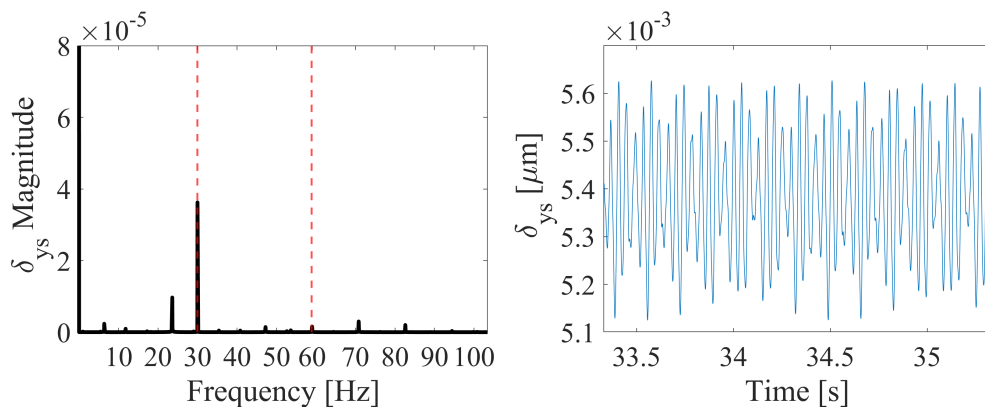
Figure 7.11. *FFT and displacement time-series by RIC=5.5[μm] n=30[Hz].*
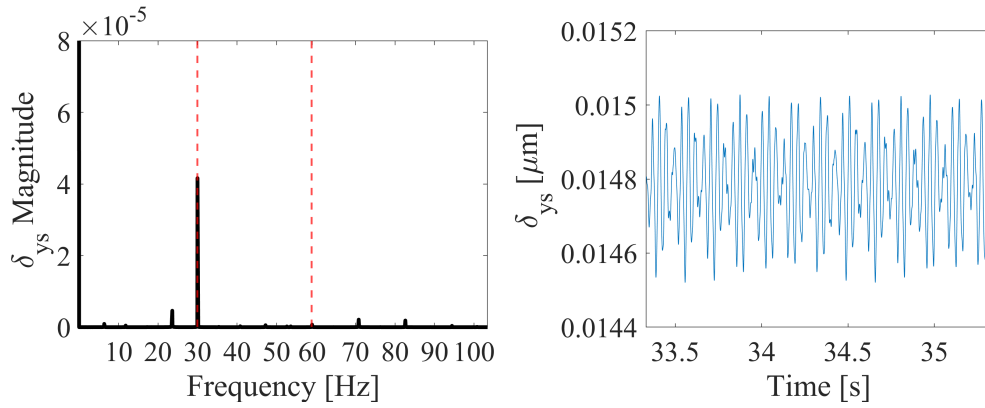
Figure 7.12. *FFT and displacement time-series by RIC=16[µm] n=30[Hz].*
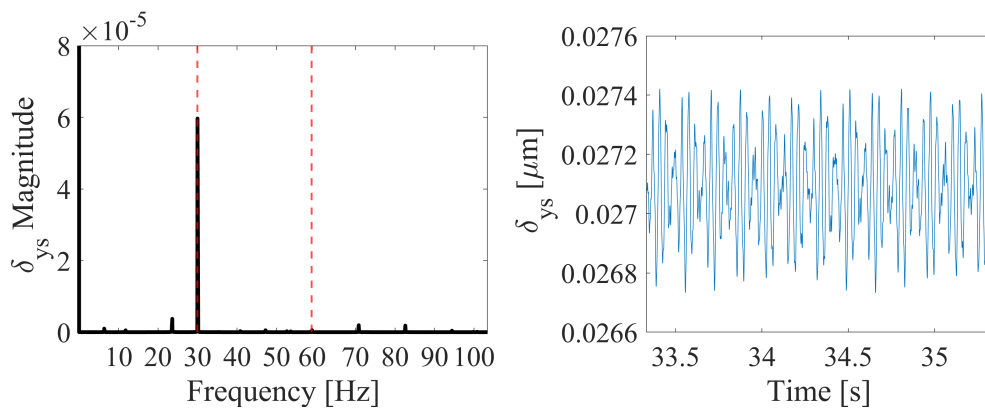
Figure 7.13. *FFT and displacement time-series by RIC=30[µm] n=30[Hz].*
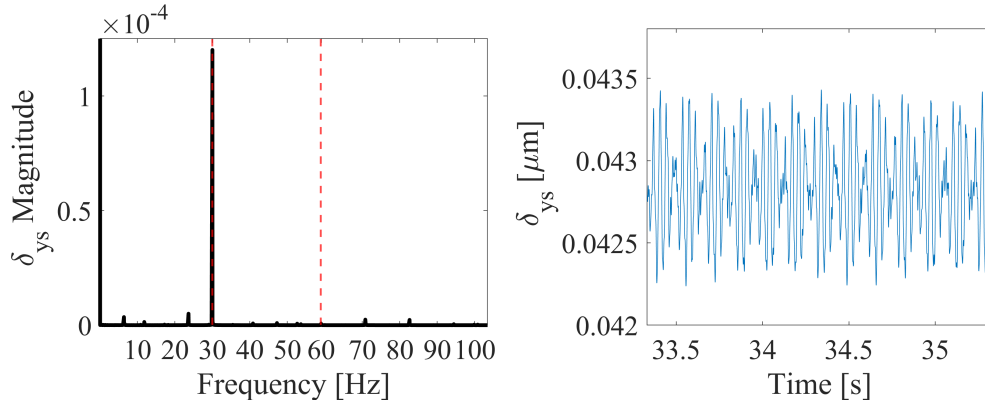
Figure 7.14. *FFT and displacement time-series by RIC=48[μm] n=30[Hz].*

7.3 Raw Data Analysis

After the analysis of the mathematical model and finding the areas of interest regarding the influence of radial internal clearance on the dynamics of ball bearing, the experiment was conducted for 10 bearings according to the assumed plan of the experiment. The obtained acceleration time series were pre-processed before the recurrence analysis. The temperature time-series for different radial internal clearance and rotational velocities didn't need special treatment and for the stable state, its mean value was calculated. In the following subsections, a short description of experimental signals analysis is described.

7.3.1 Acceleration Time-Series Analysis

After the measurement, the first step in the processing of acceleration time-series was its normalization, which means its scaling to the identical level [88, 120]. The reason is to compare the heterogeneous data obtained by different clearance and velocity, additional advantage is the decrease in the
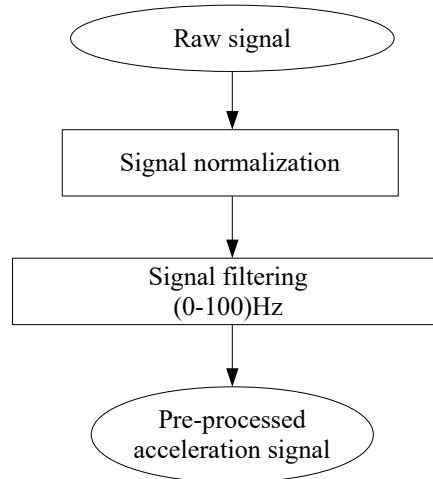
Figure 7.15. *Flowchart of signal processing of acceleration signal*

influence of errors coming during the system's refitting, i.e. bearing assembly and assembly of accelerometers. After the normalization, signal mean μ=0 and standard deviation σ=1 allowing for comparison of different time-series. Another applied signal treatment is its filtering in the band (0-100)[Hz] (low-pass Butterworth filter), the applied sampling frequency allows to study the spectra up to 800[Hz]. However, the disadvantage of recurrence analysis is its sensitivity to the number of frequencies of spectra, so the decision was made to focus on the most relevant frequency band for the spectral analysis of bearing. The current limit is equal to the second super-harmonic for the highest applied operational velocity in the experiment [86, 111, 156]. The pre-processed signal is mentioned way is applied later to the phase-space reconstruction and analysis in short-time intervals. In Figure 7.15, the flowchart of signal preprocessing is presented.

7.3.2 Temperature Time-Series Analysis

According to the measurement methodology, the data of temperature of each ring was recorded by specific radial internal clearance and five different rotational velocities. In Figure 7.16, the temperature time series are presented, distinguishing the moment of acceleration measurement (green transparent blocks) and time intervals for the temperature stabilization between cases. Results obtained (Figure 7.16) show the increasing trend of the temperature with the rotational velocity.

In Tables 7.3-7.7, the results of the temperature difference and operational radial clearance reduction are listed. The first observed dependence is that the lower the applied clearance, the mean temperature by corresponding cases has a higher value, which is related to increased frictional forces inside bearing caused by tighter assembly of bearing elements. The opposite dependence is observed by the high value of clearance, then the average mean temperatures have the lowest values what can be caused by relatively high freedom of rolling-elements movement.

The noteworthy fact is, that the biggest temperature difference is observed for the middle clearance. Both by the smallest and the biggest radial clearance, the heat transfer between rotating and the non-rotating ring is the finest, that there is no substantial temperature difference on each ring. This results in a small clearance reduction comparing to the middle clearance. The observed anomaly is convergent with the observance of bifurcation point of radial internal clearance around $30 \mu m$, this fact will be further investigated by the recurrence analysis.
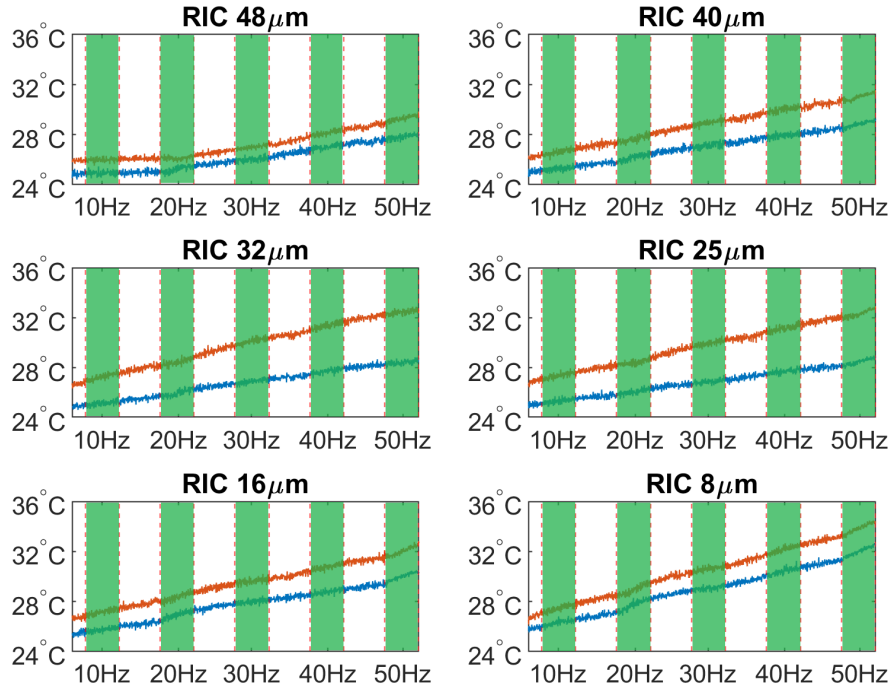
Figure 7.16. *Registered temperature time series on inner ring (IR - red) and (OR - blue) by different rotational velocity. Green transparent squares denote the time interval (circa 10 minutes), when the bearing's acceleration was measured.*

Table 7.3. *Operational radial internal clearance reduction by n=10[Hz]*

-	**8** μm	**16** μm	**25** μm	**32** μm	**40** μm	**48** μm
ΔT [$°C$]	1.147	1.407	2.024	2.104	1.332	1.070
ΔRIC [μm]	0.989	1.212	1.744	1.813	1.148	0.922

Table 7.4. *Operational radial internal clearance reduction by n=20[Hz]*

-	**8** μm	**16** μm	**25** μm	**32** μm	**40** μm	**48** μm
ΔT [$^\circ C$]	1.223	1.427	2.341	2.490	1.486	0.893
ΔRIC [μm]	1.054	1.230	2.017	2.146	1.281	0.770

Table 7.5. *Operational radial internal clearance reduction by n=30[Hz]*

-	**8** μm	**16** μm	**25** μm	**32** μm	**40** μm	**48** μm
ΔT [$^\circ C$]	1.534	1.649	3.061	3.219	1.807	0.9893
ΔRIC [μm]	1.322	1.421	2.638	2.773	1.557	0.852

Table 7.6. *Operational radial internal clearance reduction by n=40[Hz]*

-	**8** μm	**16** μm	**25** μm	**32** μm	**40** μm	**48** μm
ΔT [$^\circ C$]	1.744	1.982	3.455	3.633	2.090	1.132
ΔRIC [μm]	1.503	1.708	2.977	3.131	1.801	0.975

Table 7.7. *Operational radial internal clearance reduction by n=50[Hz]*

-	**8** μm	**16** μm	**25** μm	**32** μm	**40** μm	**48** μm
ΔT [$^\circ C$]	1.852	2.040	3.843	4.016	2.188	1.478
ΔRIC [μm]	1.596	1.758	3.312	3.461	1.885	1.273

7.4   Recurrence Analysis

One of the nonlinear dynamics tools, which can be applied for the analysis of ball bearing dynamic response is the recurrence analysis providing the information on all the times when the phase space trajectory of the dynamical system visits roughly the same area in the phase space [52, 69]. Then the two points, which are in close distance to each other, are treated as the recurrence points. The distance matrix R (Equation 7.1) is for the dynamic state x created with ones (recurrence points) and zeros (no recurrence point) at the times i and j.

$$R_{i,j}^{\varepsilon} = H(\varepsilon - ||x_i|| - ||x_j||), i, j = 1, ..., N \tag{7.1}$$

where: N is the number of considered states, H is the Heaviside function, ε is the threshold distance, $||x_i - x_j||$ is the norm of the dynamic states (for the analysis, the constant recurrence point density norm at recurrence plot was applied RR=5%.

The recurrence analysis is very popular and widely applied among a variety of sciences such as physiology [54, 68], geology [38, 125], finances [71, 99]. The subject of study is also the diagnostics of the mechanical systems [18, 123, 136] and recurrences are an alternative method to the standard frequency and time-based methods. In the following subsections, the fundamentals of the recurrence-based methods are presented, i.e., recurrence plots (RP) and Recurrence Quantification Analysis (RQA).

7.4.1   Recurrence Plots Method

The forerunners of the graphical interpretation of the considered distance matrix [R] are Eckmann et al. [40] and Zbilut et al. [154], who proposed its analysis in the form of recurrence plots. The mathematical relationship

(Equations 7.2, 7.3) describes the formation of the distance matrix with recurrence points and empty spaces (lack of recurrence):

$$[R_{i,j}] = 1 : x_i \approx x_j i, j, ..., N \tag{7.2}$$

$$[R_{i,j}] = 0 : x_i \neq x_j \tag{7.3}$$

where: $x_i \approx x_j$ are the points in the close distance appointed by the threshold radius of ε creating a recurrence point.

Before the recurrence plots can be created, the three parameters must be found beforehand, i.e., time delay—τ, embedding dimension—m, and threshold—ε. According to Takens theorem [124], three mentioned parameters are demanded creating the missing coordinates, then the state of the system after reconstruction can be represented in form of a time-delayed vector [75]:

$$\vec{x_i} = [x_i, x_{i-\tau}, x_{i-2\tau}, ..., x_{i-(m-1)\tau}] \tag{7.4}$$

The first parameter to be found for the phase space reconstruction is the time delay τ for which two methods are specified (a) autocorrelation function and (b) mutual information. The first method is the autocorrelation function [45] given by the following formula:

$$c_\tau = \frac{s_n s_{n-\tau}}{\sigma^2} \tag{7.5}$$

where, n is the time index of the dynamical process, τ is the time delay, σ^2 is the variance of the considered time series. Here the characteristic τ is found to be a decay of c_τ reaching 0 or the first minimum.

Another approach for the definition of the time lag is the mutual information function (MI) [44, 135]. The method is based on the quantification between the original time series and delayed time series (shifted), the value of time lag τ for the phase space reconstruction is the first minimum. The mathematical description of MI has the following form:

$$I(x(t), x(t+\tau)) = \sum_{i,j} p_{i,j} log(\frac{p_{i,j}(\tau)}{p_i p_j}) \tag{7.6}$$

where: $I(x(t), x(t+\tau))$ is the mutual information function between the original signal and delayed time series, p_i, p_j are the probability that $x(t)$ is in bin i, j of the histogram constructed from the data points in x, $p_{i,j}(\tau)$ is the probability that $x(t)$ is in bin i and $x(t+\tau)$ is in bin j.

The most popular method of determining the embedding dimension m was proposed by Kennel et al. [76] based on the "False Nearest Neighbors" function. The FNN function detects points in a close distance to each other in the embedding space. The number of embedding dimension m is determined by zero of the FNN function, then all false neighbors disappear and no further increase of the dimension is necessary [87].

The most demanding step in the phase-space reconstruction is the choice of the threshold ε corresponding to the radius in the phase space. Marwan in his work collected a rich source of knowledge on the criteria for its selection, however, the applied method is mostly dependent on the analyzed dynamical system. For our analysis, we assume for the calculation, the method of fixed recurrence rate of 5%. Then the threshold value is adjusted to the density of the recurrence points at RP for all considered cases. This method has two following advantages:

- Considered dynamical states are dependent on only one feature at a constant level.

Table 7.8. *The parameters for the reconstruction of recurrence plots (RPs) by the constant value of recurrence rate, RR = 0.05*

Time delay τ	Embedding dimension m	Threshold ε
5	5	based on the constant *RR*

- There is no need to normalize considered time series before the phase-space reconstruction.

The first step in the analysis of each case, the short time series consisting of 3000 data points was taken for analysis, as the dynamic response is based on the mathematical model and the general character of the deformations is repeatable after the staring procedure. Based on the value of mutual information, the value of the time delay τ was equal to 5, while applying the false nearest neighbours algorithm, the value of applied threshold was equal to 5 as well. Both found phase-space reconstruction parameters were applied to all considered cases, i.e. 5 different rotational velocities and chosen radial internal clearance values. The threshold ε was automatically calculated according to the constant value of the recurrence rate $RR = 5\%$. In Table 7.8, the phase-space reconstruction parameters for the time-series obtained from the mathematical model are collected.

Obtained RPs for the considered radial clearances and the rotational velocity n=30[rpm] are presented in Figures 7.17-7.20. The general information on the recurrence plot is that they consist of isolated points, vertical and diagonal lines, and structures formed with them. Based on the acceleration time-series (Figures 7.11-7.14) by specific clearance, it can be observed the little influence of additional harmonics into the spectra, so the response is mostly periodic formed with the diagonal lines. On the plots, also some isolated points can be observed corresponding to the close states in the dynam-
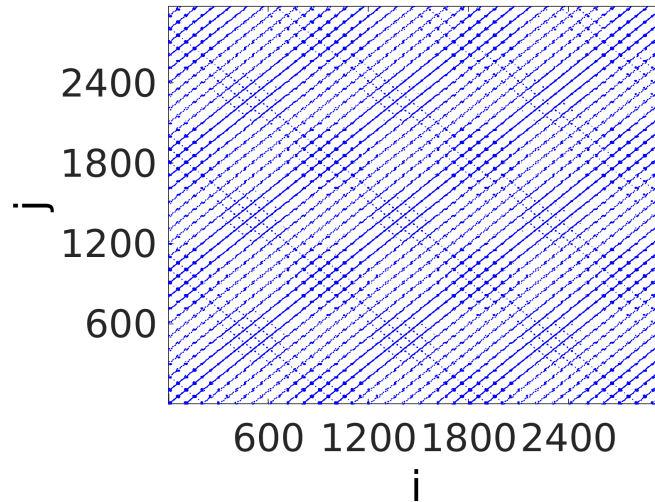
Figure 7.17. *Recurrence plot by RIC=5.5[μm] n=30[Hz].*

ics. However, the qualitative analysis provides only the general information on the bearing's dynamics, so the application of the quantitative analysis is needed in form of the recurrence analysis. The differences between recurrence plots obtained from the mathematical model differ from each other in a minor way.

7.4.2 Recurrence Quantification Analysis

As the recurrence plots (RPs) method provides only qualitative information on the bearing's dynamics, the quantitative method Recurrence Quantification Analysis (RQA) is applied in form of recurrence quantificators [131, 153] calculation. All the measures are based on the obtained topology of the recurrence plots providing a statistical description of the dynamical response. For the analysis, the quantificators determined in the CRP Toolbox [3] are employed and they can be divided by their topology (length and character of diagonal or vertical lines). In the following subsections, the
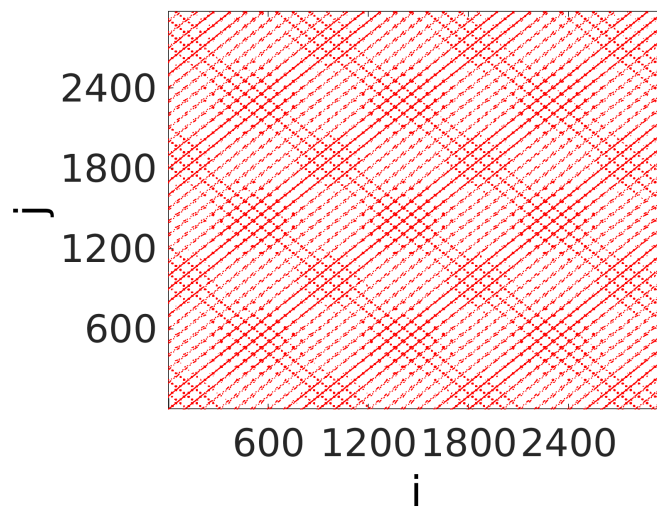
Figure 7.18. *Recurrence plot by RIC=16[µm] n=30[Hz].*
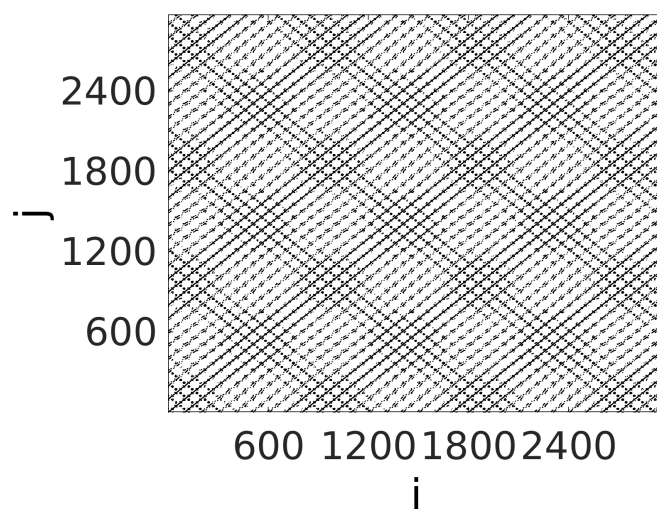
Figure 7.19. *Recurrence plot by RIC=30[µm] n=30[Hz].*
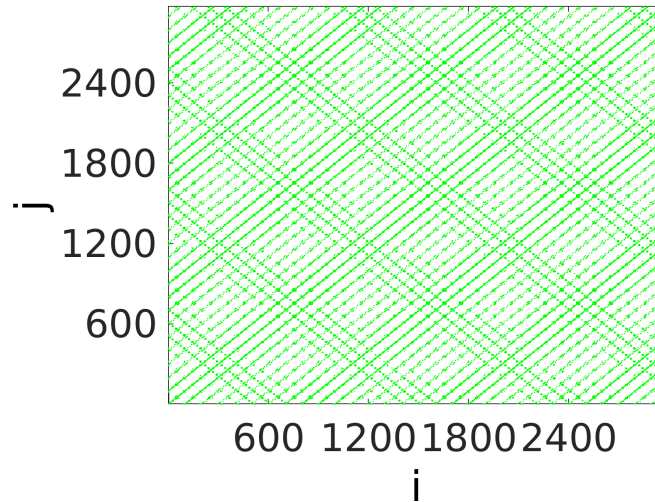
Figure 7.20. *Recurrence plot by RIC=48[μm] n=30[Hz].*

analysis of specific recurrence quantificators will be conducted, the meaning of quantificators was discussed in Chapter 4.

- Quantificators based on the Diagonal Lines - the quantificators based on the calculation of diagonal structures are determinism *DET*, averaged diagonal line lenght *L*, length of the longest diagonal L_{max} and entropy *ENTR*. Mentioned quantificators are calculated and presented in Figures 7.21-7.24. The determinism refers to the system's periodicity and predictability, and closer is to 1, the response is more periodic corresponding to stable bearing's operation. By all rotational velocities and for small values of radial clearance, the determinism is changing and fluctuating in the wide range what refers to the system's instability. Next, in the range *RIC*=5.5-16[μm], the value for determinism is stabilizing in the range between 0.8-0.9. After the found bifurcation point in 16[μm], the value of determinism is on the con-
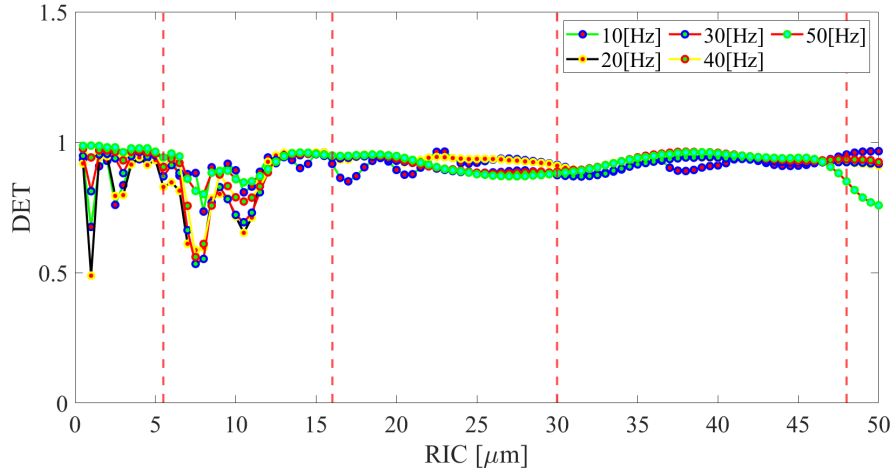
Figure 7.21. *Results of Determinism for the series of radial internal clearance.*

stant and releively high level around 1. The quantificator is rather non-sensitive to the change of the rotational velocity.

The next quantificator based on the diagonal line structures is average length of the diagonal line *L*. Observing its response in wide range (Figure 7.22), the quantificator is sensistive to the changes of the radial clearance. The same fluctuations are observed for small radial clearance. Moreover, the minima by *RIC*=30[μm] is observed at the second bifurcation point.

The third studied quantificator is the length of the longest diagonal line L_{max}, which strongly depends on the calculated phase-space reconstruction parameters. Unfortunately, the qunatificator is non-sensitive to the change of radial internal clearance and the operational velocity.

The last of diagonal lines-based quantificators is the entropy *ENTR*, which seems to be the most sensitive to the change of radial internal clearance. The calculated entropy refers to the degree of dis-
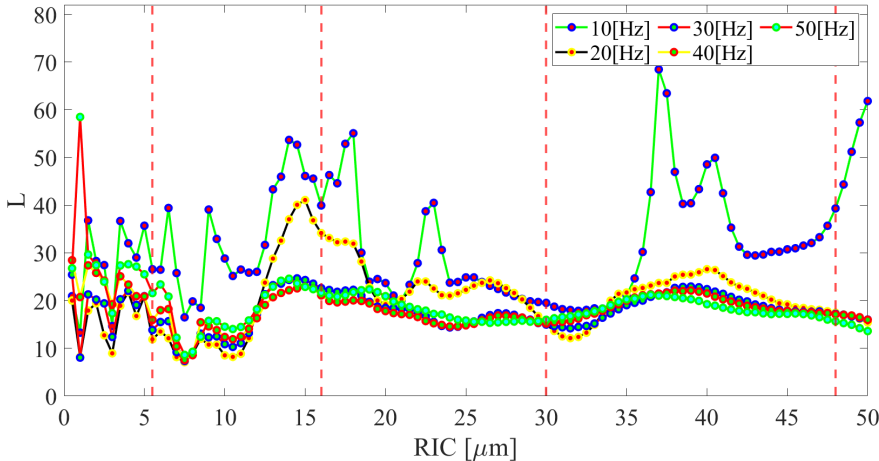
Figure 7.22. *Results of Averaged length of the diagonal line for the series of radial internal clearance.*
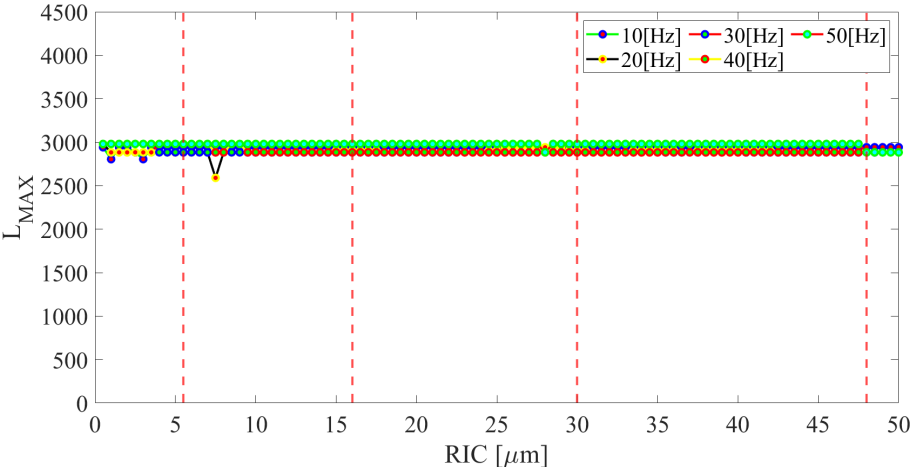
Figure 7.23. *Results of the Length of the Longest Diagonal for the series of radial internal clearance.*

102
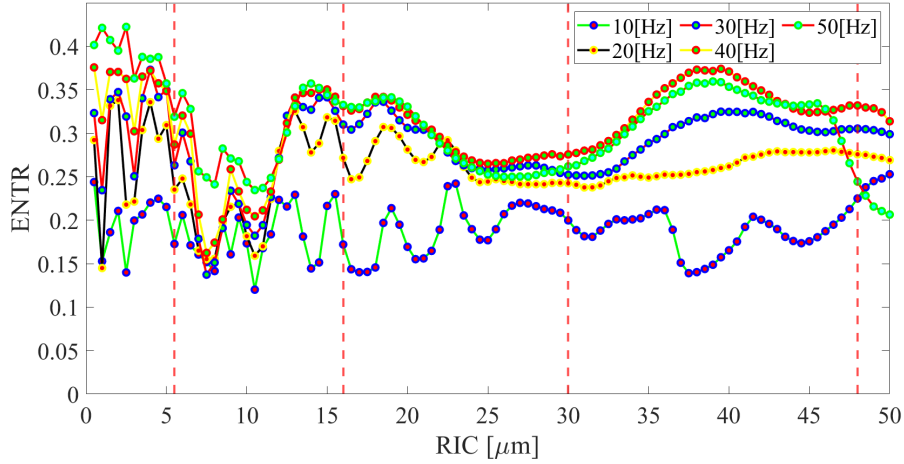
Figure 7.24. *Results of Entropy for the series of radial internal clearance.*

order of the system, by which the minima is clearly observed after the first bifurcation point and around the second bifurcation point at RIC=30[μm]. Simultaneously, the strong fluctuations for small clearance are observed. The last of quantificators seem to be the most sensitive to the change of clearance, and is dependent to the rotational velocity at the same time.

- Quantificators based on the Vertical Lines - the quantificators based on the calculation of vertical structures are laminarity *LAM*, trapping time *TT*, and length of the longest vertical V_{max}. Mentioned quantificators are calculated and presented in Figures 7.25-7.27. In the case of the first qunatificator the laminarity, it refers to the meantime, when the state of the system is trapped in some states. It also indicates switching between different states of the system. The laminarity is sensitive to the rotational velocity and the value of radial clearance at the same time. The higher the rotational velocity, the value of laminarity is closer to one, it reflects to the bearing's dynamics, that the
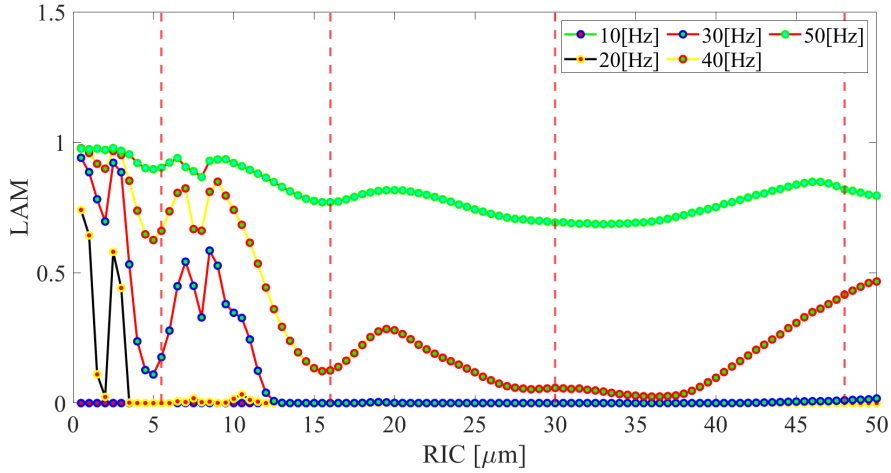
Figure 7.25. *Results of Laminarity for the series of radial internal clearance.*

higher rotational velocity neglects the influence of various terms on the dynamical response. By the *RIC*=30[μm], the minima is observed for 2 different rotational velocities and for 4 different rotational velocities, fluctuations by small clearance are observed.

Trapping time refers to the average length of the vertical lines by the measurement time scale of small changes in the response. Its shape is similar like in case of of laminarity, for few cases the minima is observed at the bifurcation point and for range of small clearance, the trapping time has the smallest value, what can be related with the influence of the frictional forces.

The last of vertical-based structures quantificators is length of the longest vertical line V_{max}. For all cases, the formed vertical lines are relatively short, what refers to the situation, when the bearing states in the same state for some time. It would not be expected, that vertical lines will be long, that they have been hardly observed at the recurrence plots. The quantificator is sensitive to the change of the
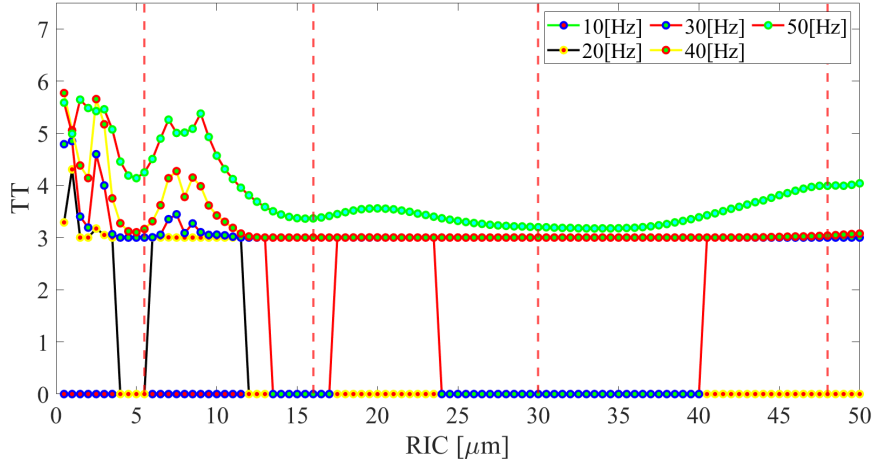
Figure 7.26. *Results of Trapping Time for the series of radial internal clearance.*

rotational velocity, and if it goes about the reference to the radial clearance, for small clarance it has the highest value and it is fluctuating. After going through the first bifurcation point at *RIC*=16[μm] it reaches its constant minima up to *RIC*=40[μm] starting again to increase.

- Quantificators based on the Recurrence Time - the quantificators based on the calculation of the recurrence time are recurrence time of the 1st type T^1, and recurrence time of the 2nd type T^2. Mentioned quantificators are calculated and presented in Figures 7.28-7.29. Recurrence time is mostly used for stochastic signals with numerous transient states, so those measures are not practical for considering the mathematical model, however they will be considered.

The recurrence time of the 1st type refers to the detection of weak transitions in signal dynamics, this quantificator is more robust to the noise level and less sensitive to the parameter change of the algo-

105
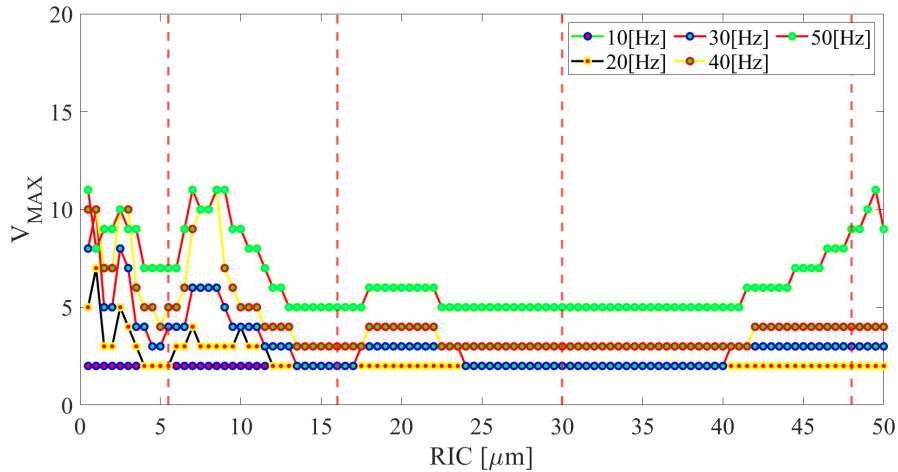
Figure 7.27. *Results of Length of the Longest Vertical Line for the series of radial internal clearance.*

rithm. Mentioned transitions and its increased value are observed for the range of small clerance up to 12[μm], later on the quantificator has its minima in wide range. The quantificator is sensitive to the change of rotational velocity and radial clearance at the same time.

The next quantificator, the recurrence time of the 2nd type detects transient states in the signal with very low energy. Similarly to previous quantificators, its fluctuations are observed for small clearances reaching the first and the second minima at bifurcation points at 16[μm] and 30[μm]. Discussed quantificator is prone to the change of the operating rotational velocity of the bearing.

- Quantificators based on the Probability - the quantificators based on the calculation of probability are recurrence period density entropy *RPDE*, clustering *C* and transitivity *TRANS*. Mentioned quantificators are calculated and presented in Figures 7.30-7.32. The first quantificator refers to the calculation of Shannon entropy, but it dif-
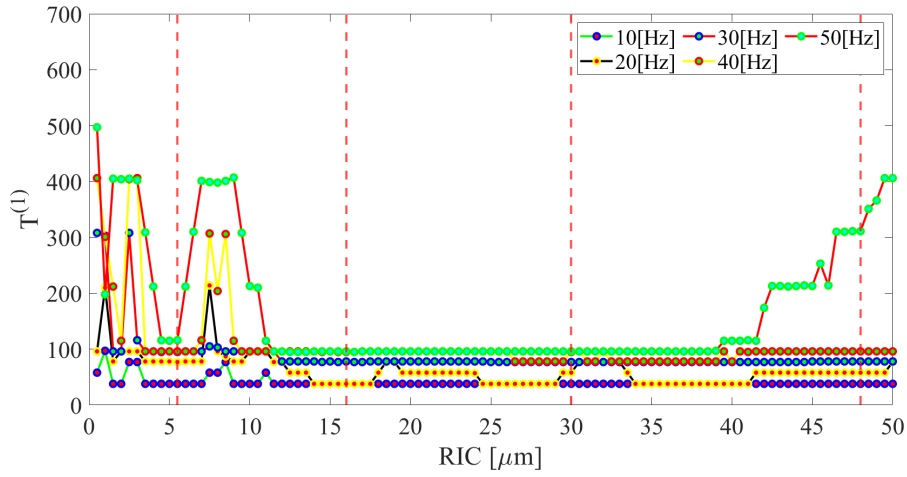
Figure 7.28. *Results of Length of the Recurrence Time of the 1st type for the series of radial internal clearance.*
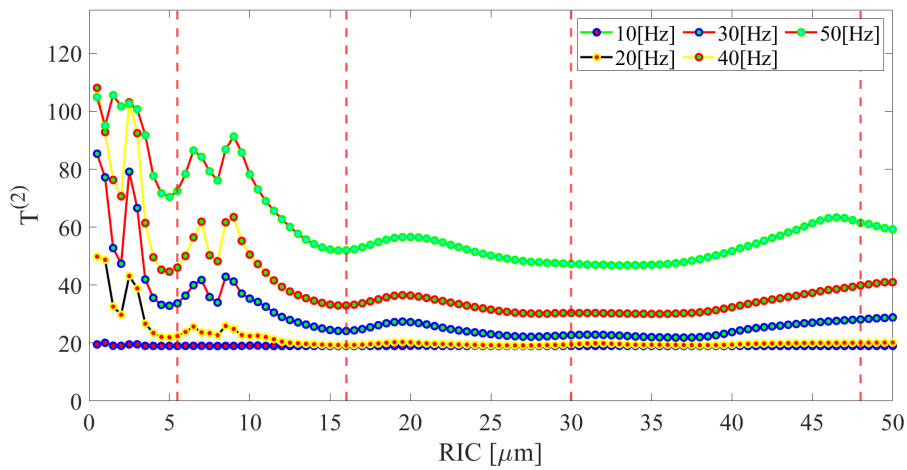
Figure 7.29. *Results of Length of the Recurrence Time of the 2nd type for the series of radial internal clearance.*
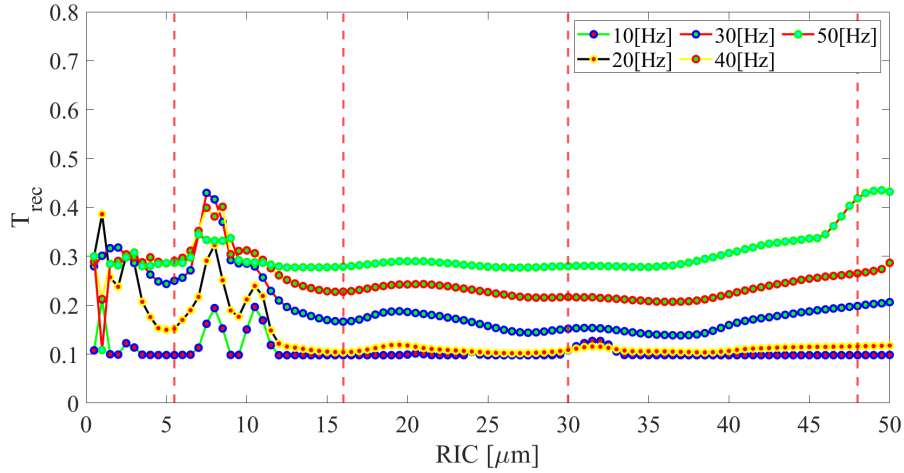
Figure 7.30. *Results of Recurrence Period Density Entropy for the series of radial internal clearance.*

fers from the calculated entropy, the quantificator is less sensitive to the change of clearance, but is shows the differences between rotational velocities. Its order is similar to the most previously calculated quantificators, it detects changes for small clearances and provides the information on qualitative change at bifurcation points.

The last quantificators are clustering, which refers to the probability that two recurrences of any state are also neighbors and transitivity, which allow to differentiate the periodic or chaotic dynamics of the system. The shape of both mentioned quantificators is similar it detects qualitative changes for small clearance and identifies the minima around the bifurcation points. They are sensitive to the change of the rotational velocity.

To sum up the conducted recurrence analysis, it helped to quantify the dynamic response of ball bearing obtained with the bifurcation analysis. Most of the recurrence quantificators are sensitive to the change of radial
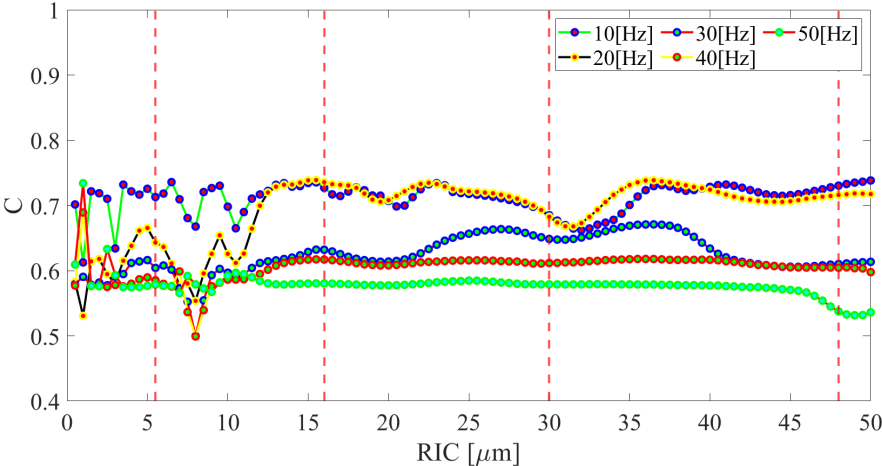
Figure 7.31. *Results of Clustering Coefficient for the series of radial internal clearance.*
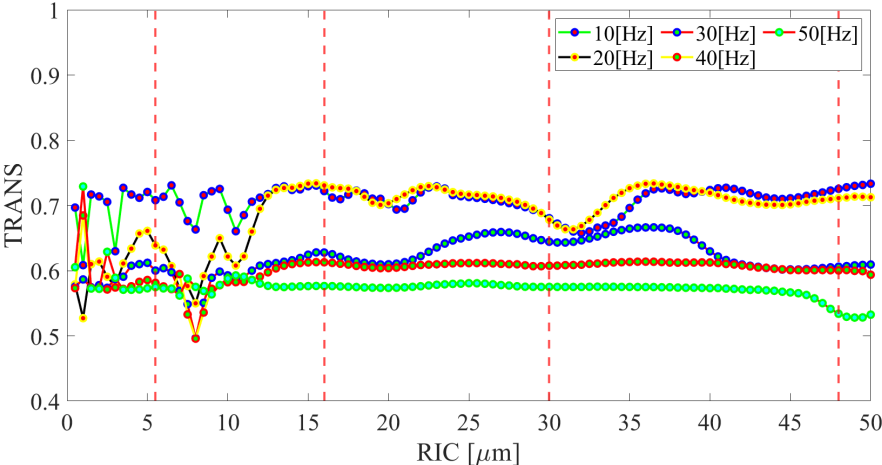
Figure 7.32. *Results of Transitivity for the series of radial internal clearance.*

clearance and allow to differentiate the cases by various rotational veloci-
ties. The characteristic areas can be observed at most of quantificators, i.e.
the quantificator's fluctuations are observed from the clearance range from 0
to 12[μm] and identyfing the first found bifurcation point at *RIC*=5.5[μm]
with vertical-based, recurrence time and probability-based quantificators.
In the clearance range up to the second bifurcation point at *RIC*=30[μm],
the response of almost all quantificators is constant with small fluctuations.
At the point of second bifurcation point, the response starts to have its min-
ima more or less remarked by some quantificators. The bearing's operation
in the range of big clearance is rather smooth without any specific quali-
tative changes. The application of the recurrence-based methods is not the
perfect tool for studying the dynamical response obtained with the mathe-
matical model, but it allowed for the initial analysis of ball bearing's dynam-
ics. In the next step, gained knowledge will be verified with the stochastic
data obtained with the experiment, the optimal clearance will be looked for
by observation of the minima around *RIC*=30[μm].

7.4.3   Experimental Verification

The aim of the experiment is to verify the dynamic response of ball bear-
ing obtained with the mathematical model. The test was conducted for 10
different bearings of the same type with different radial internal clearance,
which was adjusted according to the experimental procedure described in
Chapter 6. In Figures 7.33-7.35 the exemplary normalized time series of
acceleration signals are presented. At a first glance, there is no visible dif-
ference between cases with various radial clearance values except amplitude
and peaks distribution. The ball bearing's operation in the experiment has
not constant and strictly periodic response, that is why the detailed inves-
tigation in short signal windows with the recurrence analysis is justified.
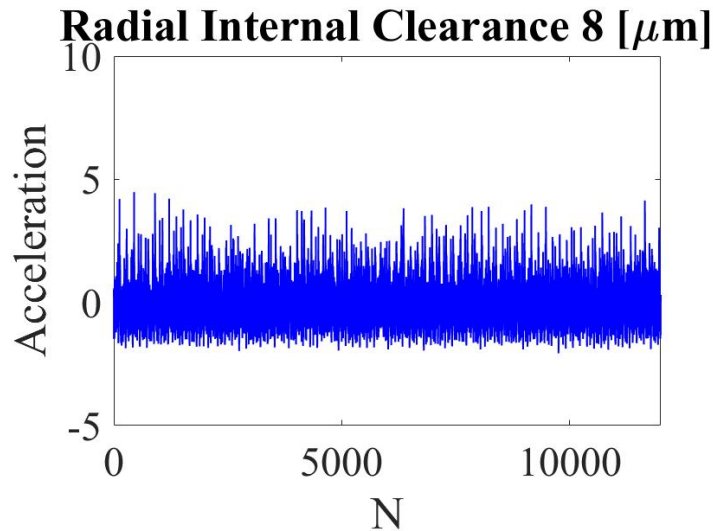
Figure 7.33. *Normalized acceleration times series for RIC=8[μm] in Bearing 1 and the operational velocity n=600[rpm].*

The time series in Figures 7.33-7.35 is only the short intervals of long time-series, the presented fragments consisting of 12000 data points are divided into smaller parts of 3000 data points (in time domain corresponding to the time t=1.92s) for which the phase space reconstruction is conducted.

In Figures 7.36-7.38, the obtained recurrence plots (RPs) are presented for earlier mentioned cases for Bearing 1, which at first glance look homogeneous. The interpretation of RP matrices is very demanding and requires a lot of experience, the mutual parts of results are isolated points corresponding to the close states, diagonal lines denoting close states for some time, and vertical lines referring to the trapping of the bearing in one state for a specific time. Regarding the phase-space reconstruction of matrices for all studied bearings the found embedding dimension m=3, while the time delay was the minimum for each case and was differing in the range τ=7-10. The threshold ε is based on constant recurrence rate *RR*.
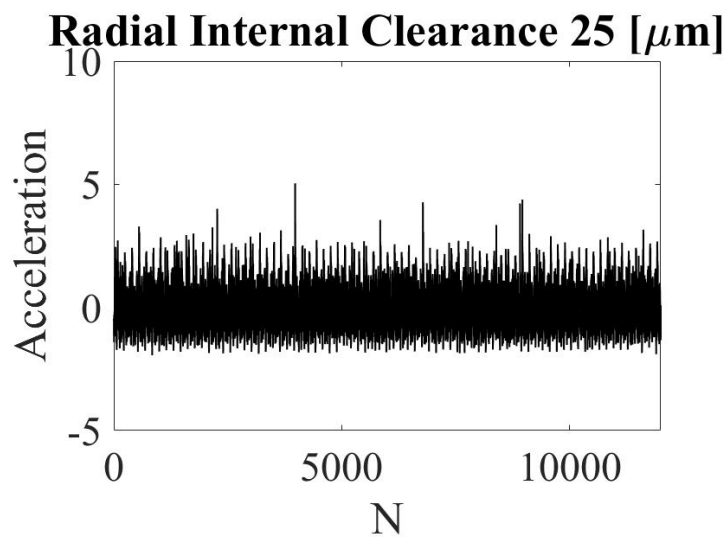
Figure 7.34. *Normalized acceleration times series for RIC=25[μm] in Bearing 1 and the operational velocity n=600[rpm].*
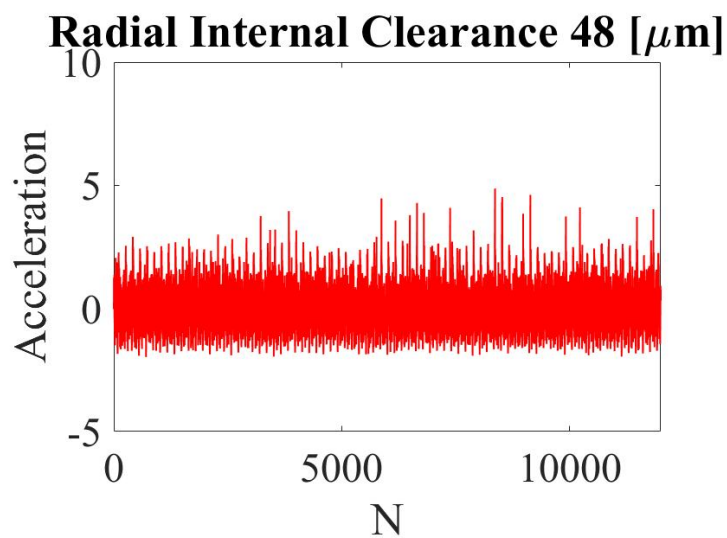
Figure 7.35. *Normalized acceleration times series for RIC=48[μm] in Bearing 1 and the operational velocity n=600[rpm].*

Table 7.9. *The parameters for the reconstruction of recurrence plots (RPs) for experimental data by the constant value of recurrence rate, RR = 0.05*

Time delay τ	Embedding dimension m	Threshold ε
7-10	3	based on the constant *RR*
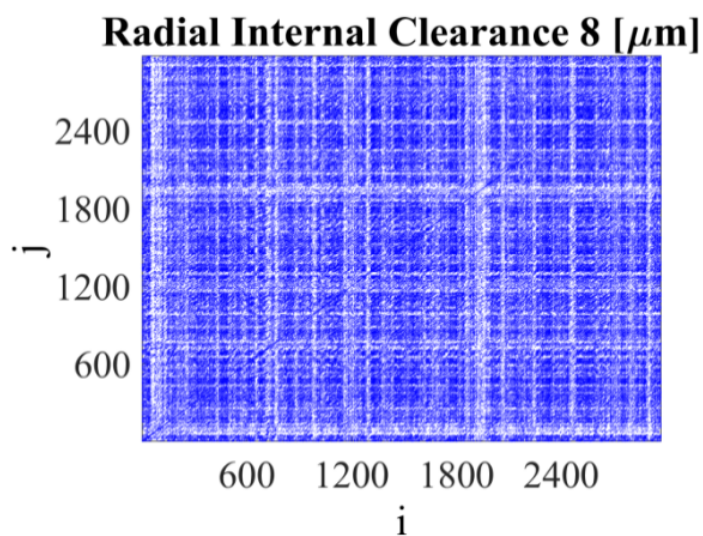
Figure 7.36. *Recurrence plot for RIC=8[µm] in Bearing 1 and the operational velocity n=600[rpm].*
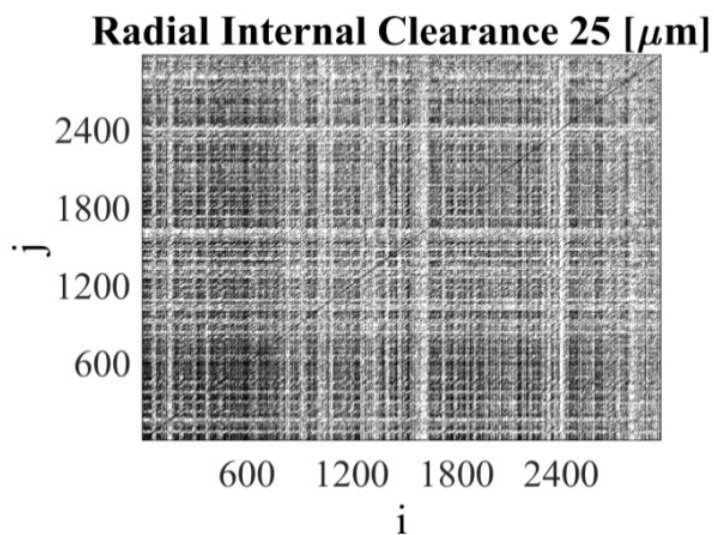
Figure 7.37. *Recurrence plot for RIC=25[μm] in Bearing 1 and the operational velocity n=600[rpm].*
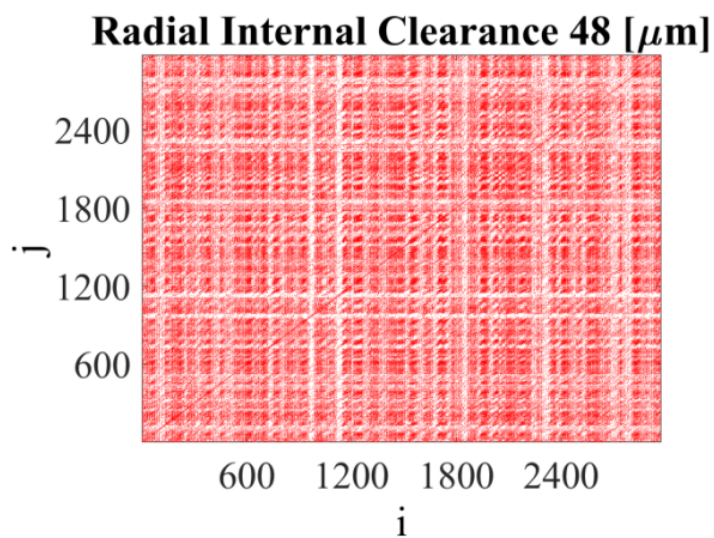
Figure 7.38. *Recurrence plot for RIC=48[μm] in Bearing 1 and the operational velocity n=600[rpm].*

Despite filtering of experimental signals it is hard to distinguish the pure dominating frequency in the spectra, so the information on frequencies is buried in the spectra. In the maps, the period of the signal cannot be found, which could be observed with equidistant diagonal lines. In this case to recognize minor changes in the dynamics of ball bearing with variable radial clearance, the recurrence quantification analysis is applied. Following the observations foudn with the mathematical model, it is worth evaluating the sensitivity of all calculated recurrence quantificators to the change of radial clearance in the batch of 10 self-aligning ball bearings and choose the best one, by which it is possible to estimate the bearing's optimal working condition referring to the clearance value. Referring to the output from the mathematical model, the minima was observed around the second bifurcation point at RIC=30[μm], and this minima with recurrence quantificators will be looked for with some tolerance caused by the thermal effects, the calculated clearance reduction for RIC=25[μm] and RIC=32[μm] was changing from around 2[μm] to 3.5[μm] depending on the operational velocity. To consider mentioned clearance range, the quadratic function fitting to the obtained mean values of qunatificators is applied (Figures 7.39-7.43) comparing fitting to the entire range of clearance (all 6 values) and by neglecting the smallest and the biggest (4 middle clearance values). The red line refers to the fitting to 4 middle clearance values, while the blue one corresponds to the entire range of considered clearance values. The motivation of showing two fittings is the fact that for considered extreme clearances, there is strong influence by external physical factors taking the role over pure rolling. For small values of clearance, there is the strong influence of frictional forces, while by big value the freedom of alignment of bearing's assembly allows to free and uncontrolled movement of rolling elements. We point out the sensitivity of quantificator if the found minima lie on the range for normal
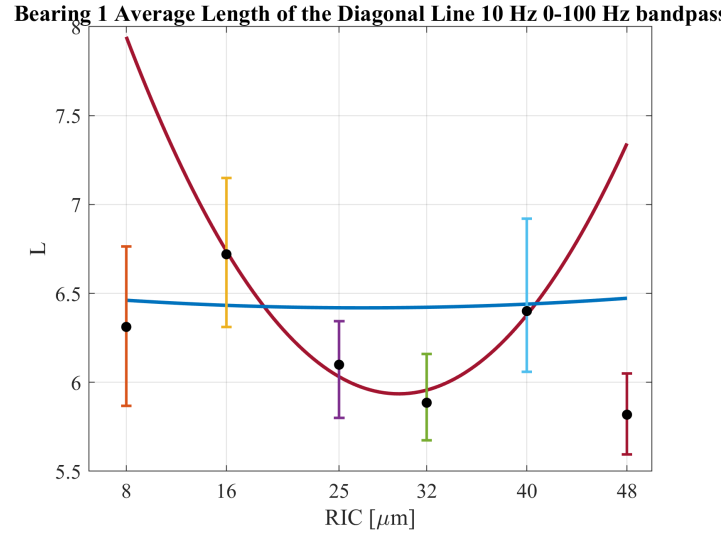
Figure 7.39. *Average length of the diagonal line from the experimental data for Bearing 1 and the rotational velocity n=10[Hz].*

clearance, the calculations are performed for all 10 bearings and 5 different operational velocities considered in the experiment.

The results of sensitivity analysis are collected in Table 6.9 and they are presented in the percentage domain. Exemplary the sensitivity at the 100% level corresponds to the situation when in case of 10 bearings and by the same operational velocity, observed minima for specific quantificator was in the range of normal clearance. Referring to the sensitivity of recurrence quantificators, the average accuracy is equal to 73.33% while referring to the operational velocity is at a similar level of 73.50%. This observation allows for the identification of optimal working conditions by normal clearance. Especially, three quantificators characterize with high accuracy, namely entropy *ENTR*, trapping time *TT*, and recurrence period density entropy *RPDE*. Other quantificators with an efficiency higher than average can be as well the powerful tool in the identification of optimal
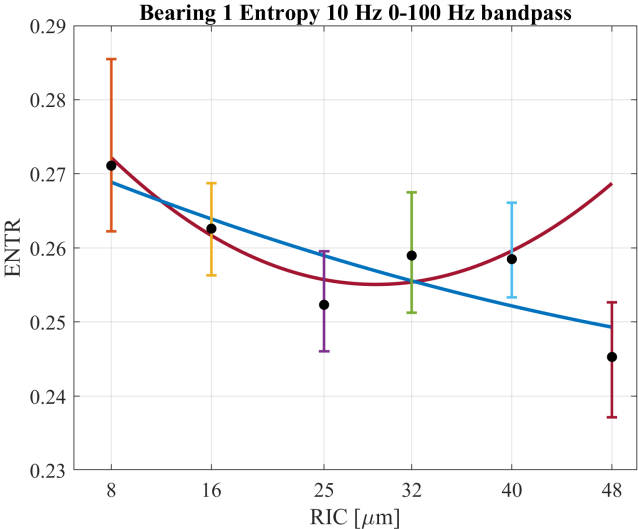
Figure 7.40. *Entropy from the experimental data for Bearing 1 and the rotational velocity n=10[Hz].*
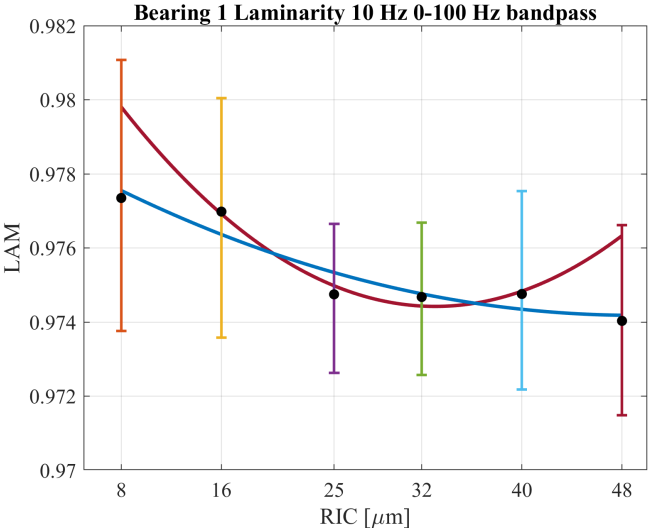
Figure 7.41. *Laminarity from the experimental data for Bearing 1 and the rotational velocity n=10[Hz].*
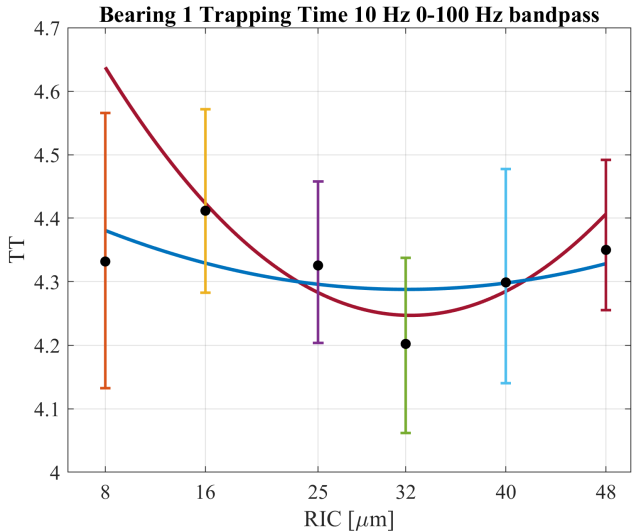
Figure 7.42. *Trapping Time from the experimental data for Bearing 1 and the rotational velocity n=10[Hz].*
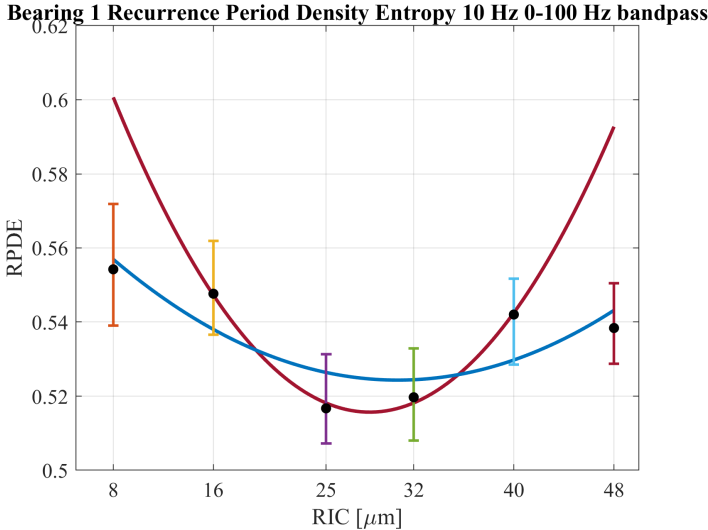
Figure 7.43. *Recurrence Period Density Entropy from the experimental data for Bearing 1 and the rotational velocity n=10[Hz].*

Table 7.10. *Sensitivity of recurrence quantificators to the optimal working conditions due to the radial internal clearance.*

RQA	10Hz	20Hz	30Hz	40Hz	50Hz	Sensitivity percentage
DET	80%	50%	20%	60%	80%	58%
L	70%	70%	30%	70%	90%	66%
L_{max}	80%	60%	70%	80%	80%	74%
ENTR	90%	70%	60%	70%	100%	78%
LAM	90%	60%	60%	90%	80%	76%
TT	80%	80%	60%	90%	100%	82%
V_{max}	70%	70%	70%	90%	90%	78%
$T^{(1)}$	80%	70%	90%	80%	60%	76%
$T^{(2)}$	60%	60%	60%	80%	90%	70%
RPDE	80%	70%	80%	100%	100%	86%
CLS	90%	50%	60%	90%	50%	68%
TRANS	90%	50%	60%	90%	50%	68%

clearance, but we focus our research on the three the best one and discuss their reference to the bearing's dynamics.

Entropy refers to the complexity of the signal, i.e. number of additional frequencies in the spectra, level of periodicity, or level of white noise in the signal. Despite relatively small differences in the mean value of entropy between various radial clearances (Figure 7.40), the minima are visible at RIC=30[μm]. The small value of entropy can denote the smallest influence of external factors such as increased friction caused by the tight alignment of rolling surfaces as well as the coupling with the test rig, i.e. external vibrations. A relatively high level of entropy by almost all velocities allows applying this quantificator for the estimation of seamless bearing operation undisturbed by external factors.

The best accuracy of quantificators based on the vertical lines has trapping time, which refers to the specific time when the system is trapped in. Similar to the entropy, the trapping time has its minima in the range of normal clearance what can signalize the optimal bearing's operation. A high level of TT on extreme clearance values can refer to the influence of increased frictional forces (C2 clearance) and increased vibrations caused by the loose alignment of rolling elements (C3 clearance and bigger). Referring to the normal clearance, the rotating elements are in the finest position and have freedom of rotation with relatively low amplitudes of vibrations, the stick and slip [146] or balls trapping [32] phenomena are then not observed.

The last of discussed quantificators is recurrence period density entropy (RPDE), which similarly to Shannon entropy refers to the complexity of the response. The measure estimates the average uncertainty of the signal, if its level is smaller, then the level of periodicity of the signal is higher. The quantificator with the highest accuracy identifies the minima at normal clearance by almost all considered operational velocities. Like in the case of previously discussed quantificators, the minima are mostly found for a range of 27-32[μm], that bearing is not affected by other external factors. The clearance from this normal clearance range can be perceived as an optimal one.

Based on the presented accuracy level of recurrence quantificators, it can be stated that some of them are able to quantify and identify the ball bearing's dynamics due to the variable radial internal clearance. Referring to Figures 7.39-7.43, the error range for quantificators is the smallest for denoting the range of normal clearance. This fact suggests additionally well the seamless bearing's operation.

7.5 Summary

To sum up the conducted simulations with the mathematical model and its experimental verification, it can be stated that with help of the recurrence analysis it is possible to refer it to the ball bearing's dynamics with the different radial internal clearance. The application especially of the recurrence quantification analysis showed its sensitivity to the minor changes in the bearing's dynamics due to the radial clearance. Results obtained with the mathematical model showed bifurcation points corresponding to the optimal bearing operation by specific clearance. Owing to the conducted experiment for the same type of 10 bearings, considered in the mathematical model, a similar dynamic behaviour was searched for. The aim of performed sensitivity analysis was to make to comparative analysis between the mathematical model and the experiment and to find by how many bearings, the optimal clearance will be observed. The result of this investigation was a selection of 3 the most sensitive quantificators to the change of radial clearance, i.e. Entropy $ENTR$, Trapping Time TT, and Recurrence Period Density Entropy $RPDE$. Mentioned quantificators identified the optimal clearance with around 80% accuracy. The proposed method is very sensitive to the change of the dynamics of the considered system, and it succeeded in the case of analysis of the dynamical response of ball bearings.

o

CONCLUSIONS AND OUTLOOK OF FURTHER RESEARCH

In the last chapter, the main achievements and contributions to knowledge about the dynamics of rolling-element bearings are presented. In the beginning, the proof of the thesis is discussed and next, the major achievements of the thesis are described dividing them into outcomes obtained with the derived nonlinear mathematical model and novelties introduced to the experimental analysis. The chapter is finished with goals for future work and the development of the methodology presented in the dissertation.

8.1 Proof of the thesis

The research thesis of the dissertation was following: "The diagnostics of the dynamical response of rolling-element bearing due to the radial internal clearance is possible to describe in a quantitative way with help of recurrence quantificators". The study of the nonlinear mathematical model for

double-row self-aligning ball bearing showed the variable character of its dynamical response caused by different values of radial internal clearance. This observation motivated me to conduct the experimental verification with a batch of 10 bearings. For prooving the research thesis, the recurrence analysis method was applied, which is the novelty in the diagnostics of mechanical systems. Owing to the calculation of recurrence quanitificators, it was possible to find its distribution due to different radial internal clearance.

8.2 Conclusions regarding the scientific objective of the thesis

This work is an approach to use recurrence-based methods on the dynamical response of the self-aligning ball bearing with different radial internal clearance. The bifurcation analysis of the mathematical model of the bearing showed the qualitative influence of the radial internal clearance on the dynamics of rolling-element bearing, which motivated me to conduct the experiment with real bearings. The proposed methodology with the application of the recurrence quantification analysis (RQA) led to observing the specific dynamical response of the bearing with different clearance referring to its variable dynamics. The application of the recurrence plots coupled with the image processing could be used in the online-radial clearance monitoring in the bearing, while the recurrence quantificators describe the bearings' dynamics in a quantitative way. The developed method with special measuring equipment and fast-data computing could be used in industrial practice.

8.3 Novelties and contribution to knowledge

The main aspects of novelty that have been demonstrated during the research project and within this report are summarised in this section. They are focused on the phenomena being researched, applied methodology and results obtained from the mathematical model and in the experiment:

8.3.1 Nonlinear mathematical model

- In the derived 2-DOF mathematical model of the double-row self-aligning ball bearing, the damping coefficient is changing in a linear way in the radial internal clearance domain. It was proved experimentally, that the damping coefficient is dependent on the clearance value. The introduced function allows getting rid of the unknown fluctuations in the recurrence quantification analysis [19]. Moreover, the damping coefficient function was changing for the specific operational velocity. The applied assumptions make the derived mathematical model more realistic.

- Another improvement of the mathematical model is the implementation of slightly variable clearance due to the design of the bearing. A separated cage holding each row of balls can affect the small changes in operational radial internal clearance. Another effect of minor variabilities of the clearance is the axial pre-load subjected with the axial nut from one side of the bearing.

- In the derived mathematical model of self-aligning ball bearing efforts was made to refer to the realistic response of the bearing. As one of the assumptions was the introduction of shape errors on rolling surfaces. Other aspects were the possibility to subject the external force

or the eccentricity of the shaft on which the bearing was mounted. The model was referred to as the real design of self-aligning ball bearing NTN 2309SK, and their real dimensions were considered for simulation.

8.3.2 Experimental verification

- Definitely, the precise measurement of reduced radial internal clearance after mounting is the innovative approach in the study. In the next step during the dynamical test, the temperature measurement on each ring allows estimating its reduction caused by the thermal effects due to the frictional forces. The measurement of the inner ring's temperature is subjected to an error, that it is placed in the close distance to rotating ring, however, in future studies, the application of rotational connector seated on the shaft and sticked to the bearing's face is planned.

- Unquestionable advantage of the experiment is the possibility to control the value of radial internal clearance in a wide range in one bearing, i.e. its manual reduction is possible with applied axial pre-load subjected to the locknut. This operation allows avoiding the influence of variable factors such as different shape errors, amount of lubrication, or assembly quality in two different bearings. Usually, the research on the influence of radial internal clearance was conducted with two different bearings with pre-defined clearance during the assembly process, however, the manufacturing quality of their rolling surfaces could be completely different, which could mix with the specific influence of the clearance on the bearing's dynamics.

- The study on the dynamics was conducted on 10 bearings, in order to cross-check the experiment for randomly chosen bearings. Such choice of bearings for the experiment increases the resiliency of the test due to consideration of the different quality of rolling surfaces of studied bearings. Moreover, during the dynamical test, the shaft's eccentricity was measured with the eddy current sensor for different rotational velocities. This fact is usually omitted, however, it influences the bearing's dynamics as the external vibration source coming from the test rig.

8.3.3 Methodology

- The calculation of the recurrence quantificators for the experimental time-series was based on the big random sample from which the average value was calculated. This action allowed for observation of the quantificators distribution and eliminate the influence of transient states in the bearing for further consideration.

- Based on the observation of the optimal clearance in the mathematical model response, the same conditions were observed for many cases in the experiment for different bearings. The optimal clearance was found around 30 μm, which refers to the normal clearance class. By mentioned value of radial clearance, the vibrations with the smallest amplitude were observed both in the mathematical model and in the experimental verification.

- The sensitivity analysis was conducted to find the most sensitive recurrence quantificators, by which the qualitative and quantitative changes were observed by the optimal clearance. Three of the best quantificators were found, i.e. entropy $ENTR$, trapping time TT, and recurrence

period density entropy *RPDE*. The overall sensitivity of mentioned quantificators was over 80%, while for all considered quantificators, the sensitivity was over 70%. It proves, that the recurrence quantificators can be quite good indicators of the bearing's dynamics due to different radial internal clearance.

8.4 Conclusions on the further application of the proposed methodology

- One of the factors influencing the changes of the radial internal clearance is subjected external load to the bearing. During the initial tests, the case without subjected load was considered, however in the future, the tests with external load are planned. Definitely, this action will change the dynamic response and the thermal changes in studied bearing.

- In the double-row self-aligning ball bearing (SABB) with conical bore was studied in the experiment and in the mathematical model. Analyzed bearing is specific, that it was possible to control in it the value of the radial clearance in a wide range, however in the future experiment standard single row ball bearings and are going to be studied.

- As the outcome of the study was the sensitivity of chosen recurrence quantificators for identification of radial internal clearance in the bearing. Definitely, a big advantage would be the application of the Artificial Intelligence (AI) methods for automatic classification of operational clearance with the quantificators. Based on the already obtained quantificators, the AI methods will be considered for future studies on the dynamics of the bearing with different radial clearance.

- Owing to the conducted experiment, the recurrence analysis proved its accuracy in the identification of the radial clearance. The results obtained will be compared in the future with diagnostics features applied to the rotational systems.

- The derived mathematical model can still be developed to reflect a more realistic operation of the bearing introducing the stochasticity to the system. One of the solutions can be the application of Monte Carlo simulation to chosen bearing's parameters, such as clearance in some range or shape errors propagating with the bearing's operation. Bearing's dynamics in the reality is unpredictable, which is why the consideration of the stochasticity in the model is justified.

8.5 Published research

The parts of the research presented in the thesis are contained in the series of own published papers regarding the diagnostics of the rotational systems. The research on the diagnostics on the damage of the planetary gearbox and radial internal clearance with recurrences was initiated with paper [20]. In the next conference, paper [96], the results obtained with the recurrence analysis were compared with kurtosis and neural networks. The initial analysis with the recurrence quantification analysis and experimental data was described in the following paper [17]. The next research was considering the derivation of the mathematical model for the ball bearing and application of recurrence-based methods for the analysis of the dynamics [16, 19]. Based on the results obtained, the research will be continued and its results will be presented in future joint papers.

o

Bibliography

[1] Bearing Assembly. https://commons.wikimedia.org/wiki/%20w/index.php?title=File:Adapter-sleeve_DIN5415_assembly_ex.png&oldid=245907301. Accessed: 2021-08-15.

[2] Contact in Rolling-element bearings. https://www.linearmotiontips.com/what-are-hertz-contact-stresses-how-do-they-affect/. Accessed: 2021-08-15.

[3] Cross-Recurrence Plot Matlab Toolbox. https://tocsy.pik-potsdam.de/CRPtoolbox/. Accessed: 2021-09-15.

[4] Damping coefficient. https://evolution.skf.com/damping-in-a-rolling-bearing-arrangement/. Accessed: 2021-08-15.

[5] Design of the plummer block. https://www.timken.com/resources/snt-plummer-blocks-brochure/. Accessed: 2021-08-15.

[6] Differences between Rolling-element bearings. https://koyo.jtekt.co.jp/en/2019/09/column01-04.html. Accessed: 2021-08-15.

[7] Internal Clearance. https://koyo.jtekt.co.jp/en/support/bearing-knowledge/10-0000.html. Accessed: 2021-08-15.

[8] Radial internal clearance classes. https://shop.eriks.nl/en/bearing-clearance/. Accessed: 2021-08-15.

[9] Types of Internal Clearance. https://www.skf.com/group/products/rolling-bearings/principles-of-rolling-bearing-selection/

`bearing-selection-process/bearing-execution/`
`selecting-internal-clearance-or-preload`.   Accessed:
2021-08-15.

[10] Weibull   Distribution.   `https://www.oxfordreference.com/`
`view/10.1093/oi/authority.20110803121608170`.   Accessed:
2021-08-15.

[11] ABDI, H., AND WILLIAMS, L. Principal component analysis. *Wiley Interdisciplinary Reviews: Computational Statistics 2*, 4 (2010), 433–459.

[12] ADAMCZAK, S., AND ZMARZŁY, P. Influence of raceway waviness on the level of vibration in rolling-element bearings. *Bulletin of the Polish Academy of Sciences: Technical Sciences 65*, 4 (2017), 541–551.

[13] AFSAR, O., TIRNAKLI, U., AND MARWAN, N. Recurrence quantification analysis at work: Quasi-periodicity based interpretation of gait force profiles for patients with parkinson disease. *Scientific Reports 8*, 1 (2018).

[14] AI, Y.-T., GUAN, J.-Y., FEI, C.-W., TIAN, J., AND ZHANG, F.-L. Fusion information entropy method of rolling bearing fault diagnosis based on n-dimensional characteristic parameter distance. *Mechanical Systems and Signal Processing 88* (2017), 123–136.

[15] AL-BADOUR, F., SUNAR, M., AND CHEDED, L. Vibration analysis of rotating machinery using time–frequency analysis and wavelet techniques. *Mechanical Systems and Signal Processing 25*, 6 (2011), 2083–2101. Interdisciplinary Aspects of Vehicle Dynamics.

[16] AMBROŻKIEWICZ, B., LITAK, G., GEORGIADIS, A., MEIER, N., AND GASSNER, A. Analysis of dynamic response of a two degrees of freedom (2-dof) ball bearing nonlinear model. *Applied Sciences 11*, 2 (2021).

[17] AMBROŻKIEWICZ, B., SYTA, A., MEIER, N., LITAK, G., AND GEORGIADIS, A. Radial internal clearance analysis in ball bearings. *Eksploatacja i Niezawodnosc 23*, 1 (2021), 42–54.

[18] AMBROZKIEWICZ, B., GUO, Y., LITAK, G., AND WOLSZCZAK, P. Dynamical response of a planetary gear system with faults using recurrence statistics. vol. 228, pp. 177–185.

[19] AMBROZKIEWICZ, B., LITAK, G., GEORGIADIS, A., SYTA, A., MEIER, N., AND GASSNER, A. Effect of radial clearance on ball bearing's dynamics using a 2-dof model. *International Journal of Simulation Modelling 20*, 3 (2021), 513–524.

[20] AMBROŻKIEWICZ, B., MEIER, N., GUO, Y., LITAK, G., AND GEORGIADIS, A. Recurrence-based diagnostics of rotary systems. 012014.

[21] ATTOUI, I., FERGANI, N., BOUTASSETA, N., OUDJANI, B., AND DELIOU, A. A new time–frequency method for identification and classification of ball bearing faults. *Journal of Sound and Vibration 397* (2017), 241–265.

[22] BALAKRISHNAN, V., NICOLIS, G., AND NICOLIS, C. Recurrence time statistics in deterministic and stochastic dynamical systems in continuous time: A comparison. *Phys. Rev. E 61* (Mar 2000), 2490–2499.

[23] BECKMANN, C., DELUCA, M., DEVLIN, J., AND SMITH, S. Investigations into resting-state connectivity using independent component analysis. *Philosophical Transactions of the Royal Society B: Biological Sciences 360*, 1457 (2005), 1001–1013.

[24] BEN ALI, J., CHEBEL-MORELLO, B., SAIDI, L., MALINOWSKI, S., AND FNAIECH, F. Accurate bearing remaining useful life prediction based on Weibull distribution and artificial neural network. *Mechanical Systems and Signal Processing 56-57* (2015), 150–172.

[25] CAO, M., AND XIAO, J. A comprehensive dynamic model of double-row spherical roller bearing—model development and case studies on surface defects, preloads, and radial clearance. *Mechanical Systems and Signal Processing 22*, 2 (2008), 467–489.

[26] CASTANEDO, F. A review of data fusion techniques. *The Scientific World Journal 2013* (2013).

[27] CASTEJÓN, C., LARA, O., AND GARCÍA-PRADA, J. Automated diagnosis of rolling bearings using mra and neural networks. *Mechanical Systems and Signal Processing 24*, 1 (2010), 289–299.

[28] CHANGQING, B., AND QINGYU, X. Dynamic model of ball bearings with internal clearance and waviness. *Journal of Sound and Vibration 294*, 1 (2006), 23–48.

[29] CHEN, L., ÇETIN, M., AND WILLSKY, A. Distributed data association for multi-target tracking in sensor networks. vol. 1, pp. 9–16.

[30] CHENG, L., LIU, D., WANG, Y., AND CHEN, A. Load distribution and contact of axle box bearings in electric multiple units. *International Journal of Simulation Modelling 18*, 2 (2019), 290–301.

[31] CHENGLIN, W., FEIYA, L., ZHEJING, B., AND MEIQIN, L. A review of data driven-based incipient fault diagnosis.

[32] COLAS, G., SAULOT, A., MICHEL, Y., FILLETER, T., AND MERSTALLINGER, A. Experimental analysis of friction and wear of self-lubricating composites used for dry lubrication of ball bearing for space applications. *Lubricants 9*, 4 (2021).

[33] CRISAN, D., AND DOUCET, A. A survey of convergence results on particle filtering methods for practitioners. *IEEE Transactions on Signal Processing 50*, 3 (2002), 736–746.

[34] CUI, L., HUANG, J., ZHANG, F., AND CHU, F. Hvsrms localization formula and localization law: Localization diagnosis of a ball bearing outer ring fault. *Mechanical Systems and Signal Processing 120* (2019), 608–629.

[35] CUI, L., AND WANG, Q. S. On the bifurcation of periodic motion of rotor ball bearing system considering five degrees of freedom. In *Advances in Manufacturing Science and Engineering V* (7 2014), vol. 945 of *Advanced Materials Research*, Trans Tech Publications Ltd, pp. 707–710.

[36] DELGADO, M., CIRRINCIONE, G., ESPINOSA, A. G., ORTEGA, J. A., AND HENAO, H. Dedicated hierarchy of neural networks applied to bearings degradation assessment. In *2013 9th IEEE International Symposium on Diagnostics for Electric Machines, Power Electronics and Drives (SDEMPED)* (2013), pp. 544–551.

[37] DEMPSTER, A. P. *A Generalization of Bayesian Inference.* Springer Berlin Heidelberg, Berlin, Heidelberg, 2008, pp. 73–104.

[38] DONNER, R., BALASIS, G., STOLBOVA, V., GEORGIOU, M., WIEDERMANN, M., AND KURTHS, J. Recurrence-based quantification of dynamical complexity in the earth's magnetosphere at geospace storm timescales. *Journal of Geophysical Research: Space Physics 124*, 1 (2019), 90–108.

[39] DONNER, R. V., ZOU, Y., DONGES, J. F., MARWAN, N., AND KURTHS, J. Recurrence networks—a novel paradigm for nonlinear time series analysis. *New Journal of Physics 12*, 3 (mar 2010), 033025.

[40] ECKMANN, J.-P., OLIFFSON KAMPHORST, O., AND RUELLE, D. Recurrence plots of dynamical systems. *EPL 4*, 9 (1987), 973–977.

[41] ELSAYED, S., ELKHATIB, A., AND YAKOUT, M. Vibration modal analysis of rolling element bearing.

[42] FAN, X., LIANG, M., YEAP, T., AND KIND, B. A joint wavelet lifting and independent component analysis approach to fault detection of rolling element bearings. *Smart Materials and Structures 16*, 5 (2007), 1973–1987.

[43] FORTMANN, T. E., BAR-SHALOM, Y., AND SCHEFFE, M. Multitarget tracking using joint probabilistic data association. vol. 2, pp. 807–812.

[44] FRASER, A. M., AND SWINNEY, H. L. Independent coordinates for strange attractors from mutual information. *Phys. Rev. A 33* (Feb 1986), 1134–1140.

[45] FRISWELL, M., LITAK, G., AND SAWICKI, J. Crack identification in rotating machines with active bearings. pp. 2843–2855.

[46] GANGIL, M., PRADHAN, M., AND PUROHIT, R. Review on modelling and optimization of electrical discharge machining process using modern techniques. *Materials Today: Proceedings 4*, 2, Part A (2017), 2048–2057. 5th International Conference of Materials Processing and Characterization (ICMPC 2016).

[47] GAO, J., CAO, Y., GU, L., HARRIS, J., AND PRINCIPE, J. Detection of weak transitions in signal dynamics using recurrence time statistics. *Physics Letters A 317*, 1 (2003), 64–72.

[48] GAO, J. B. Recurrence time statistics for chaotic systems and their applications. *Phys. Rev. Lett. 83* (Oct 1999), 3178–3181.

[49] GAO, P., CHEN, Y., AND HOU, L. Nonlinear thermal behaviors of the inter-shaft bearing in a dual-rotor system subjected to the dynamic load. *Nonlinear Dynamics 101*, 1 (2020), 191–209.

[50] GAO, S., CHATTERTON, S., NALDI, L., AND PENNACCHI, P. Ball bearing skidding and over-skidding in large-scale angular contact

ball bearings: Nonlinear dynamic model with thermal effects and experimental results. *Mechanical Systems and Signal Processing 147* (2021).

[51] GOMEZ, J., BOURDON, A., ANDRÉ, H., AND RÉMOND, D. Modelling deep groove ball bearing localized defects inducing instantaneous angular speed variations. *Tribology International 98* (2016), 270–281.

[52] GORSKI, G., LITAK, G., MOSDORF, R., AND RYSAK, A. Two phase flow bifurcation due to turbulence: transition from slugs to bubbles. *European Physical Journal B 88*, 9 (2015).

[53] GREDILLA, A., FDEZ-ORTIZ DE VALLEJUELO, S., DE DIEGO, A., MADARIAGA, J., AND AMIGO, J. Unsupervised pattern-recognition techniques to investigate metal pollution in estuaries. *TrAC Trends in Analytical Chemistry 46* (2013), 59–69.

[54] GROOT, V., REZAEE, N., WU, W., CAMERON, J., FISHMAN, E., HRUBAN, R., WEISS, M., ZHENG, L., WOLFGANG, C., AND HE, J. Patterns, timing, and predictors of recurrence following pancreatectomy for pancreatic ductal adenocarcinoma. *Annals of Surgery 267*, 5 (2018), 936–945.

[55] GUNDUZ, A., DREYER, J. T., AND SINGH, R. Effect of bearing preloads on the modal characteristics of a shaft-bearing assembly: Experiments on double row angular contact ball bearings. *Mechanical Systems and Signal Processing 31* (2012), 176–195.

[56] GUO, J., SHI, Z., LI, H., ZHEN, D., GU, F., AND BALL, A. D. Early fault diagnosis for planetary gearbox based wavelet packet energy and modulation signal bispectrum analysis. *Sensors 18*, 9 (2018).

[57] GUO, J., ZHEN, D., LI, H., SHI, Z., GU, F., AND BALL, A. Fault feature extraction for rolling element bearing diagnosis based on a multi-stage noise reduction method. *Measurement 139* (2019), 226–235.

[58] HAMADACHE, M., AND LEE, D. Principal component analysis based signal-to-noise ratio improvement for inchoate faulty signals: Application to ball bearing fault detection. *International Journal of Control, Automation and Systems 15*, 2 (2017), 506–517.

[59] HARSHA, S. Non-linear dynamic response of a balanced rotor supported on rolling element bearings. *Mechanical Systems and Signal Processing 19*, 3 (2005), 551–578.

[60] HARSHA, S. Nonlinear dynamic response of a balanced rotor supported by rolling element bearings due to radial internal clearance effect. *Mechanism and Machine Theory 41*, 6 (2006), 688–706.

[61] HARSHA, S., SANDEEP, K., AND PRAKASH, R. The effect of speed of balanced rotor on nonlinear vibrations associated with ball bearings. *International Journal of Mechanical Sciences 45*, 4 (2003), 725–740.

[62] HIRANO, F., AND TANOUE, H. Motion of a ball in a ball bearing. *Wear 4*, 3 (1961), 177–197.

[63] HOCHMANN, D., AND BECHHOEFER, E. Envelope bearing analysis: Theory and practice. vol. 2005, pp. 3658 – 3666.

[64] HOSEINZADEH, M. S., KHADEM, S. E., AND SADOOGHI, M. S. Modifying the hilbert-huang transform using the nonlinear entropy-based features for early fault detection of ball bearings. *Applied Acoustics 150* (2019), 313–324.

[65] HUANG, S.-J., CHIU, N.-H., AND CHEN, L.-W. Integration of the grey relational analysis with genetic algorithm for software effort estimation. *European Journal of Operational Research 188*, 3 (2008), 898–909.

[66] HYVÄRINEN, A., AND OJA, E. Independent component analysis: Algorithms and applications. *Neural Networks 13*, 4-5 (2000), 411–430.

[67] ILIEV, A., SCORDILIS, M., PAPA, J., AND FALCÃO, A. Spoken emotion recognition through optimum-path forest classification using glottal features. *Computer Speech and Language 24*, 3 (2010), 445–460.

[68] IWANIEC, J., AND IWANIEC, M. Heart work analysis by means of recurrence-based methods. *Diagnostyka 18*, 4 (2017), 89–96.

[69] IWANIEC, J., UHL, T., STASZEWSKI, W., AND KLEPKA, A. Detection of changes in cracked aluminium plate determinism by recurrence analysis. *Nonlinear Dynamics 70*, 1 (2012), 125–140.

[70] JEDLIŃSKI, ., AND JONAK, J. A disassembly-free method for evaluation of spiral bevel gear assembly. *Mechanical Systems and Signal Processing 88* (2017), 399–412.

[71] JIANG, Z.-Q., WANG, G.-J., CANABARRO, A., PODOBNIK, B., XIE, C., STANLEY, H., AND ZHOU, W.-X. Short term prediction of extreme returns based on the recurrence interval analysis. *Quantitative Finance 18*, 3 (2018), 353–370.

[72] JOLLIFE, I., AND CADIMA, J. Principal component analysis: A review and recent developments. *Philosophical Transactions of the Royal Society A: Mathematical, Physical and Engineering Sciences 374*, 2065 (2016).

[73] KANKAR, P., SHARMA, S., AND HARSHA, S. Vibration based performance prediction of ball bearings caused by localized defects. *Nonlinear Dynamics 69*, 3 (2012), 847–875.

[74] KANKAR, P., SHARMA, S. C., AND HARSHA, S. Fault diagnosis of ball bearings using machine learning methods. *Expert Systems with Applications 38*, 3 (2011), 1876–1886.

[75] KANTZ, H., AND SCHREIBER, T. *Nonlinear Time Series Analysis*, 2 ed. Cambridge University Press, 2003.

[76] KENNEL, M. B., BROWN, R., AND ABARBANEL, H. D. I. Determining embedding dimension for phase-space reconstruction using a geometrical construction. *Phys. Rev. A 45* (Mar 1992), 3403–3411.

[77] KHONSARI, M., AND BOOSER, E. *Applied Tribology: Bearing Design and Lubrication: Second Edition*. 2008.

[78] KNEŽEVIĆ, I., ŽIVKOVIĆ, A., RACKOV, M., KANOVIĆ, Ž., BUL-JEVIĆ, A., ŠEJAT, M. B., AND NAVALUŠIĆ, S. Prediction of radial clearance based on bearing vibration using artificial neural network. *IOP Conference Series: Materials Science and Engineering 1009* (jan 2021), 012028.

[79] KONG, F., HUANG, W., JIANG, Y., WANG, W., AND ZHAO, X. A vibration model of ball bearings with a localized defect based on the hertzian contact stress distribution. *Shock and Vibration 2018* (2018).

[80] KUO, Y.-C., HSIEH, C.-T., YAU, H.-T., AND LI, Y.-C. Research and development of a chaotic signal synchronization error dynamics-based ball bearing fault diagnostor. *Entropy 16*, 10 (2014), 5358–5376.

[81] LANIADO-JCOME, E., MENESES-ALONSO, J., AND DIAZ-LPEZ, V. A study of sliding between rollers and races in a roller bearing with a numerical model for mechanical event simulations. *Tribology International 43*, 11 (2010), 2175–2182.

[82] LEI, Y., ZUO, M. J., HE, Z., AND ZI, Y. A multidimensional hybrid intelligent method for gear fault diagnosis. *Expert Systems with Applications 37*, 2 (2010), 1419–1430.

[83] LEITE, V. C. M. N., DA SILVA, J. G. B., DA SILVA, L. E. B., VELOSO, G. F. C., LAMBERT-TORRES, G., BONALDI, E. L., AND DE OLIVEIRA, L. E. L. Experimental bearing fault detection, identification, and prognosis through spectral kurtosis and envelope spectral analysis. *Electric Power Components and Systems 44*, 18 (2016), 2121–2132.

[84] LEÃO, L., CAVALINI, A., MORAIS, T., MELO, G., AND STEFFEN, V. Fault detection in rotating machinery by using the modal state observer approach. *Journal of Sound and Vibration 458* (2019), 123–142.

[85] LI, J., CAO, Y., YING, Y., AND LI, S. A rolling element bearing fault diagnosis approach based on multifractal theory and gray relation theory. *PLOS ONE 11*, 12 (12 2016), 1–16.

[86] LI, Y., XU, M., WANG, R., AND HUANG, W. A fault diagnosis scheme for rolling bearing based on local mean decomposition and improved multiscale fuzzy entropy. *Journal of Sound and Vibration 360* (2016), 277–299.

[87] LIN, J., HUANG, Z., WANG, Y., AND SHEN, Z. Selection of proper embedding dimension in phase space reconstruction of speech signals. *Journal of Electronics (China) 17* (04 2012), 161–169.

[88] LITAK, G., SYTA, A., GAJEWSKI, J., AND JONAK, J. Detecting and identifying non-stationary courses in the ripping head power consumption by recurrence plots. *Meccanica 45*, 4 (2010), 603–608.

[89] LITTLE, M., MCSHARRY, P., ROBERTS, S., COSTELLO, D., AND MOROZ, I. Exploiting nonlinear recurrence and fractal scaling properties for voice disorder detection. *BioMedical Engineering Online 6* (2007).

[90] LIU, J., XU, Y., WANG, L., XU, Z., AND TANG, C. Influence of the local defect distribution on vibration characteristics of ball

bearings [wplyw rozkladu wad lokalnych na charakterystyke drgan lozysk kulkowych]. *Eksploatacja i Niezawodnosc 21*, 3 (2019), 485–492.

[91] LU, Y., LI, Q., PAN, Z., AND LIANG, S. Y. Prognosis of bearing degradation using gradient variable forgetting factor RLS combined with time series model. *IEEE Access 6* (2018), 10986–10995.

[92] LUO, R., YIH, C.-C., AND SU, K. Multisensor fusion and integration: Approaches, applications, and future research directions. *IEEE Sensors Journal 2*, 2 (2002), 107–119.

[93] LYNAGH, N., RAHNEJAT, H., EBRAHIMI, M., AND AINI, R. Bearing induced vibration in precision high speed routing spindles. *International Journal of Machine Tools and Manufacture 40*, 4 (2000), 561–577.

[94] MARWAN, N., CARMEN ROMANO, M., THIEL, M., AND KURTHS, J. Recurrence plots for the analysis of complex systems. *Physics Reports 438*, 5 (2007), 237–329.

[95] MARWAN, N., KURTHS, J., AND FOERSTER, S. Analysing spatially extended high-dimensional dynamics by recurrence plots. *Physics Letters A 379*, 10-11 (May 2015), 894–900.

[96] MEIER, N., AMBROŻKIEWICZ, B., GEORGIADIS, A., AND LITAK, G. Verification of measuring the bearing clearance using kurtosis, recurrences and neural networks and comparison of these approaches. In *2019 IEEE SENSORS* (2019), pp. 1–4.

[97] MEIER, N., AND GEORGIADIS, A. Automatic assembling of bearings including clearance measurement. vol. 41, pp. 242–246.

[98] MEIER, N., PAPADOUDIS, J., AND GEORGIADIS, A. Automated system for measuring the radial clearance of rolling bear-ings. pp. 410–413.

[99] MEINECKE, A., HANDKE, L., MUELLER-FROMMEYER, L., AND KAUFFELD, S. Capturing non-linear temporally embedded processes in organizations using recurrence quantification analysis. *European Journal of Work and Organizational Psychology 29*, 4 (2020), 483–500.

[100] MISHRA, C., SAMANTARAY, A., AND CHAKRABORTY, G. Ball bearing defect models: A study of simulated and experimental fault signatures. *Journal of Sound and Vibration 400* (2017), 86–112.

[101] MISHRA, C., SAMANTARAY, A., AND CHAKRABORTY, G. Rolling element bearing fault diagnosis under slow speed operation using wavelet de-noising. *Measurement 103* (2017), 77–86.

[102] MITROVIĆ, R., ATANASOVSKA, I., SOLDAT, N., AND MOMČILOVIĆ, D. Effects of operation temperature on thermal expansion and main parameters of radial ball bearings. *Thermal Science 19*, 5 (2015), 1835–1844.

[103] MOHANTY, S., GUPTA, K., AND RAJU, K. Adaptive fault identification of bearing using empirical mode decomposition-principal component analysis-based average kurtosis technique. *IET Science, Measurement and Technology 11*, 1 (2017), 30–40.

[104] MORTADA, M.-A., YACOUT, S., AND LAKIS, A. Diagnosis of rotor bearings using logical analysis of data. *Journal of Quality in Maintenance Engineering 17*, 4 (2011), 371–397.

[105] MOSDORF, R., AND GÓRSKI, G. Detection of two-phase flow patterns using the recurrence network analysis of pressure drop fluctuations. *International Communications in Heat and Mass Transfer 64* (2015), 14–20.

[106] MOSHREFZADEH, A., AND FASANA, A. Planetary gearbox with localised bearings and gears faults: simulation and time/frequency analysis. *Meccanica 52* (05 2017).

[107] OLFATI-SABER, R. *Distributed Kalman Filtering and Sensor Fusion in Sensor Networks*, vol. 331. 07 2006, pp. 157–167.

[108] OSWALD, F., ZARETSKY, E., AND POPLAWSKI, J. Effect of internal clearance on load distribution and life of radially loaded ball and roller bearings. *Tribology Transactions - TRIBOL TRANS 55* (03 2012), 245–265.

[109] PARMAR, V., SARAN, V. H., AND HARSHA, S. Effect of an unbalanced rotor on dynamic characteristics of double-row self-aligning ball bearing. *European Journal of Mechanics - A/Solids 82* (2020), 104006.

[110] PETERSEN, D., HOWARD, C., SAWALHI, N., MOAZEN AHMADI, A., AND SINGH, S. Analysis of bearing stiffness variations, contact forces and vibrations in radially loaded double row rolling element bearings with raceway defects. *Mechanical Systems and Signal Processing 50-51* (2015), 139–160.

[111] RENAUDIN, L., BONNARDOT, F., MUSY, O., DORAY, J., AND RÉMOND, D. Natural roller bearing fault detection by angular measurement of true instantaneous angular speed. *Mechanical Systems and Signal Processing 24*, 7 (2010), 1998–2011.

[112] SAMUEL, P. D., AND PINES, D. J. A review of vibration-based techniques for helicopter transmission diagnostics. *Journal of Sound and Vibration 282*, 1 (2005), 475–508.

[113] SARIBULUT, L., TEKE, A., AND TUMAY, M. Fundamentals and literature review of fourier transform in power quality issues.

[114] SAWALHI, N., RANDALL, R., AND ENDO, H. The enhancement of fault detection and diagnosis in rolling element bearings using minimum entropy deconvolution combined with spectral kurtosis. *Mechanical Systems and Signal Processing 21*, 6 (2007), 2616–2633.

[115] SEERA, M., WONG, M. D., AND NANDI, A. K. Classification of ball bearing faults using a hybrid intelligent model. *Applied Soft Computing 57* (2017), 427–435.

[116] SHAFER, G. *A Mathematical Theory of Evidence*. Princeton University Press, 1976.

[117] SHANI, A., COGHLAN, D., AND ALEXANDER, B. Rediscovering abductive reasoning in organization development and change research. *Journal of Applied Behavioral Science 56*, 1 (2020), 60–72.

[118] SHI, H., AND BAI, X. Model-based uneven loading condition monitoring of full ceramic ball bearings in starved lubrication. *Mechanical Systems and Signal Processing 139* (2020), 106583.

[119] SHI, Z., LI, Y., AND LIU, S. A review of fault diagnosis methods for rotating machinery. In *2020 IEEE 16th International Conference on Control Automation (ICCA)* (2020), pp. 1618–1623.

[120] SOHN, H., AND FARRAR, C. Damage diagnosis using time series analysis of vibration signals. *Smart Materials and Structures 10*, 3 (2001), 446–451.

[121] SOUALHI, A., MEDJAHER, K., AND ZERHOUNI, N. Bearing health monitoring based on hilbert–huang transform, support vector machine, and regression. *IEEE Transactions on Instrumentation and Measurement 64*, 1 (2015), 52–62.

[122] SUN, S., PRZYSTUPA, K., WEI, M., YU, H., YE, Z., AND KOCHAN, O. Fast bearing fault diagnosis of rolling element using

lévy moth-flame optimization algorithm and naive bayes. *Eksploatacja i Niezawodnosc 22*, 4 (2020), 730–740.

[123] SYTA, A., JONAK, J., JEDLISKI, U., AND LITAK, G. Failure diagnosis of a gear box by recurrences. *Journal of Vibration and Acoustics, Transactions of the ASME 134*, 4 (2012).

[124] TAKENS, F. Detecting strange attractors in turbulence. In *Dynamical Systems and Turbulence, Warwick 1980* (Berlin, Heidelberg, 1981), D. Rand and L.-S. Young, Eds., Springer Berlin Heidelberg, pp. 366–381.

[125] TAMURA, T., OLIVER, T., CUNNINGHAM, A., AND WOODROFFE, C. Recurrence of extreme coastal erosion in se australia beyond historical timescales inferred from beach ridge morphostratigraphy. *Geophysical Research Letters 46*, 9 (2019), 4705–4714.

[126] TIAN, J., MORILLO, C., AZARIAN, M., AND PECHT, M. Motor bearing fault detection using spectral kurtosis-based feature extraction coupled with k-nearest neighbor distance analysis. *IEEE Transactions on Industrial Electronics 63*, 3 (2016), 1793–1803.

[127] TIAN, X., XI GU, J., REHAB, I., ABDALLA, G. M., GU, F., AND BALL, A. A robust detector for rolling element bearing condition monitoring based on the modulation signal bispectrum and its performance evaluation against the kurtogram. *Mechanical Systems and Signal Processing 100* (2018), 167–187.

[128] TIWARI, M., GUPTA, K., AND PRAKASH, O. Dynamic response of an unbalanced rotor supported on ball bearings. *Journal of Sound and Vibration 238*, 5 (2000), 757–779.

[129] TIWARI, M., GUPTA, K., AND PRAKASH, O. Effect of radial internal clearance of a ball bearing on the dynamics of a balanced horizontal rotor. *Journal of Sound and Vibration 238*, 5 (2000), 723–756.

[130] TIWARI, M., GUPTA, K., AND PRAKASH, O. Experimental study of a rotor supported by deep groove ball bearing. *International Journal of Rotating Machinery 8*, 4 (2002), 243–258. cited By 16.

[131] TRULLA, L., GIULIANI, A., ZBILUT, J., AND WEBBER JR., C. Recurrence quantification analysis of the logistic equation with transients. *Physics Letters, Section A: General, Atomic and Solid State Physics 223*, 4 (1996), 255–260.

[132] UHLMANN, J. Covariance consistency methods for fault-tolerant distributed data fusion. *Information Fusion 4* (09 2003), 201–215.

[133] UPADHYAY, S., HARSHA, S., AND JAIN, S. Analysis of nonlinear phenomena in high speed ball bearings due to radial clearance and unbalanced rotor effects. *Journal of Vibration and Control 16*, 1 (2010), 65–88.

[134] VASHISHT, R. K., AND PENG, Q. Crack detection in the rotor ball bearing system using switching control strategy and short time fourier transform. *Journal of Sound and Vibration 432* (2018), 502–529.

[135] WALLOT, S., AND MØNSTER, D. Calculation of average mutual information (ami) and false-nearest neighbors (fnn) for the estimation of embedding parameters of multidimensional time series in matlab. *Frontiers in Psychology 9* (2018), 1679.

[136] WANG, D.-F., GUO, Y., WU, X., NA, J., AND LITAK, G. Planetary-gearbox fault classification by convolutional neural network and recurrence plot. *Applied Sciences (Switzerland) 10*, 3 (2020).

[137] WANG, H., HAN, Q., LUO, R., AND QING, T. Dynamic modeling of moment wheel assemblies with nonlinear rolling bearing supports. *Journal of Sound and Vibration 406* (2017), 124–145.

[138] WANG, H., HAN, Q., AND ZHOU, D. Nonlinear dynamic modeling of rotor system supported by angular contact ball bearings. *Mechanical Systems and Signal Processing 85* (2017), 16–40.

[139] WANG, J., XU, M., ZHANG, C., HUANG, B., AND GU, F. Online bearing clearance monitoring based on an accurate vibration analysis. *Energies 13*, 2 (2020).

[140] WANG, Y., YANG, H., CHEN, G., AND JIA, Y. Influence of fit clearance on the stability of "three oil film-rotor" structure. *International Journal of Simulation Modelling 20*, 1 (2021), 170–180.

[141] WARDLE, F. 1 - introduction. In *Ultra-Precision Bearings*, F. Wardle, Ed. Woodhead Publishing, Oxford, 2015, pp. 1–35.

[142] WILLIAMS, T., RIBADENEIRA, X., BILLINGTON, S., AND KURFESS, T. Rolling element bearing diagnostics in run-to-failure lifetime testing. *Mechanical Systems and Signal Processing 15*, 5 (2001), 979–993.

[143] WOLD, S., ESBENSEN, K., AND GELADI, P. Principal component analysis. *Chemometrics and Intelligent Laboratory Systems 2*, 1-3 (1987), 37–52.

[144] WU, S., JING, X.-Y., ZHANG, Q., WU, F., ZHAO, H., AND DONG, Y. Prediction consistency guided convolutional neural networks for cross-domain bearing fault diagnosis. *IEEE Access 8* (2020), 120089–120103.

[145] XIA, X., AND MENG, F. Grey relational analysis of measure for uncertainty of rolling bearing friction torque as time series. *Journal of Grey System 23*, 2 (2011), 135–144.

[146] XIANG, W., YAN, S., AND WU, J. Dynamic analysis of planar mechanical systems considering stick-slip and stribeck effect in revolute clearance joints. *Nonlinear Dynamics 95*, 1 (2019), 321–341.

[147] XIAOLI, R., JIA, Z., AND GE, R. Calculation of radial load distribution on ball and roller bearings with positive, negative and zero clearance. *International Journal of Mechanical Sciences 131-132* (2017), 1–7.

[148] XU, M., FENG, G., HE, Q., GU, F., AND BALL, A. Vibration characteristics of rolling element bearings with different radial clearances for condition monitoring of wind turbine. *Applied Sciences 10*, 14 (2020).

[149] XU, M., HAN, Y., SUN, X., SHAO, Y., GU, F., AND BALL, A. D. Vibration characteristics and condition monitoring of internal radial clearance within a ball bearing in a gear-shaft-bearing system. *Mechanical Systems and Signal Processing 165* (2022), 108280.

[150] XU, X., HUANG, Q., REN, Y., ZHAO, D.-Y., AND YANG, J. Sensor fault diagnosis for bridge monitoring system using similarity of symmetric responses. *Smart Structures and Systems 23*, 3 (2019), 279–293.

[151] YAKOUT, M., NASSEF, M., AND BACKAR, S. Effect of clearances in rolling element bearings on their dynamic performance, quality and operating life. *Journal of Mechanical Science and Technology 33* (05 2019), 2037–2042.

[152] ZAVADSKAS, E., TURSKIS, Z., TAMOŠAITIENE, J., AND MARINA, V. Multicriteria selection of project managers by applying grey cri-

teria. *Technological and Economic Development of Economy 14*, 4 (2008), 462–477.

[153] ZBILUT, J., GIULIANI, A., AND WEBBER JR., C. Detecting deterministic signals in exceptionally noisy environments using cross-recurrence quantification. *Physics Letters, Section A: General, Atomic and Solid State Physics 246*, 1-2 (1998), 122–128.

[154] ZBILUT, J., GIULIANI, A., AND WEBBER JR., C. Recurrence quantification analysis and principal components in the detection of short complex signals. *Physics Letters, Section A: General, Atomic and Solid State Physics 237*, 3 (1998), 131–135.

[155] ZHANG, X., HAN, Q., PENG, Z., AND CHU, F. A comprehensive dynamic model to investigate the stability problems of the rotor-bearing system due to multiple excitations. *Mechanical Systems and Signal Processing 70-71* (2016), 1171–1192.

[156] ZHANG, Y., AND RANDALL, R. Rolling element bearing fault diagnosis based on the combination of genetic algorithms and fast kurtogram. *Mechanical Systems and Signal Processing 23*, 5 (2009), 1509–1517.

[157] ZHANG, Z., CHEN, Y., AND CAO, Q. Bifurcations and hysteresis of varying compliance vibrations in the primary parametric resonance for a ball bearing. *Journal of Sound and Vibration 350* (2015), 171–184.

[158] ZHANG, Z., SATTEL, T., ZHU, Y., LI, X., DONG, Y., AND RUI, X. Mechanism and characteristics of global varying compliance parametric resonances in a ball bearing. *Applied Sciences (Switzerland) 10*, 21 (2020), 1–28.

[159] ZHUO, Y., ZHOU, X., AND YANG, C. Dynamic analysis of double-row self-aligning ball bearings due to applied loads, internal clearance, surface waviness and number of balls. *Journal of Sound and Vibration 333*, 23 (2014), 6170–6189.

List of Figures

List of Tables

LIST OF ABBREVIATIONS

AI	Artificial intelligence
ANN	Artificial Neural Networks
BPFI	Ball Passing Frequency Inner
BPFO	Ball Passing Frequency Outer
BSF	Ball Spin Frequency
CF	Crest Factor
CLS	Clustering
DET	Determinism
DGBB	Deep Groove Ball Bearing
DOF	Degree of Freedom
ENTR	Entropy
ER	Energy Ratio
FC	Frequency Center
FFT	Fast Fourier Transform
FNN	False Nearest Neighbors
FTF	Fundamental Train Frequency
GI	Gini Index
GRA	Grey Relational Anlysis
HHT	Hilbert-Huang Transform
ICA	Independent Component Analysis
IR	Inner Ring
L	Average Length of the Diagonal Line
L_{max}	Length of the Longest Diagonal Line
LAM	Laminarity
MEMS	Micro-Electro-Mechanical-System
MF	Mean Frequency
MI	Mutual Information
MSB	Modulation Signal Bispectrum
MSB	Modulation Signal Bispectrum
OR	Outer Ring
PCA	Principal Component Analysis

PS	Power Spectrum
RIC	Radial Internal Clearance
RMS	Root Mean Square
RMSF	Root Mean Square Frequency
RP	Recurrence Plot
RPDE	Recurrence Period Density Entropy
RQA	Recurrence Quantification Analysis
SABB	Self Aligning Ball Bearing
SC	Spectral Centroid
SK	Spectral Kurtosis
SOTA	State of the Art
STFT	Short Time Fourier Transform
T^1	Recurrence Time of 1st Type
T^2	Recurrence Time of 2nd Type
TRANS	Transitivity
TT	Trapping Time
V_{max}	Maximal Length of the Vertical Line